USAAVLABS TECHNICAL REPORT 65-81

AN INVESTIGATION OF PROPELLER SLIPSTREAM EFFECTS ON V/STOL AIRCRAFT PERFORMANCE AND STABILITY

By

L. Butler

K. P. Huang

L. Goland

February 1966

U. S. ARMY AVIATION MATERIEL LABORATORIES

FORT EUSTIS, VIRGINIA

Disclaimers

The findings in this report are not to be construed as an
official Department of the Army position, unless so desig-
nated by other authorized documents.

When Government drawings, specifications, or other data are
used for any purpose other than in connection with a defi-
nitely related Government procurement operation, the United
States Government thereby incurs no responsibility nor any
obligation whatsoever; and the fact that the Government may
have formulated, furnished, or in any way supplied the said
drawings, specifications, or other data is not to be regarded
by implication or otherwise as in any manner licensing the
holder or any other person or corporation, or conveying any
rights or permission, to manufacture, use, or sell any pat-
ented invention that may in any way be related thereto.

Disposition Instructions

Destroy this report when it is no longer needed. Do not
return it to the originator.

The study summarized in this report was undertaken to extend knowledge of performance and stability characteristics of V/STOL aircraft.

The report has been reviewed by the U. S. Army Aviation Materiel Laboratories and is considered to be technically sound. It is published for the exchange of information and stimulation of ideas.

Task 1D121401A14203
Contract DA 44-177-AMC-48(T)
USAAVLABS Technical Report 65-81
February 1966

AN INVESTIGATION OF PROPELLER SLIPSTREAM
EFFECTS ON V/STOL AIRCRAFT
PERFORMANCE AND STABILITY

Dynasciences Report No. DCR-174

by
L. Butler
K.P. Huang
L. Goland

Prepared by

Dynasciences Corporation
Blue Bell, Pennsylvania

for

U. S. ARMY AVIATION MATERIEL LABORATORIES
FORT EUSTIS, VIRGINIA

SUMMARY

An investigation was made of the effects of
propeller slipstream on several aspects of V/STOL aircraft
performance and stability. Specific areas investigated
include wing stall during transition, minimum wing size for
stall-free transition, and the effects of slipstream on
aircraft pitching moments. In addition, a stability analysis
was performed, and analog computer techniques were used to
determine the feasibility of utilizing the slipstream for
stability augmentation. Finally, the effects of the
nonuniformity of slipstream velocity and wing geometry
modifications on performance were analyzed.

FOREWORD

This report presents the results of the investigation made for the U.S. Army Aviation Materiel Laboratories* (USAAVLABS), Fort Eustis, Virginia, under Phases IV through VI of Contract DA 44-177-AMC-48(T), during the period April 1964 through March 1965.

The results of the work performed for the preceding phases of the above mentioned contract are covered by TRECOM Technical Report 64-47, published in August 1964.

*Formerly, U.S. Army Transportation Research Command

CONTENTS

ILLUSTRATIONS

SYMBOLS

A_j	cross-sectional area of fully developed slipstream, square feet
AR	wing aspect ratio
a	basic wing lift curve slope, per radian
a_o	airfoil section lift curve slope, per radian
a_x	aircraft longitudinal acceleration, feet per second per second
a_z	aircraft vertical acceleration, feet per second per second
b	wing span, feet
b_s	distance from wing root to slipstream centerline, feet
C_{D_o}	section profile drag coefficient of wing area not immersed in slipstream (evaluated at free stream wing geometric angle of attack)
$C_{D_{o_F}}$	fuselage profile drag coefficient
$C_{D_{o,S}}$	section profile drag coefficient of wing area immersed in slipstream (evaluated at slipstream wing geometric angle of attack)
$C_{D_{o_t}}$	tail profile drag coefficient
C_{D_W}	wing drag coefficient, including effect of slipstream, $D_W/q_s S$
C_M	pitching moment coefficient, $M/q_s S\bar{c}$

xiii

C_L basic wing lift coefficient

$C_{L,s}$ total lift coefficient, including contributions due to propeller thrust and normal force components, and effect of slipstream, based on q_s

$\Delta C_{L,s}$ increment of lift coefficient due to effect of slipstream

C_{Lw} wing lift coefficient, including effect of slipstream, $L_w/q_s S$

C_l airfoil section lift coefficient; also local wing lift coefficient

C_{lmax} airfoil section maximum lift coefficient

C_{lpeak} maximum local wing lift coefficient of wing area immersed in slipstream, based on q_s

$C_{l,s}$ local lift coefficient of wing area immersed in slipstream, based on q_s

$\Delta C_{l,s}$ increment of local lift coefficient due to effect of slipstream

C_{Mp} propeller pitching moment coefficient, $M_p/\rho n^2 D^4$

$C_{M,s}$ total pitching moment coefficient about wing quarter-chord, including contributions due to propeller pitching moment and normal force, and effect of slipstream

C_{Mw} wing pitching moment coefficient, $M_{wc/4}/q_s S \bar{c}$

C_{Np} propeller normal force coefficient, $N_p/\rho n^2 D^4$

C_p	propeller power coefficient, $P/\rho n^3 D^5$
C_Q	propeller torque coefficient, $C_p/2\pi$
C_T	propeller thrust coefficient, $T_p/q_o(\pi D^2/4)$
C_T'	propeller thrust coefficient, $T_p/\rho n^2 D^4$
C_{Ts}	propeller thrust coefficient, $T_p/q_s(\pi D^2/4)$
$C_{X,s}$	longitudinal force coefficient, $X/q_s S$
c	wing chord, feet
$\bar{c}$	average wing chord, feet
c_f	flap chord, feet
c_s	wing chord at slipstream centerline, feet
$c.g.$	center of gravity
$c.p.$	center of pressure
D	propeller diameter, feet
D_F	fuselage drag, pounds
D_t	tail drag, pounds
D_w	wing drag, including effect of slipstream, pounds
D_{w_u}, D_{w_α}	wing drag derivatives
g	acceleration due to gravity, feet per second per second
I_{yy}	aircraft pitching moment of inertia, slug-square feet

i_p	geometric angle between propeller thrust axis and X-axis, radians
i_T	angle of incidence between propeller thrust axis and wing-chord line, radians
i_w	geometric angle between wing-chord line and X-axis, radians
J	propeller advance ratio, V_o/nD
J'	propeller advance ratio, $V_o \cos\alpha_p/nD$
j	index number
K, K_l	empirical constants for correction of additional angle of attack due to flap deflections
$k_1, k_2, \ldots$	slipstream stabilizer constants
L	basic wing lift, pounds
L_F	fuselage lift, pounds
L_t	tail lift, pounds
L_w	wing lift, pounds
L_{w_u}, L_{w_α}	wing lift derivatives
ℓ_t	distance from c.g. of aircraft to quarter-chord of horizontal tail, feet
$M, M_{c.g.}$	aircraft pitching moment about c.g. of aircraft, pound-feet
M_F	fuselage pitching moment, pound-feet
M_p	propeller pitching moment, pound-feet

M_{p_u}, M_{p_α}	propeller pitching moment derivatives
$M_u, M_w, \ldots$	aircraft pitching moment derivatives
$M_{w_{c/4}}$	wing pitching moment about wing quarter-chord, pound-feet
M_{y_p}	propeller yawing moment, pound-feet
m	mass, slugs
N	number of propellers
N_p	propeller normal force, pounds
N_T	tail rotor normal force, pounds
n	propeller rotational speed, revolutions per second
n_o	propeller rotational speed preceding engine power failure, revolutions per second
P	propeller power, foot-pounds per second
Q	propeller torque, pound-feet
q_o	free stream dynamic pressure, pounds per square foot
q_s	slipstream dynamic pressure, pounds per square foot
R_n	reynolds number
r_s	radius of fully developed slipstream, feet
r_1, r_2	radii of slipstream velocity zones, feet
S	total wing area, square feet

S_p	propeller side force, pounds
S_s	slipstream-immersed wing area, square feet
T_p	propeller thrust, pounds
T_r	tail rotor thrust, pounds
U	slipstream-induced velocity in fully developed slipstream, feet per second
U_1, U_2	slipstream-induced velocities, feet per second
$\overline{U}'$	nondimensionalized slipstream-induced velocity
U_1', U_2'	nondimensionalized slipstream-induced velocities
u	longitudinal component of free stream velocity, feet per second
V_o	free stream velocity, feet per second
V_j	velocity of fully developed slipstream, feet per second
V_t	airflow velocity at horizontal tail, feet per second
V_1, V_2	slipstream velocities in velocity zones, feet per second
W	aircraft gross weight, pounds
w	normal component of free stream velocity, feet per second
X	force acting in X-axis direction, pounds

$X_u, X_w, \cdots$	derivatives of forces acting in the X-axis direction
x	longitudinal distance from wing leading-edge, feet
$x_p, x_w, \cdots$	distances in X-axis direction, feet
y	spanwise distance from wing root, feet
y_s	spanwise distance from slipstream centerline, positive towards wing tip, feet
$\overline{y}$	nondimensionalized spanwise distance from slipstream centerline, y_s / r_s
Z	force acting in Z-axis direction, pounds
$Z_u, Z_w, \cdots$	derivatives of forces acting in Z-axis direction
z	vertical distance from wing trailing-edge to plane of horizontal tail, feet
$z_p, z_w, \cdots$	distances in Z-axis direction, feet
α	effective wing angle of attack without slipstream, $\alpha_w - \alpha_{Lo} + \Delta\alpha_F$, radians
α_{Lo}	angle of zero lift of basic airfoil section (with no flap), radians
α_F	angle of attack between X-axis and free stream, radians
$\Delta\alpha_f$	change in wing effective angle of attack due to flap deflection (without slipstream), radians

α_p	angle of attack between propeller thrust axis and free stream, radians
$\Delta\alpha_a$	spanwise local change in wing angle of attack due to slipstream rotation, radians
α_s	mean effective wing angle of attack in slipstream, $\phi + i_T - \alpha_{lo} + \delta_f$, radians
α_{sc}	effective wing angle of attack at slipstream centerline, radians
α_t	horizontal tail angle of attack, radians
α_w	wing geometric angle of attack, radians
$\beta, \beta_{0.75}$	propeller blade pitch at three-quarter blade radius, degrees
γ_o	aircraft climb angle, radians
δ	slipstream stabilizer deflection, radians
δ_f	wing trailing-edge flap deflection angle, radians
γ	ratio of slipstream induced velocities in two velocity zones
η	ratio of radii of slipstream velocity zones
ϵ	downwash angle at tail, radians
ϵ_s	wing twist from slipstream centerline to periphery, radians
θ	fuselage attitude, radians
μ	ratio of free stream to jet velocity

ρ mass density of air, slugs per cubic foot

ϕ deflection angle of resultant slipstream flow from propeller thrust axis (slipstream velocity assumed uniform and irrotational), radians

$\Phi, \Phi_o, \Phi_1, \ldots$ velocity potentials

INTRODUCTION

The present work is a continuation of the investigation of propeller-wing aerodynamics reported in Reference 3. In Reference 3, simple analytical expressions are presented for the lift and drag of a wing immersed in propeller slipstream. These expressions were correlated with experimental data and it was found that fair to good agreement is obtained for unstalled wings. Also, a preliminary investigation of wing stall was presented. Furthermore, the previously mentioned expressions were utilized to evaluate the use of slipstream to augment stability and it was found that the use of a servo-flap on the wing trailing edge results in positive dynamic stability in the hovering flight condition.

In the program reported herein the problem of wing stall is further investigated and an expression is given for the determination of wing stall within the slipstream. This expression is then utilized to formulate a method for the determination of the minimum wing size for stall-free transition of tilt-wing type VTOL aircraft. The above analyses for stall and minimum wing size are presented in the two following sections.

The effect of propeller-wing interaction on pitching moments is presented in the section titled Propeller and Slipstream-Induced Moments. Data are given for propeller normal force and pitching moment with and without the presence of a wing. Furthermore, the effect of propeller slipstream on wing pitching moment and center of pressure is examined for a range of flap deflections. In addition, slipstream effects on the horizontal tail are discussed.

The next topic in the present investigation pertains to stability during the transition maneuver and is presented in the section title Slipstream Effects on VTOL Aircraft Stability. The derivatives, which in Reference 3 are obtained for the hovering flight condition, are extended to the transition conditions. A number of stabilization augmentation systems are investigated by means of an analog computer study.

In the section titled Modification of Slipstream to Augment Lift and Control, an analysis is made on the possibility of increasing the lift of a slipstream-immersed wing by changing the propeller-induced velocity profile of the slipstream. Finally, the effects of large flap deflections, wing twist and relative propeller-wing orientation and position on wing lift are investigated.

STALL OF A WING IMMERSED IN PROPELLER SLIPSTREAM

Wing stall constitutes a serious problem if encountered during the transition maneuver of a tilt-wing VTOL aircraft. The stalled wing not only modifies the lift and drag characteristics of the aircraft but also has an adverse effect on stability and control.

In formulating a method for the prediction of stall of a wing immersed in a slipstream, it is useful to review the analyses which are being utilized for conventional wings.

The first and probably still the most successful approach to the analysis of wing stall is contained in NACA Report 572 (Reference 1) published in 1936. This method can be summarized as follows:

1. The spanwise distribution of the maximum section lift coefficient, $C_{\ell max}$, of the wing is determined using experimental two-dimensional airfoil data.

2. The spanwise distribution of local lift coefficient, C_ℓ, is calculated for increasing angles of attack, until the C_ℓ curve first reaches the $C_{\ell max}$ curve. When this occurs initial stall is considered to begin at the point of tangency of the two curves.

Initial wing stall as defined by the above method is illustrated in the sketch below.

3
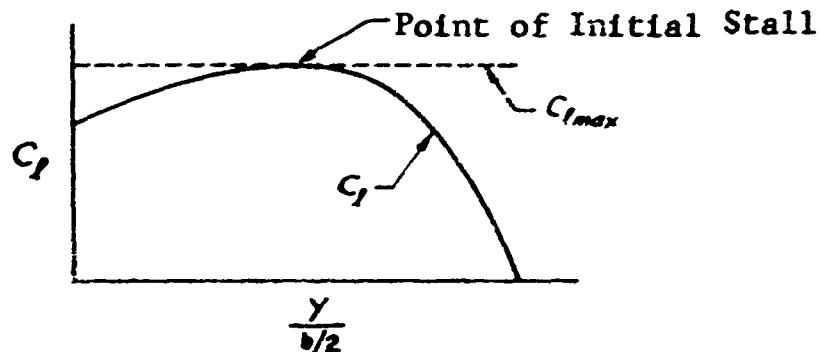
As reported in Reference 8 the above method has been used with success in analyzing unswept wings of mild taper.

Following World War II, the above method was applied to the analysis of swept wings, but it was found that the resulting stall predictions were less accurate than those for unswept wings. In part this is due to the boundary layer flow which for swept wings is significantly different from what occurs on a two-dimensional airfoil. As indicated in Reference 8, the difference in boundary layer conditions is, for the most part, due to the spanwise component of velocity over the swept wing, although the wing planform also contributes to this difference. In spite of these inaccuracies, the above method provides useful results for the swept wing in that it gives a conservative estimate of the condition of initial stall.

It is assumed that this method is applicable also to wings partially or fully immersed in a slipstream. The formulation of the appropriate equations for the wing-propeller case is now presented.

STALL ANALYSIS

The slipstream is assumed to consist of a circular jet of uniform velocity with a linear variation of flow direction between the jet centerline and the jet to free stream boundary, as illustrated in Figure 1.

Spanwise Distribution of Maximum Section Lift Coefficient

Experimental data show that $C_{\ell_{max}}$ is affected both by Reynolds number and flow turbulence. The present analysis utilizes data from Reference 10, which are corrected for tunnel turbulence.

A typical spanwise $C_{\ell_{max}}$ distribution of a wing immersed in a uniform slipstream is shown in the sketch at the top of page 6.

4

FIGURE 1. Velocity and Angle-of-Attack Distribution
of Assumed Slipstream at the Wing.

5
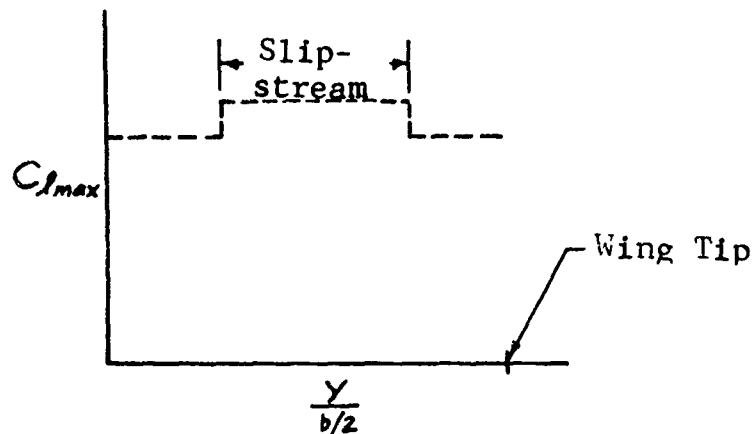
The step in the $C_{\ell max}$ distribution is due to the different Reynolds numbers in and outside of the slipstream.

Spanwise Distribution of Local Lift Coefficient

Using the approach of Reference 3, the lift coefficient of a wing partially immersed in a slipstream is obtained by the addition of a basic wing lift coefficient and an increment due to the slipstream effects. The spanwise distribution of C_{ℓ} outside of the slipstream is obtained using Schrenk's method (Reference 24), as follows:

$$C_{\ell} = \frac{C_L}{2}\left[1 + \frac{4}{\pi}\frac{\bar{c}}{c}\sqrt{1 - \left(\frac{y}{b/2}\right)^2}\right] \qquad (1)$$

The total lift coefficient, C_L, is obtained from the relationship,

$$C_L = a \sin \alpha \qquad (2)$$

6

where

$$a = \frac{a_o}{\sqrt{1 + \left(\frac{a_o}{\pi R}\right)^2} + \frac{a_o}{\pi R}}$$

In Equation (2), $\sin\alpha$ is used rather then α to better approximate C_L at large values of $\alpha_{,i/}$.

Within the slipstream, the basic distribution, Equation (1), is modified to account for the slipstream dynamic pressure and is expressed in terms of Y_s/r_s . The equation for the increment lift coefficient, $\Delta C_{\ell,s}$, is obtained from Reference 3. Hence, the lift coefficient distribution inside the slipstream is given by

$$C_{\ell,s} = C_\ell \frac{q_o}{q_s} + \Delta C_{\ell,s} \tag{3}$$

For a rectangular wing, $\bar{c}/c = 1$, and

$$C_{\ell,s} = \frac{a \sin\alpha}{2}\left[1 + \frac{4}{\pi}\sqrt{1 - \left(\frac{b_s + Y_s}{b/2}\right)^2}\right]\frac{q_o}{q_s}$$

$$+ \frac{1.87\left(\frac{r_s}{c}\right)(1-\mu^2)\alpha_s}{\frac{\pi^2}{4}-1}\left(\frac{1}{\frac{Y_s}{r_s}} - \frac{Y_s}{r_s}\right)\ell_n\left(\frac{1 + \frac{Y_s}{r_s}}{1 - \frac{Y_s}{r_s}}\right) \tag{4}$$

where

$$\alpha_s = \phi + i_T - \alpha_{Lo} + \delta_f - \Delta\alpha_Q \tag{5}$$

The term $\Delta\alpha_Q$ accounts for the change in local angle of attack due to slipstream rotation, and is given by

7

$$\Delta \alpha_Q = \left[\frac{32\, C_Q \sqrt{1 - C_{T,s}}}{\pi\, J^2 \left(\cos \alpha_p + \sqrt{\cos^2 \alpha_p - \dfrac{C_{T_s}}{1 - C_{T,s}}} \right)} \right] \frac{Y_s}{r_s} \qquad (6)$$

CORRELATION

To determine its accuracy, the above method is correlated with test data presented in Reference 27. The geometric parameters of the test model are as follows:

Span	5.0 feet
Chord	1.0 feet
Taper Ratio	1.0
Aspect Ratio	5.0
Airfoil Section	NACA 0015
Propeller Diameter	2.0 feet
Number of Propellers	2

The predicted region of wing stall and estimated spanwise distributions are shown for this model at an angle of attack, $\alpha_w = 15$ degrees, and thrust coefficient, $C_{T,s} = 0.58$, on Figures 2 and 3 for different directions of propeller rotation, respectively. The $C_{l_{max}}$ curves are based on "Effective Reynolds Number" data from Reference 10. For $C_{T,s} = 0.58$,

$R_n = 550,000$ (in the slipstream)
$R_n = 356,000$ (outside of the slipstream).

In Figures 2 and 3, stall has occurred over the inboard portion of the wing outside of the slipstream. On the other hand, wing stall has not occurred in the slipstream since $C_{l,s} < C_{l_{max}}$. Calculations performed for increasing angles of attack show that the immersed portion of the wing begins to stall at $\alpha_w = 19$ and 23 degrees for the propeller rotating down and up at the wing tip, respectively. This difference in stall angles results from the shift of the maximum value of $C_{l,s}$ toward the wing tip.

8
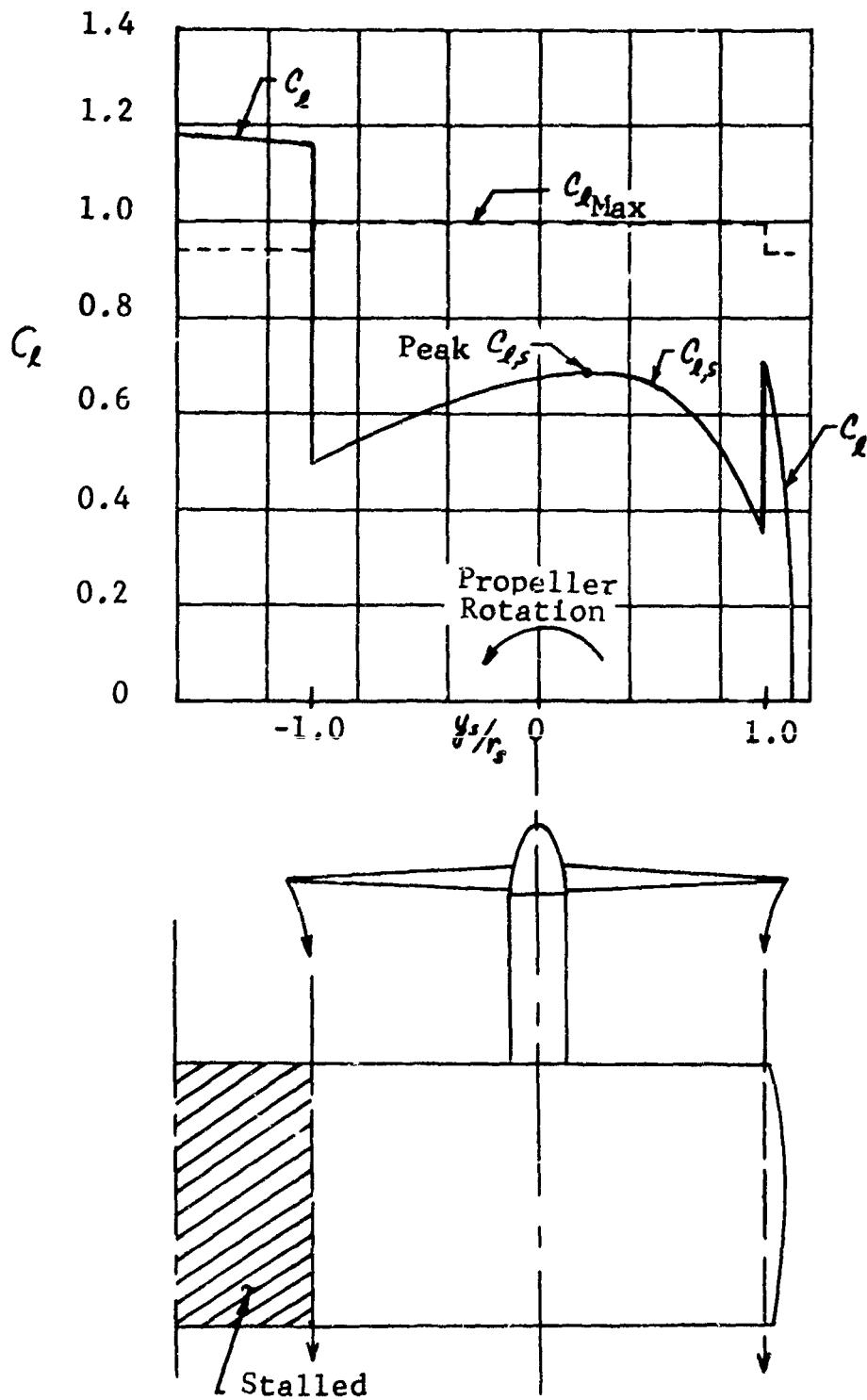
FIGURE 2. Estimated Spanwise Lift Coefficient Distribution and Extent of Wing Stall (Propeller Rotating Down at Wing Tip, α_w = 15 Degrees, $C_{T,s}$ = 0.58, $\mathcal{R}$ = 5.00, NACA 0015 Airfoil Section).
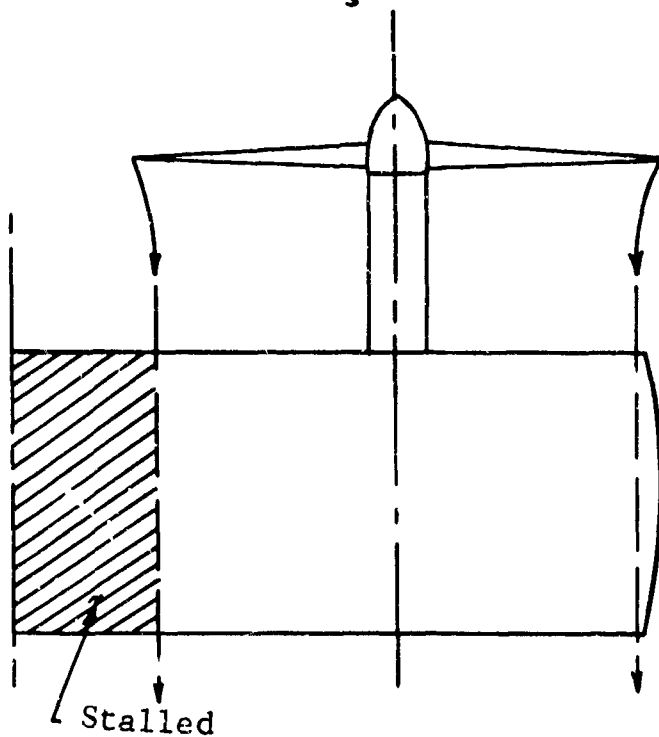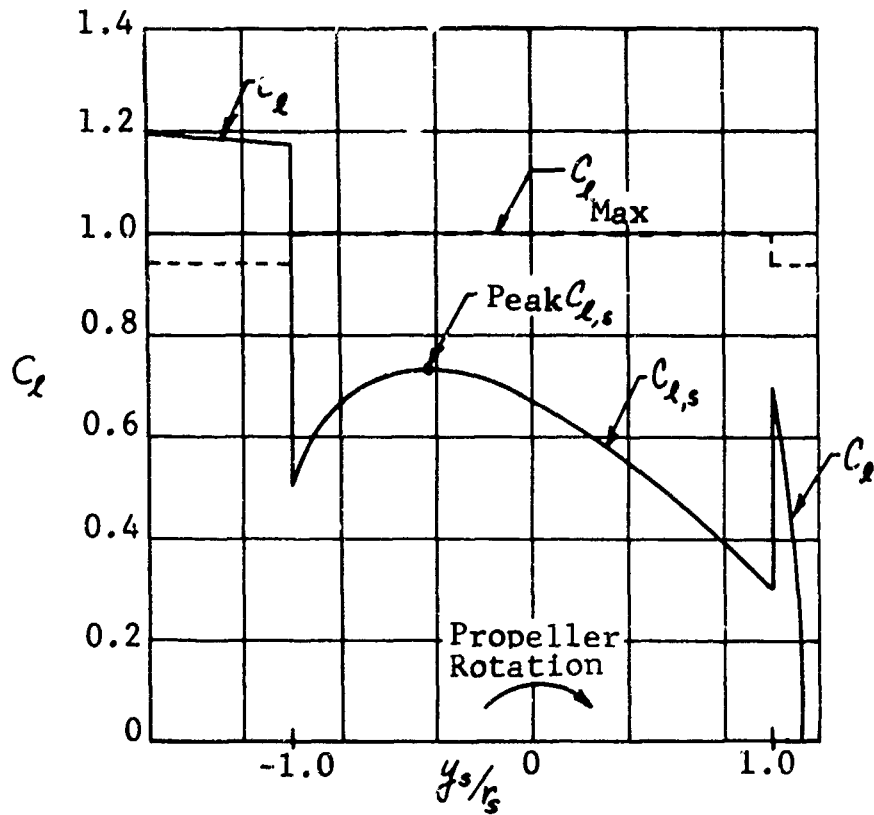
FIGURE 3. Estimated Spanwise Lift Coefficient Distribution and Extent of Wing Stall (Propeller Rotating up at Wing Tip, α_w = 15 Degrees, $C_{T,s}$ = 0.58, R = 5.00, NACA 0015 Airfoil Section).

Similar calculations were performed for α_w = 50 degrees and C_{TS} = 0.88. The $C_{l_{max}}$ curves are based on Reynolds numbers of 550,000 and 346,000 in and outside of the slipstream, respectively. The results are presented in Figures 4 and 5 for the propeller rotating down and up at the wing tip. It is noted again that stall within the slipstream occurs earlier for the case of the propeller rotating down at the wing tip.

Correlation between estimated stall and experimental data for the model analyzed is shown in Figure 6. The experimental data points shown correspond to the wing angle of attack where the lift curve slope begins to change noticeably as illustrated in the sketch at the top of Figure 6. It is seen that at constant C_{TS}, the calculated values of the wing angle of attack at initial stall correlate well with test data up to C_{TS} = 0.5. At larger thrust coefficients, the predicted stall angle increases more rapidly than the measured value. Additional test data are required to determine the reason for this discrepancy.

11
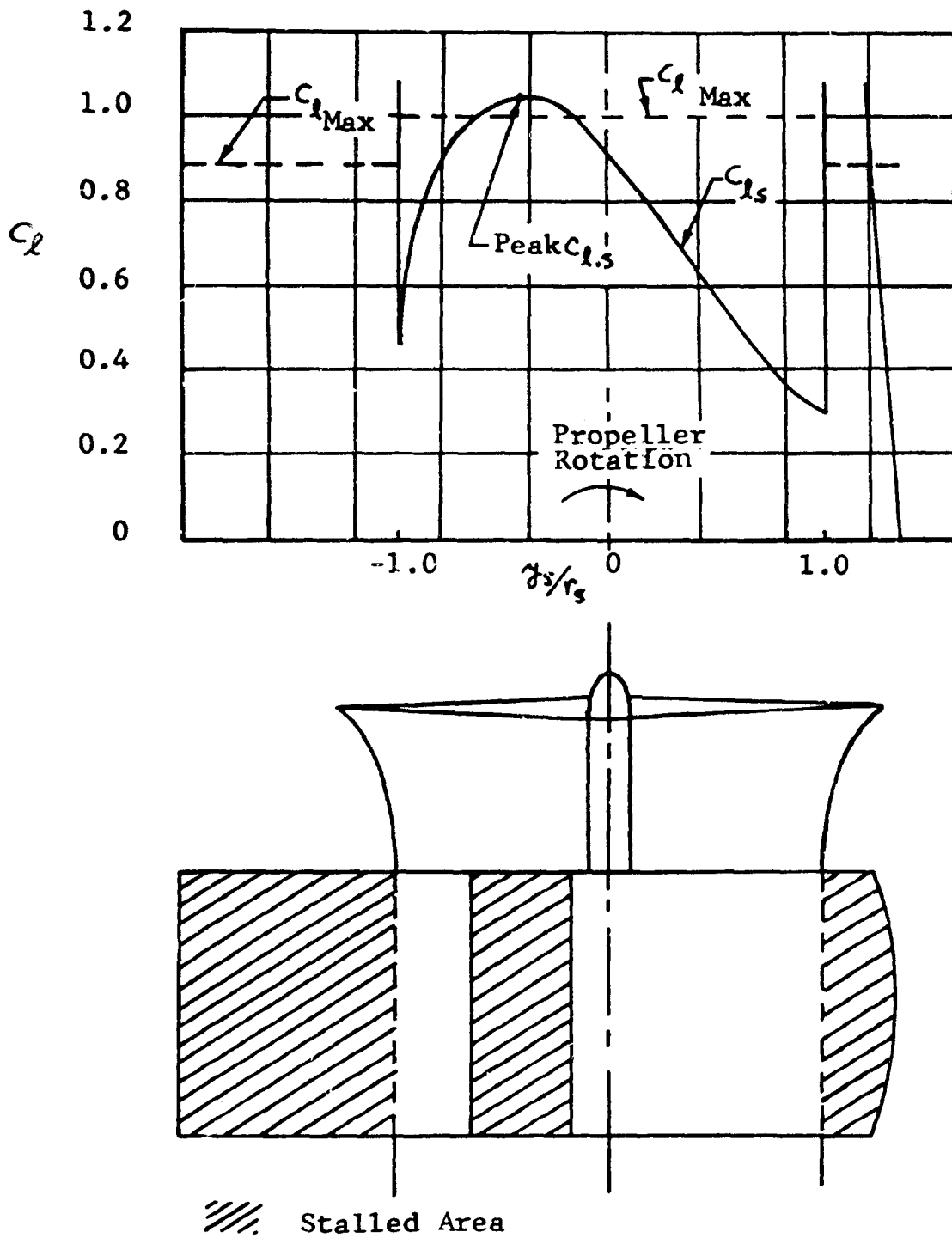
FIGURE 4. Estimated Spanwise Lift Coefficient Distribution and Extent of Wing Stall (Propeller Rotating down at Wing Tip, α_w = 50 Degrees, $C_{T,s}$ = 0.88, R = 5.0, NACA 0015 Airfoil Section).
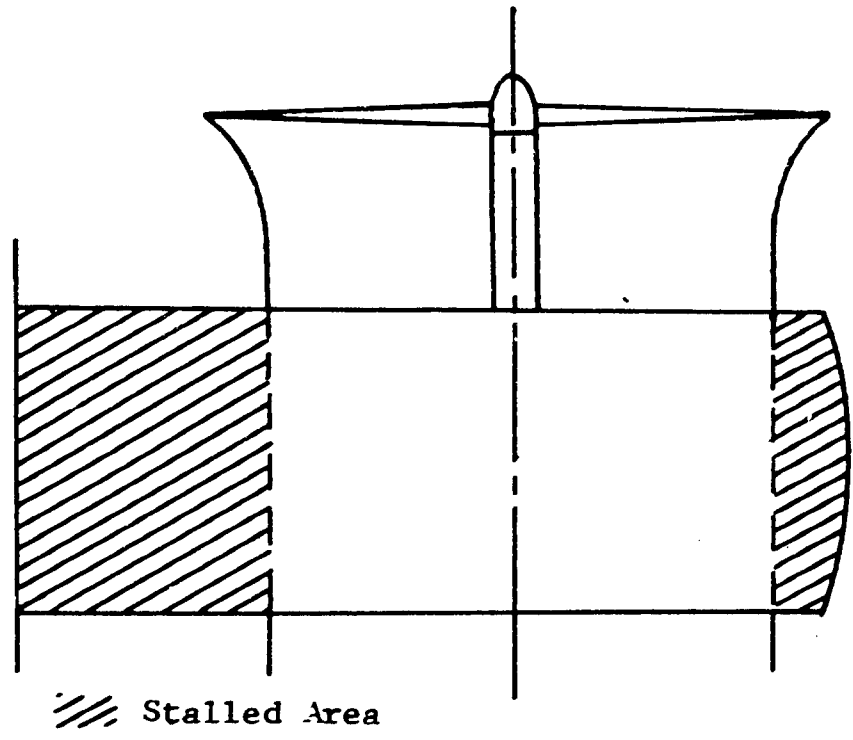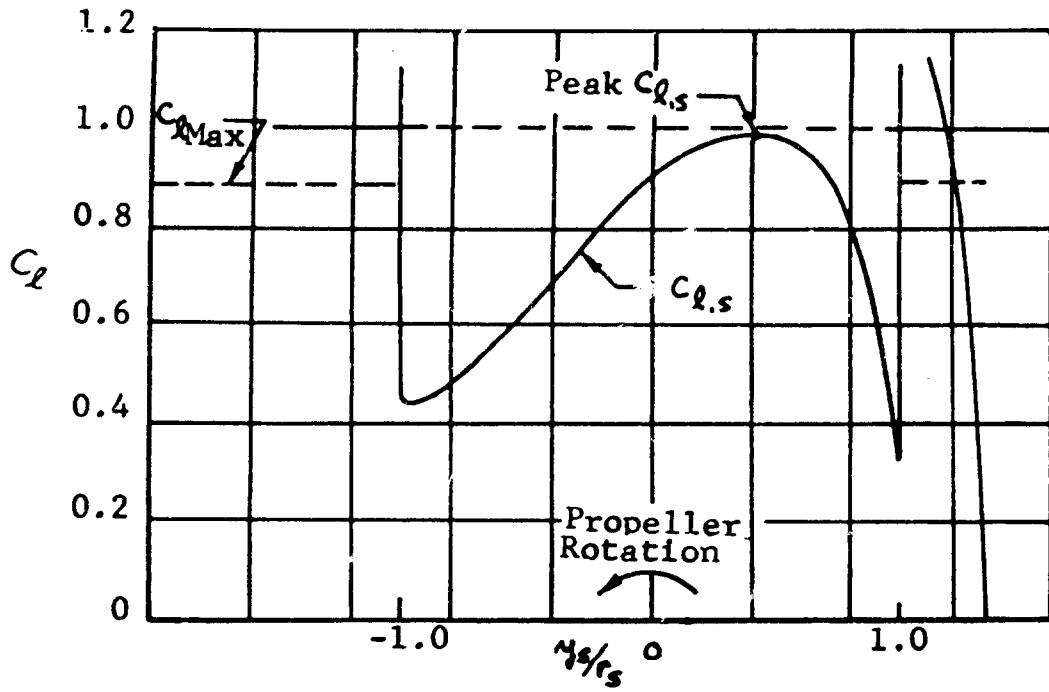
FIGURE 5. Estimated Spanwise Lift Coefficient Distribution and Extent of Wing Stall (Propeller Rotating Up at Wing Tip, α_w =50 Degrees, $C_{T,s}$ = 0.88, R =5.0, NACA 0015 Airfoil Section).
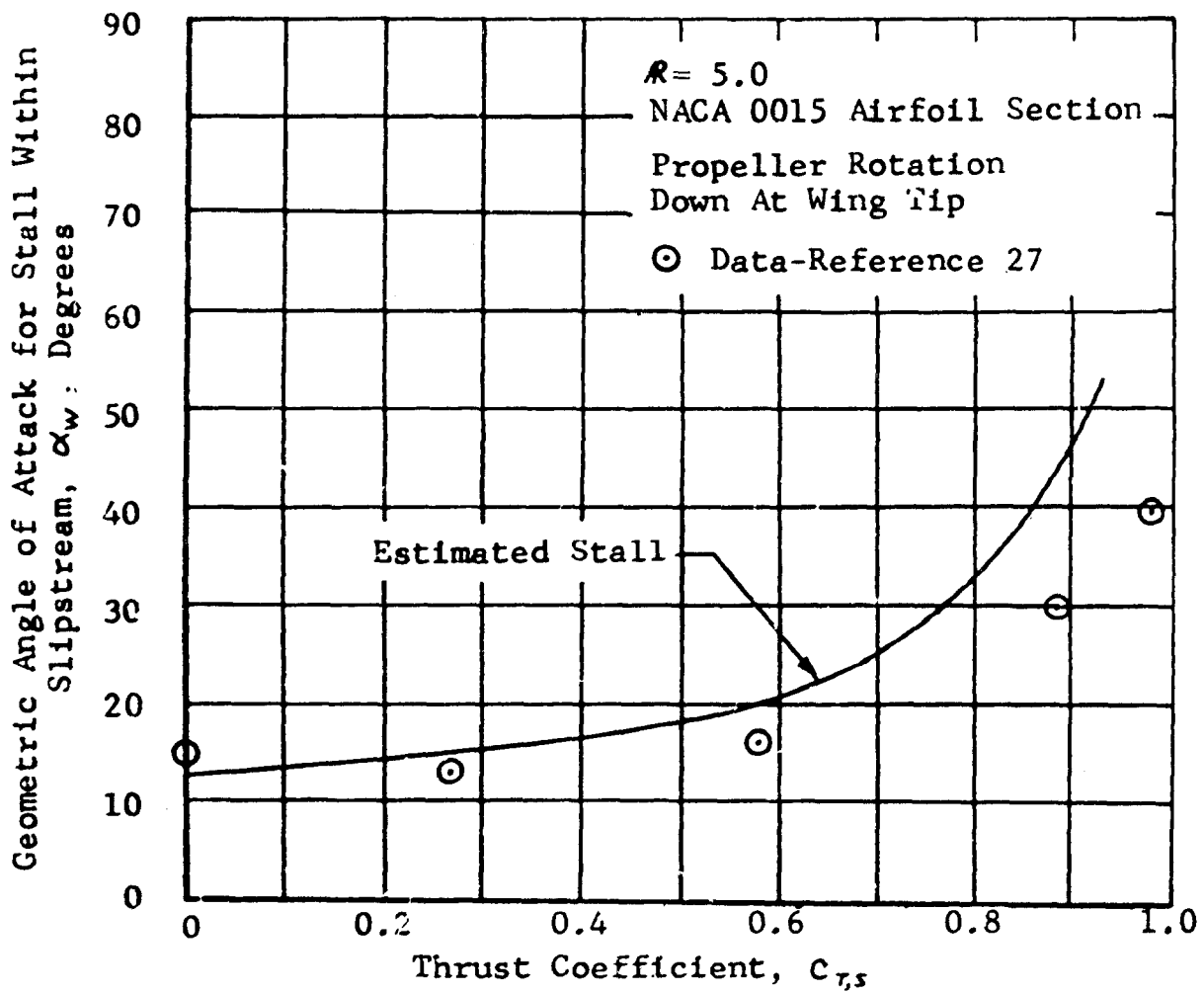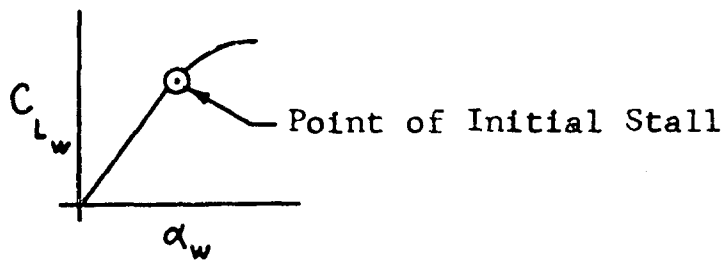
FIGURE 6. Correlation of Estimated Wing Stall Within
Slipstream with Test Data.

14

MINIMUM WING SIZE FOR VTOL AIRCRAFT
TRANSITION WITHOUT STALL

The stall analysis of the preceding section is now utilized to determine the minimum wing size for VTOL aircraft transition without stall of the slipstream-immersed portion of the wing. This is accomplished as follows:

1. For an aircraft of a particular gross weight and configuration, a wing size is selected in accordance with the mission requirement of the aircraft, i.e., high-speed flight or stalling-speed considerations. Also, the span should be such that most of the wing is immersed within the propeller slipstreams.

2. Next, the trim values of the thrust coefficient, $C_{T,s}$, and airspeed, V_o, are determined for a number of wing tilt angles between 10 to 90 degrees. This is accomplished by use of the lift and drag equations of Reference 3. First, at a selected wing tilt angle, the total longitudinal force coefficient, $C_{x,s}$, including fuselage and tail drag, is calculated using the following expression (all angles in degrees):

$$C_{x,s} = \frac{\pi N D^2}{4S} C_{T,s} \cos\alpha_p - 0.000338 \frac{ND^2}{S}\left(\frac{r_s}{D}\right)^2 (1-\mu^2)^2 \alpha_s^2 \cos(\alpha_p - \phi)$$

$$- 0.0653 \frac{ND^2}{S}\left(\frac{r_s}{D}\right)^2 (1-\mu^2) \alpha_s \sin(\alpha_p - \phi)$$

$$- \frac{2NDc_s}{S}\left(\frac{r_s}{D}\right) C_{Do,s} \cos(\alpha_p - \phi) - \frac{C_{Lw}^2}{\pi \mathcal{R}} \frac{q_o}{q_s}$$

$$- \left[1 - \frac{2NDc_s}{S}\left(\frac{r_s}{D}\right)\right] C_{Do} \frac{q_o}{q_s} - (C_{Do_f} + C_{Do_t}) \frac{q_o}{q_s} \qquad (7)$$

15

where

$$\frac{q_o}{q_s} = 1 - C_{T,s}$$

Calculations are made for several values of $C_{T,s}$ for each value of α_w. Curves of $C_{x,s}$ versus $C_{T,s}$ are plotted as shown in the following sketch:
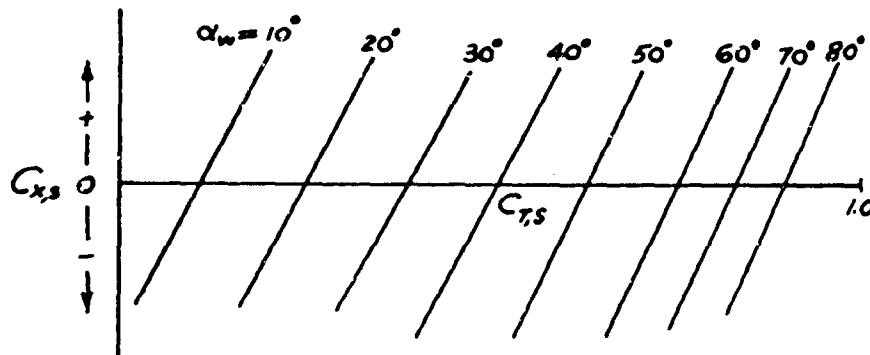
The values of $C_{T,s}$ at $C_{x,s} = 0$ are determined for each α_w. These values are then utilized to calculate the lift coefficient, $C_{L,s}$, where

$$C_{L,s} = \frac{\pi N D^2}{4S} C_{T,s} \sin \alpha_p + C_L \frac{q_o}{q_s}$$

$$+ 0.0653 \frac{ND^2}{S}\left(\frac{r_s}{D}\right)^2 (1-\mu^2)\, \alpha_s \cos(\alpha_p - \phi)$$

$$- 0.000338 \frac{ND^2}{S}\left(\frac{r_s}{D}\right)^2 (1-\mu^2)^2 \alpha_s^2 \sin(\alpha_p - \phi)$$

$$- \frac{2NDc_s}{S}\left(\frac{r_s}{D}\right) C_{D_{q,s}} \sin(\alpha_p - \phi) \tag{8}$$

16

Next, the airspeed is calculated as follows:

$$V_o = \sqrt{\frac{2}{\rho} q_o}$$

$$= \sqrt{\frac{2W(1 - C_{T,s})}{\rho S C_{L,s}}} \tag{9}$$

3. The spanwise lift coefficient distribution of the slipstream-immersed portion of the wing is calculated for each trim condition using Equation (4). The resulting peak values of $C_{\ell,s}$ are plotted versus α_w .

4. The local $C_{\ell max}$ corresponding to the peak value of $C_{\ell,s}$ in step 3 above is determined as discussed in the preceding section. These values are plotted on the same graph as the $C_{\ell,s}$ values in step 3 above.

5. If the maximum value of $C_{\ell,s}$ is nearly equal to but not greater than the corresponding value of $C_{\ell max}$, the wing size selected above corresponds to the minimum size for stall-free transition.

6. If the above is not the case, the calculation procedure is repeated for another wing size, and so on, until the condition of step 5 is satisfied.

To illustrate the above procedure sample calculations were performed and the results of these calculations are now discussed.

The basic aircraft analyzed corresponds to the Vertol V-76. The characteristics of this vehicle are summarized in Table I. Calculations were performed for three different wing chords, at constant wing span, corresponding to aspect ratios of 3.0, 5.24, and 7.0. The calculated values of the longitudinal force coefficient, $C_{x,s}$, are presented in Figure 7. The trim values of total lift coefficient, $C_{L,s}$, are presented in Figure 8

17

TABLE I

PHYSICAL CHARACTERISTICS OF THE VERTOL V-76 AIRCRAFT

Rotor:

Diameter, feet 9.5
Blade Chord, inches 13
Blade Twist (linear, root to tip), degrees 19.2
Airfoil Section .... NACA 0009*
Blade Taper Ratio 1
Solidity 0.218
Distance Between Propeller Axes, feet 14.67
Operational Speed, rpm 1416

Wing:

Span (excluding tips), feet 24.88
Chord, feet 4.75
Airfoil Section .... NACA 4415
Taper Ratio 1
Sweep, degrees 0
Dihedral, degrees 0
Pivot, percent chord 37.6
Ailerons
  Chord, feet 1.25
  Span, feet 5
Tilt Range (referenced to upper longeron), degrees .... 9 to 85

*with 0.5-inch cusp
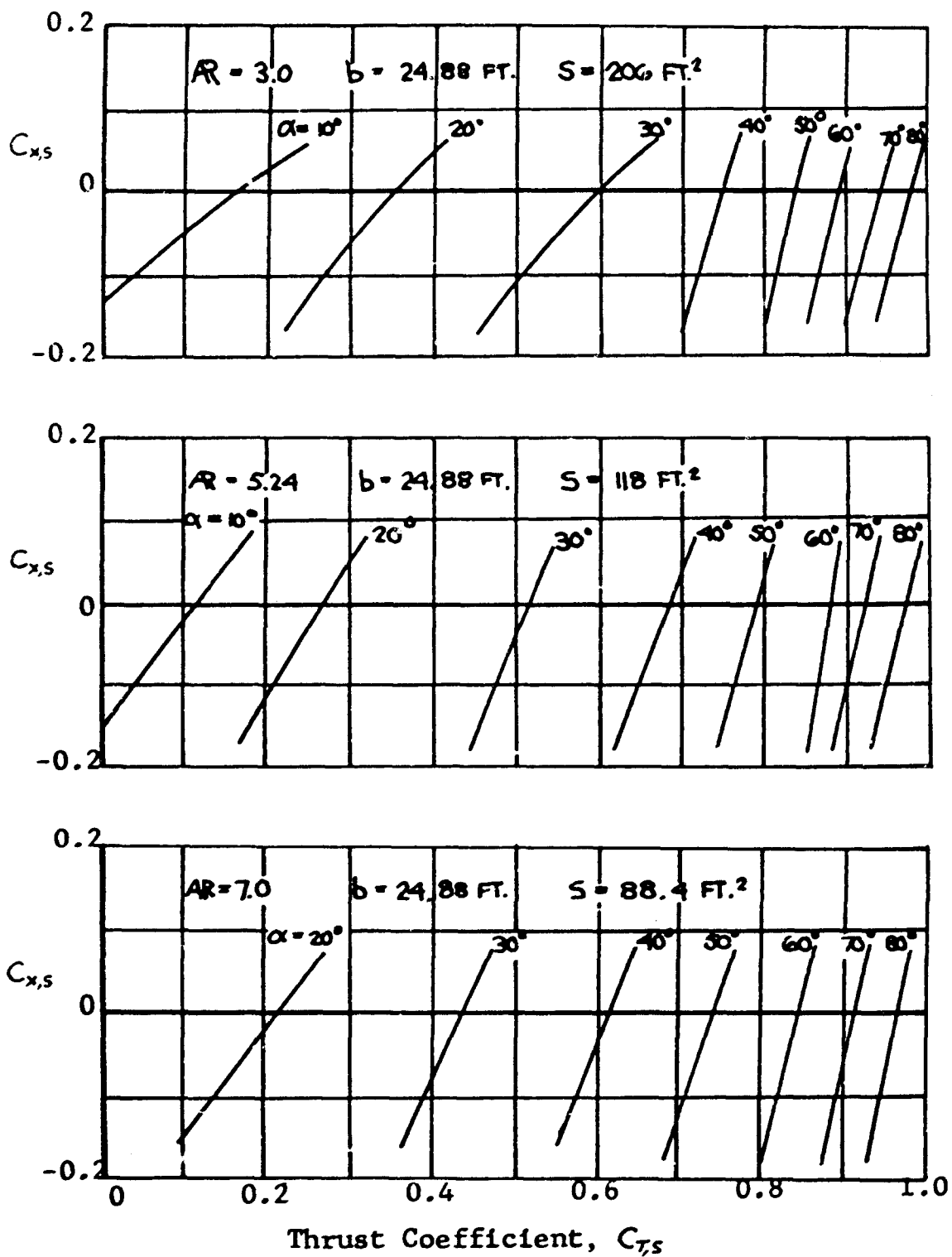
FIGURE 7. Estimated Longitudinal Force Coefficients for a 3500-Pound, Tilt-Wing VTOL Aircraft, Showing Conditions of $C_{x,s} = 0$.

19
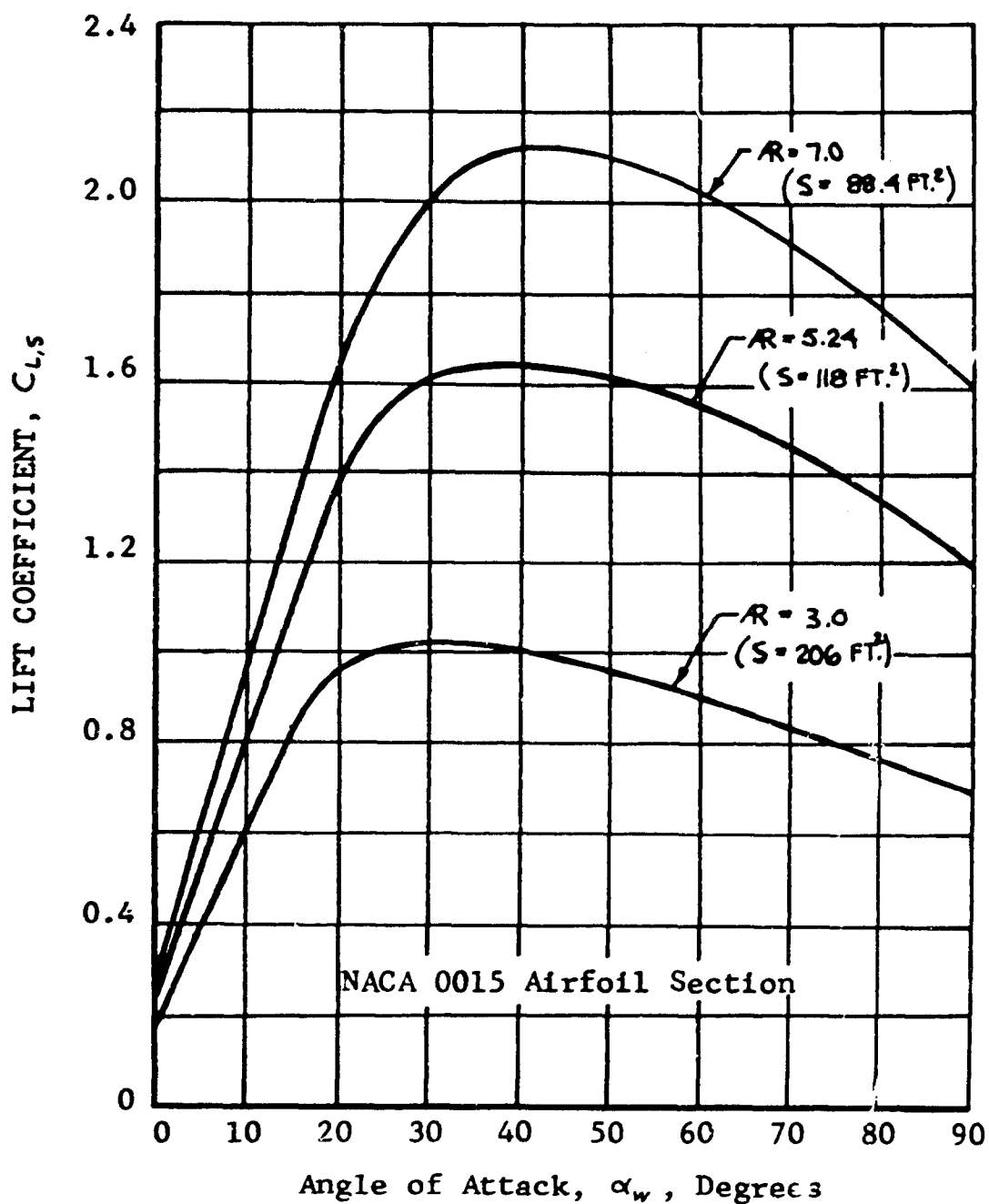
FIGURE 8. Effects of Wing Size on Lift Coefficient During Transition Maneuver of a 3500-Pound, Tilt-Wing VTOL Aircraft.

20

for all three aspect ratios. The corresponding trim speeds are plotted versus wing tilt angle, α_w , in Figure 9. Also shown in this figure are test data obtained from Reference 21. Good agreement is evident between the theory and test data.

The calculated peak values of local lift coefficients are compared with $C_{\ell_{max}}$ values on Figure 10. It is noted that for the basic aircraft, R = 5.24, the wing is stalled for the range of wing tilt angles between 19 and 43 degrees. Also, it is seen that an increase of aspect ratio to 7.0, which corresponds to a decrease of wing area, results in wing stall over an increased range of wing tilt angle. On the other hand, a wing size corresponding to an R = 3.0 results in stall-free transition.

The aspect ratio for minimum wing size for stall-free transition, as approximated by interpolation of the data presented in Figure 10, is equal to 4.5. This corresponds to a wing area of 138 square feet.

The stall boundary is plotted as airspeed versus aspect ratio in Figure 11. Also shown are two flight conditions of the V-76 aircraft obtained from Reference 21. The triangular symbol corresponds to a condition of poor handling qualities, and the circular symbol corresponds to a condition of unacceptable flying qualities. As indicated in Reference 21, these conditions of unfavorable flying qualities are related to wing stall.
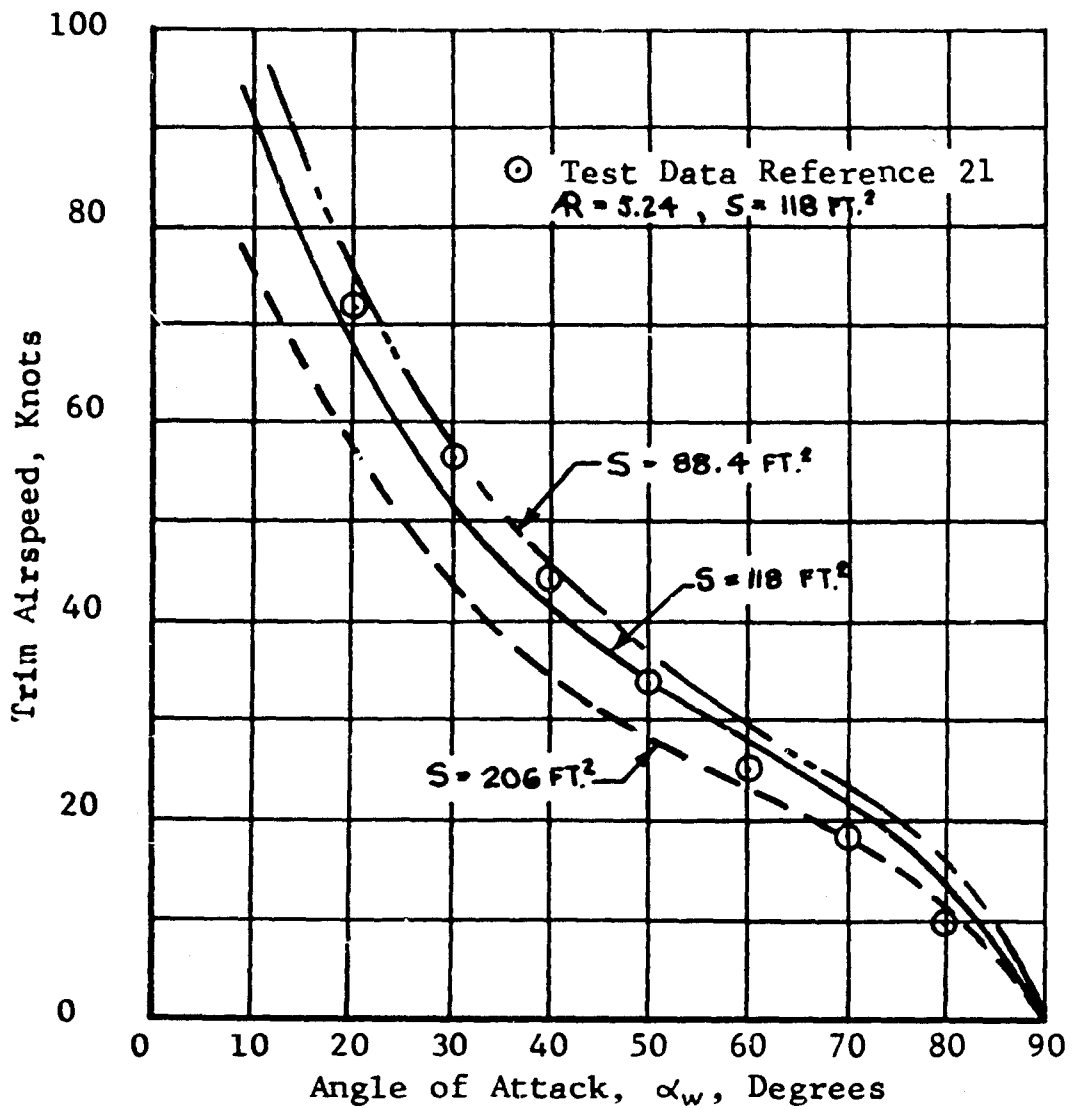
FIGURE 9. Effects of Wing Area on Airspeed Versus Wing Angle of Attack for a 3500-Pound, Tilt-Wing VTOL Aircraft.
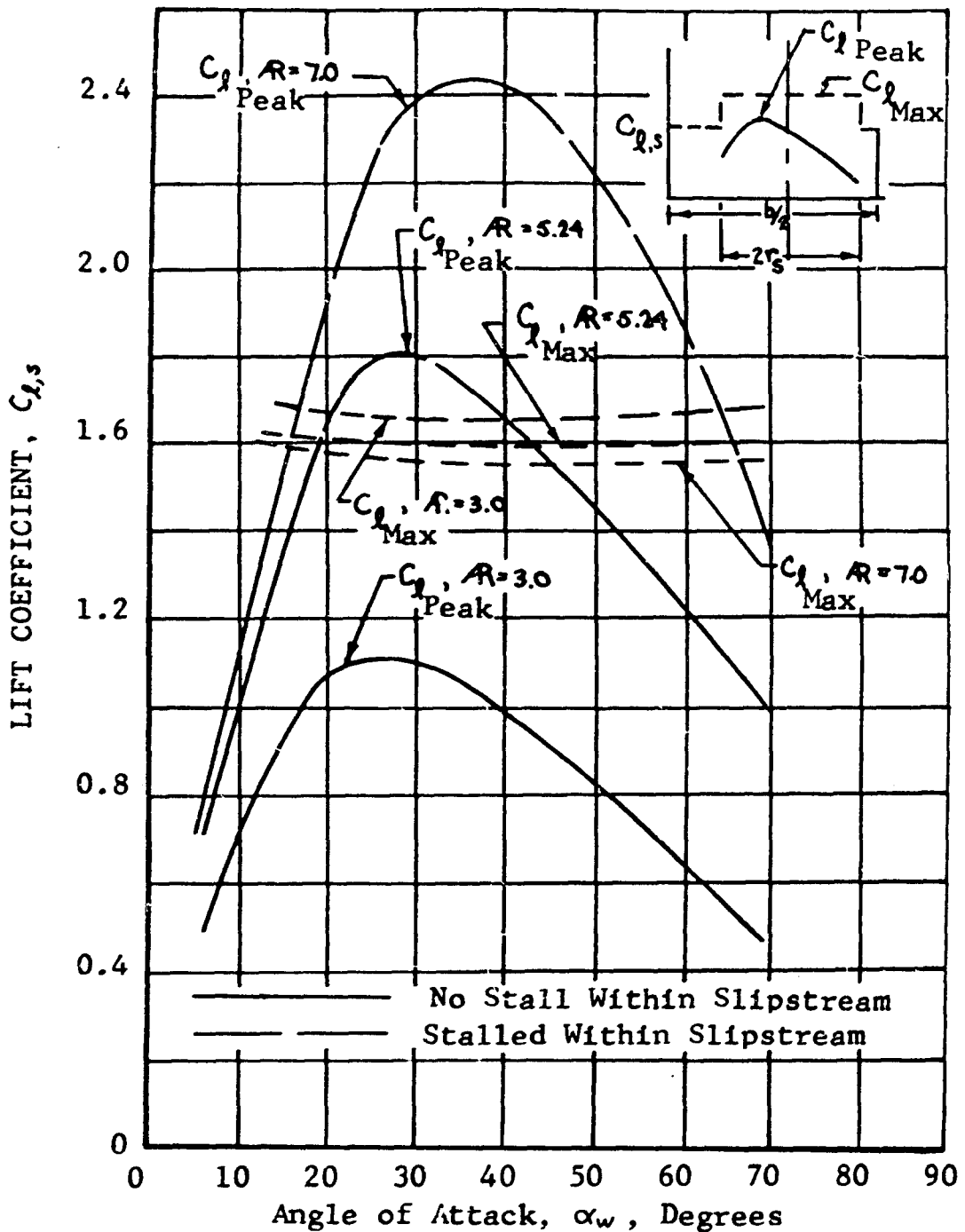
FIGURE 10. Effects of Aspect Ratio (Wing Size) on Peak Local
Lift Coefficient and Stall within the Slipstream for a 3500-
Pound, Tilt-Wing VTOL Aircraft.

V-76 Flight Test Handling Qualities
(Reference 21)

⊙   Unacceptable - Dangerous (Wing Dropping)

△   Poor

Minimum Wing Size
For Stall-Free Transition
$S = 138$ Ft.^{2}
$R = 4.5$

Flight Regime Where
Stall in Slipstream
Occurs

AIRSPEED, KNOTS
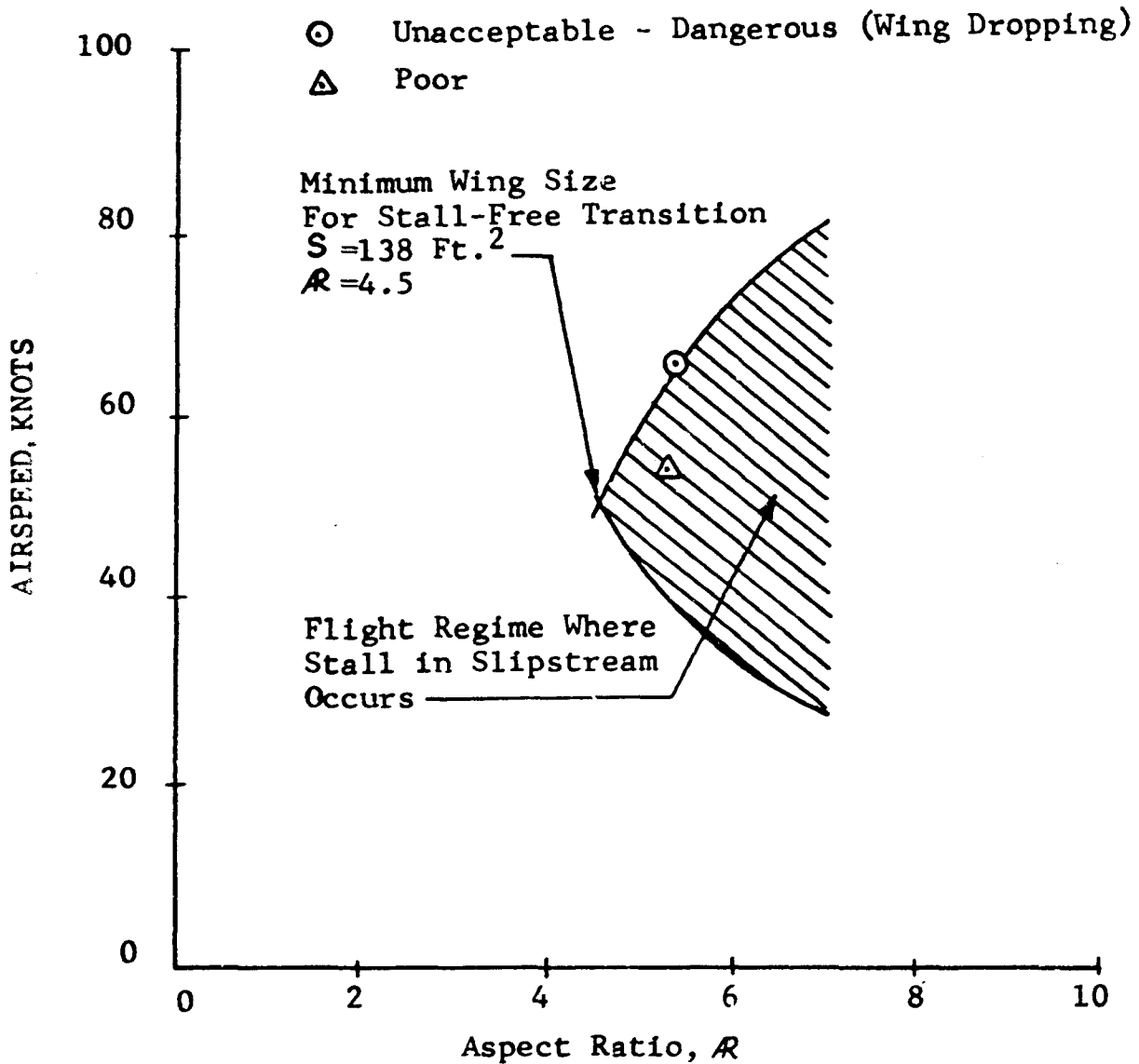
Aspect Ratio, R

FIGURE 11. Estimated VTOL Stall Regime as a Function of Aspect Ratio (Wing Size) for a 3500-Pound, Tilt-Wing VTOL Aircraft (Wing Span 24.88 feet).

PROPELLER AND SLIPSTREAM-INDUCED MOMENTS

The propeller forces and moments and the effects of the slipstream on the VTOL wing pitching moment are discussed in this section. These forces and moments are defined in Figure 12.

PROPELLER SIDE FORCE

The measurements made in Reference 30 indicate that the propeller side force is negligible for the range of flight parameters occurring throughout tilt-wing aircraft transition.

PROPELLER NORMAL FORCE

A summary of propeller normal force data is shown in Figure 13. This figure serves to indicate trends of magnitude of C_{NP} for conditions of α_p and J' corresponding to the entire range of the transition maneuver. It should be noted that all C_{NP} data have been converted to correspond to the definition of C_{NP} used in this report.

In general, at constant α_p, C_{NP} increases with J'. The figure also indicates that throughout the transition the magnitude of C_{NF} varies between 0 and 0.01. The figure shows isolated propeller data (plain symbols) as well as data for propellers mounted on wings (solid symbols). The scatter of the data is due to the effect of propeller configuration. Information on these configurations is presented in Table II. All data on Figure 13 were obtained for a blade pitch angle, $\beta_{0.75}$, equal to 8 degrees.

A specific propeller configuration (3a of Table II) is examined in more detail in Figure 14. The transition regime is bracketed by arrows. It is seen that C_{NP} increases with J' at constant α_p. Also the derivative $\partial C_{NP}/\partial \alpha_p$ is positive for all values of α_p. Finally, as expected, C_{NP} increases with $\beta_{0.75}$ at constant J' and α_p.
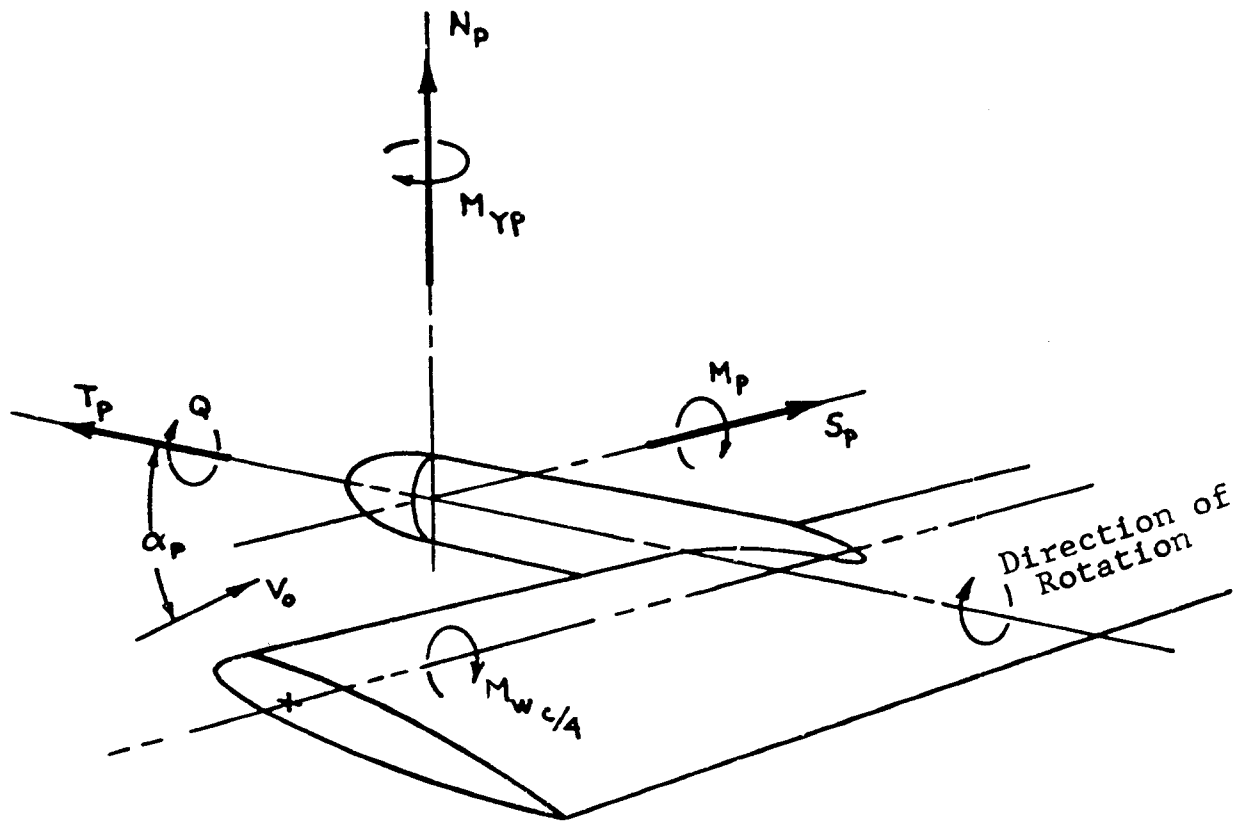
FIGURE 12. Propeller-Wing Force and Moment Notation.
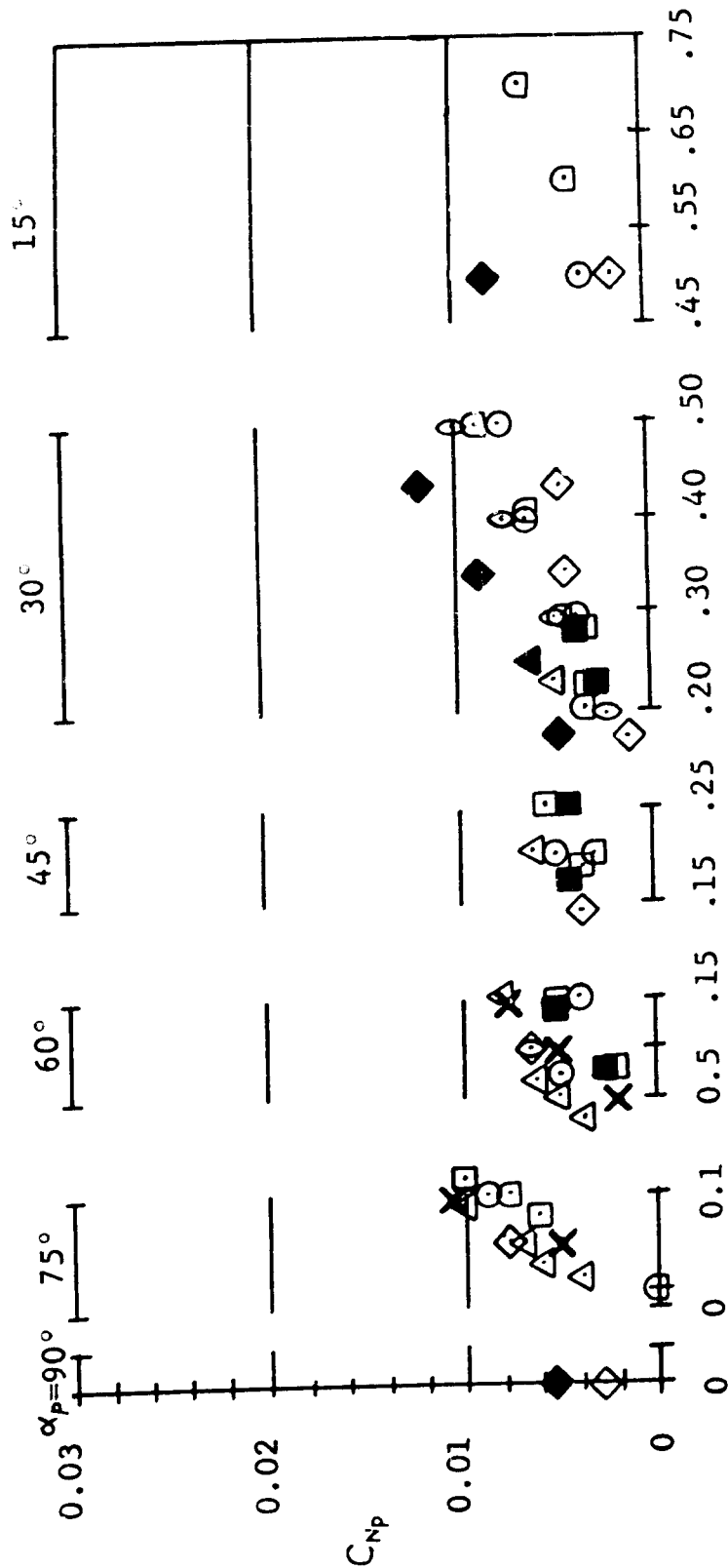
FIGURE 13. Summary of Propeller Normal Force Coefficient Data.

TABLE II

FORCE DATA AVAILABILITY

PROPELLER GEOMETRIC CHARACTERISTICS

Prop. No.	Ref.	Diam. Feet	No. Blades	Airfoil Section	Activity Factor	$\beta_{0.75}$	Remarks
1	14	2.00	3	Clark Y	-	8°	Forces measured with and without wing behind the propeller
2	15	2.00	3	-	-	8° & 16°	Forces measured with and without wing behind the propeller
3a	30	12.00	3	NACA 16 Ser.	150	Variable	Conventional propeller
3b	30	10.00	3	NACA 64 Ser.	188	Variable	Fiber glass VTOL propeller
3c	30	9.50	3	NACA 0009	178	Variable	Propeller similar to that used on Vertol V-76 tilt wing aircraft, flapping with 3" hinge offset
4	16	9.67	3	NACA 00C	178	Variable	Propeller used on Vertol VZ2 tilt wing VTOL flapping blades, 3" hinge offset
5a	29	9.50	3	NACA 0009	178	Variable	Same propeller as Ref.30 above, tests for descending flight
5b	29	12.00	3	NACA 16 Ser.	150	Variable	Same propeller as Ref.30 above, tests for descending flight
6	20	1.21	3	Circular Arc	100	12°	
7	19	21	3	-	-	Variable	Model propeller similar to an XC-142 VTOL propeller

28
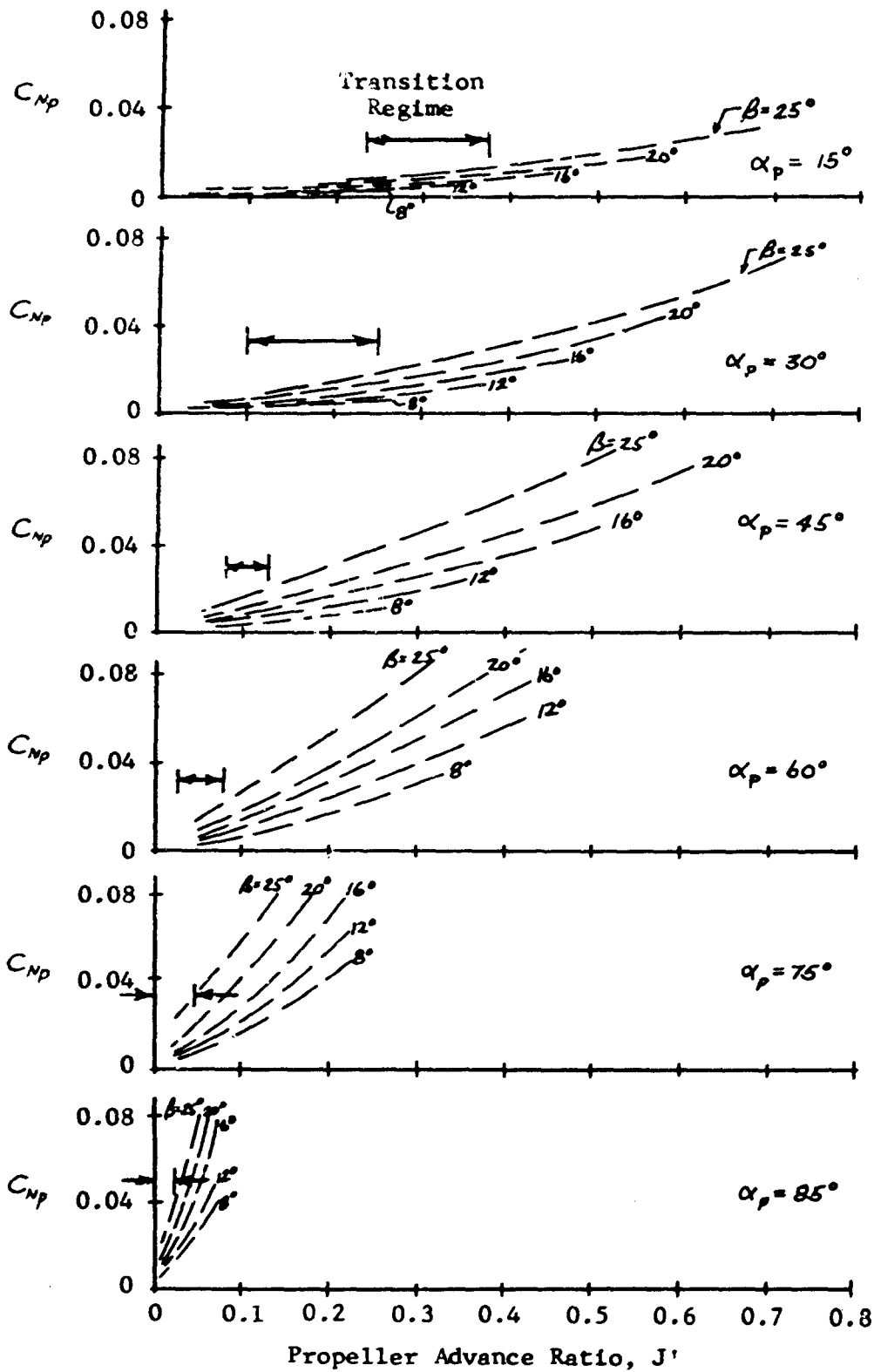
FIGURE 14. Effect of Propeller Blade Pitch, β, on Propeller Normal Force Coefficient, C_{Np}.

The effect of the wing on C_{N_p} is presented in Figure 15 for flap angles of 0 and 50 degrees, respectively. It is noted that in all cases the presence of the wing causes an increased value of C_{N_p} .

Correlation between several published theories and experimental data of C_{N_p} is presented in Figure 16. It is noted that the theory of Reference 6, which actually was derived for helicopter rotor drag force, results in very poor correlation. Better agreement is obtained by use of the theories presented in References 7 and 23.

PROPELLER PITCHING MOMENT

A summary of propeller pitching moment data is presented in Figure 17. It is seen that, as in the case of normal force, the magnitude of C_{M_p} varies between 0 and 0.01 throughout the transition range. The figure also shows isolated propeller data (plain symbols) and data for propellers mounted on wings. The effect of propeller configuration on the magnitude of C_{M_p} is apparent from the scatter of the data. Again these data are for a blade pitch of 8 degrees.

Pitching moment coefficient data for propeller 3a of Table II are plotted separately on Figure 18. The range of J' typical of the transition maneuver at each α_p is bracketed by the arrows. From these curves it is apparent that C_{M_p} increases with J' at constant α_p . At angles of attack below 45 degrees, $\partial C_{M_p}/\partial \alpha_p$ is approximately 0; however, for α_p from 45 degrees to 85 degrees, $\partial C_{M_p}/\partial \alpha_p$ becomes increasingly positive. Also at angles of attack below 45 degrees the effect of $\beta_{0.75}$ on C_{M_p} is small. At $\alpha_p = 45$, 60 and 75 degrees, the effect of $\beta_{0.75}$ is significant but C_{M_p} is nonlinear.

The effect of a wing on C_{M_p} is illustrated in Figure 19. It is noted that the presence of the wing results in a substantial increase of C_{M_p} . This increase, in part, is believed to be due to a wing-induced change in axial velocity distribution through the propeller. No applicable analytical methods have been found in the reviewed technical literature pertaining to prediction of propeller pitching moment.

30

Angle of Attack, α_p, Degrees

Angle of Attack, α_p, Degrees
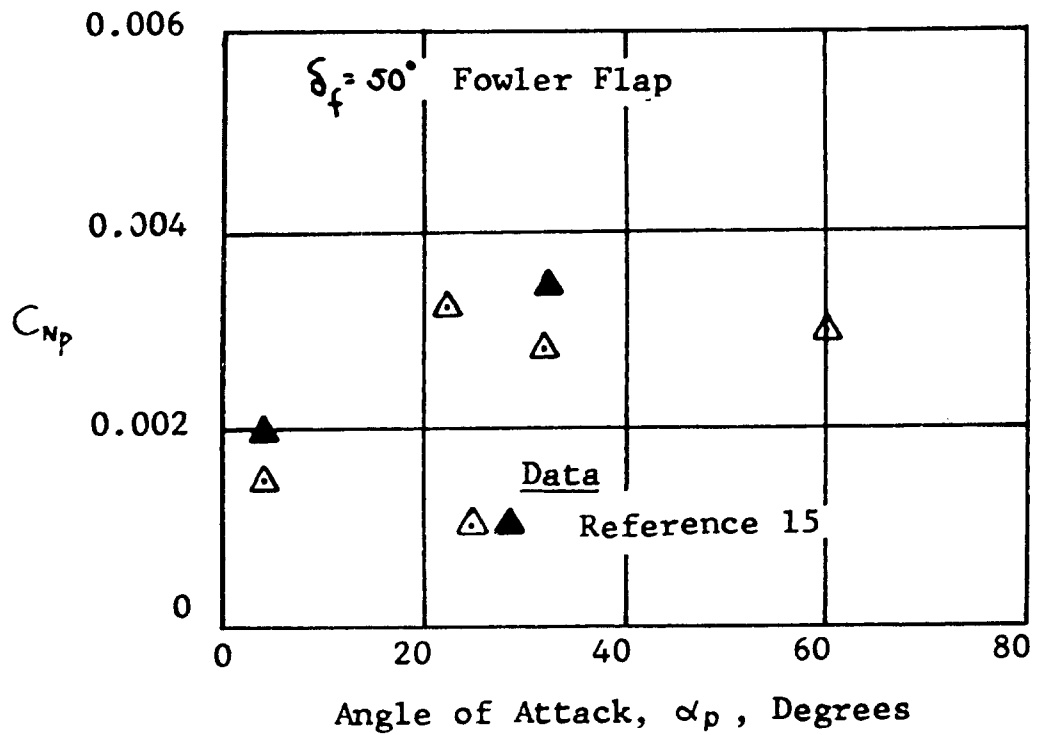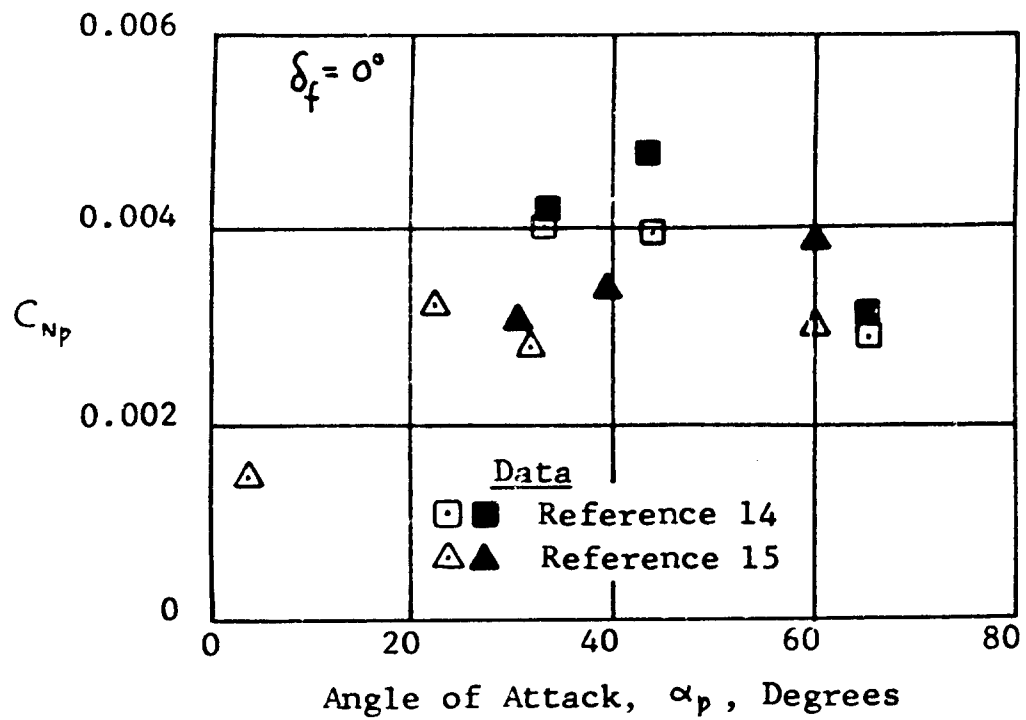
FIGURE 15. Effect of Wing on Propeller Normal Force Coefficient.

31
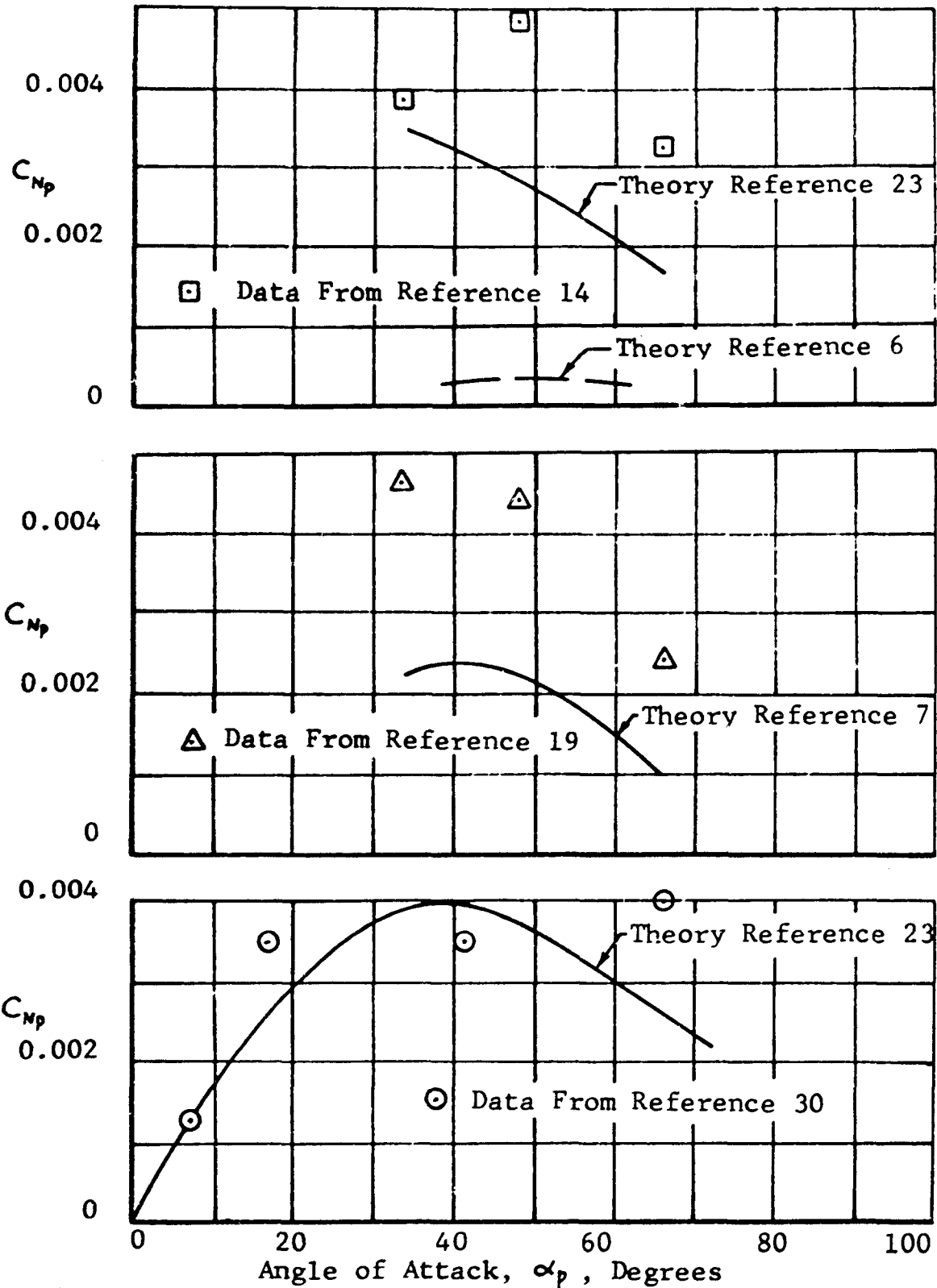
FIGURE 16. Correlation Between Propeller Normal Force Theory and Test Data.
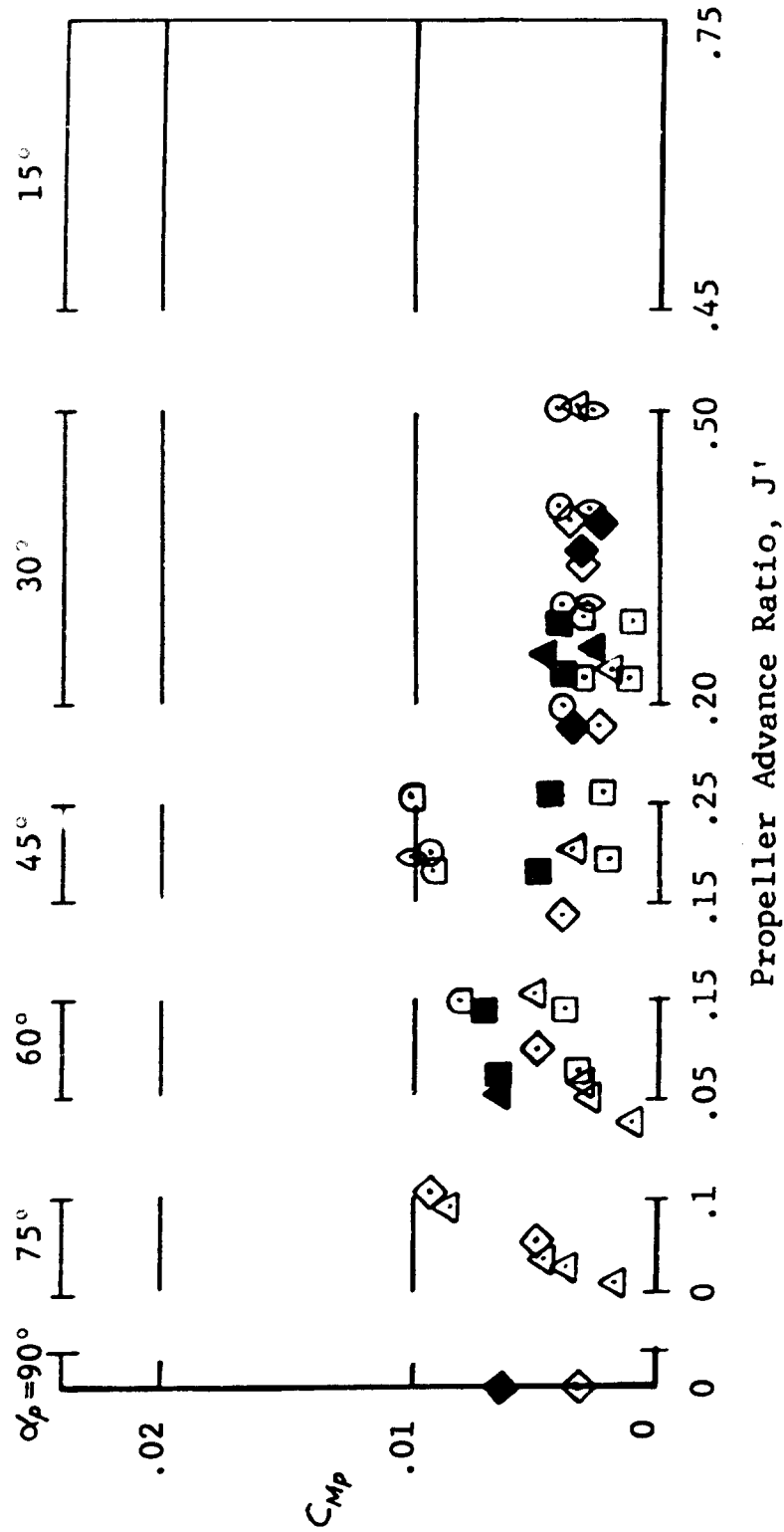
FIGURE 17. Summary of Propeller Pitching Moment Coefficient Data.

33
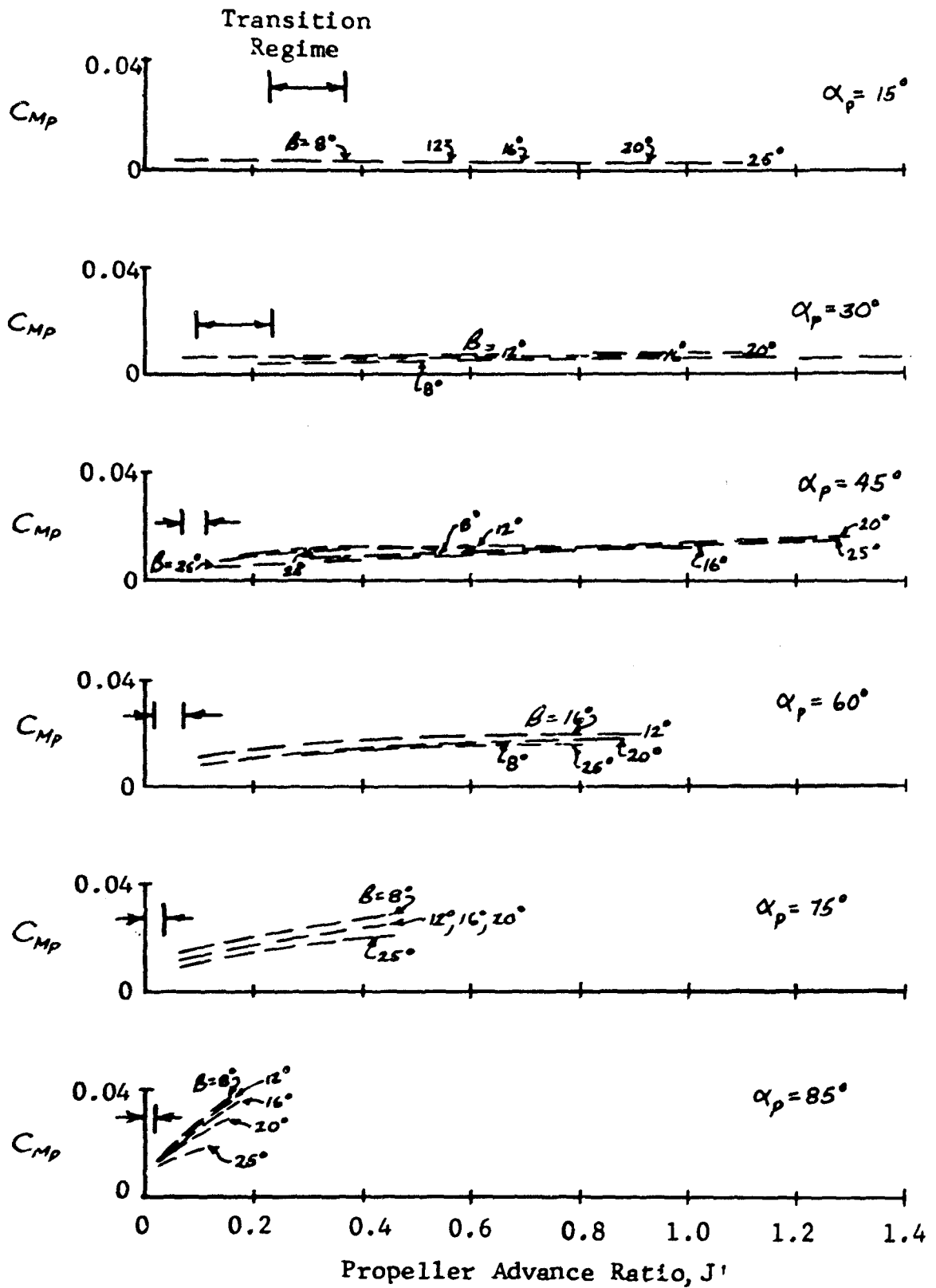
FIGURE 18 Effect of Propeller Blade Pitch, β, on Propeller Pitching Moment Coefficient, C_{Mp} .
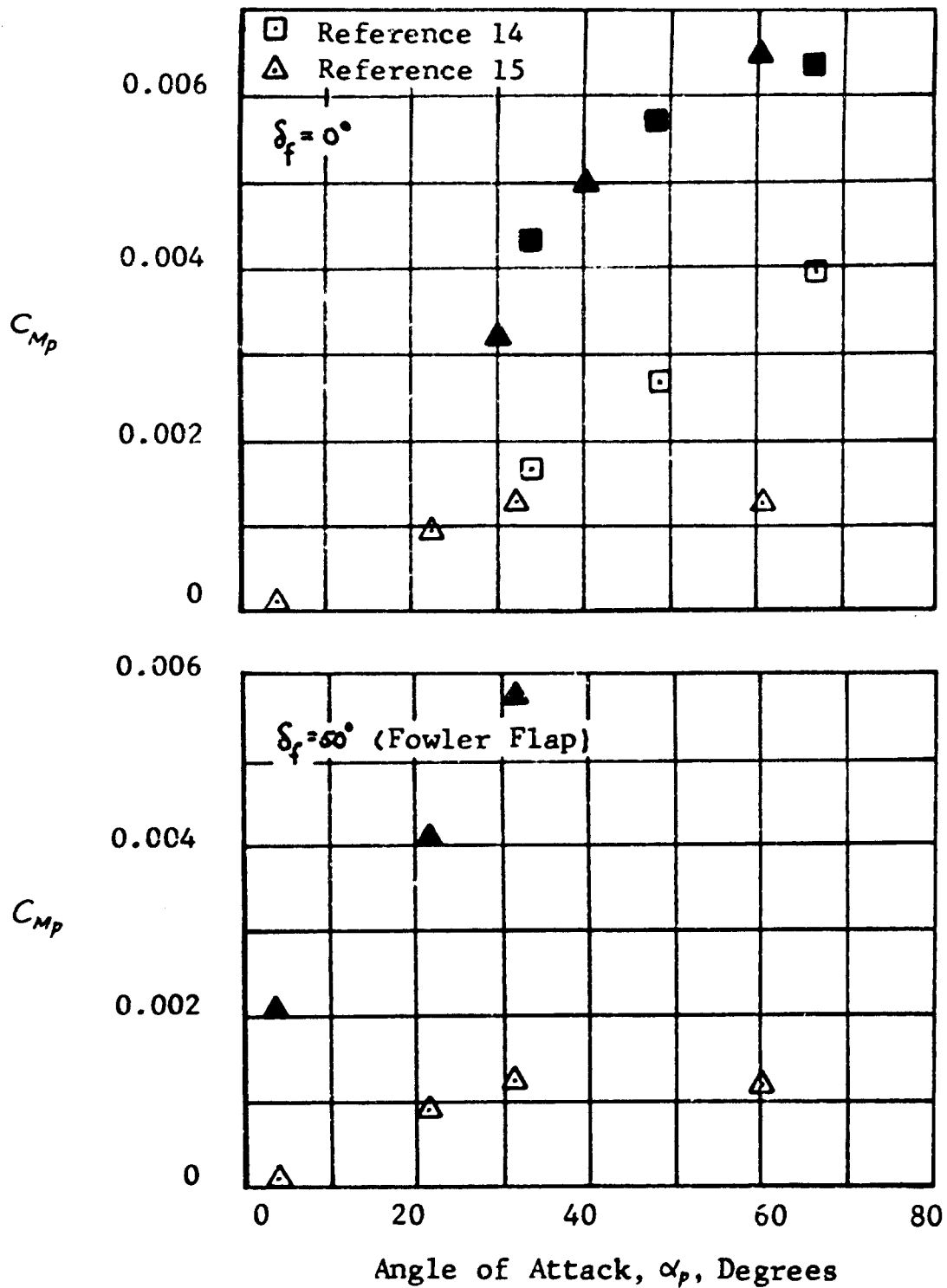
FIGURE 19. Effect of Wing on Propeller Pitching Moment Coefficient.

35

WING PITCHING MOMENT AND CENTER OF PRESSURE

Pitching moment and center of pressure data of several wing-propeller configurations are evaluated in this section. The physical characteristics of these configurations are presented in Table III. The pitching moment coefficient, C_{Mw}, as used herein, is

$$C_{Mw} = \frac{M_{wc/4}}{q_s S c} \qquad (10)$$

where

c = chord, measured from the wing leading edge to the trailing edge of the flap

$M_{wc/4}$ = pitching moment about quarter chord (definition of chord as above).

q_s = slipstream dynamic pressure

S = wing area based on the chord as defined above

The center of pressure location, $x/\bar{c}$, is defined as

$$\frac{x}{\bar{c}} = \frac{1}{\bar{c}} \left[\frac{M_{wc/4}}{(L_w \cos \alpha_w + D_w \sin \alpha_w)} + \frac{\bar{c}}{4} \right] \qquad (11)$$

To utilize the data from References 4 and 5, the propeller contribution to the pitching moment was deducted, where such was included in the test data. Also, the data of Reference 4 were corrected to account for the above mentioned definition of chord.

The resulting data are presented in Figures 20 through 24. The solid symbols correspond to data obtained with windmilling propellers, and the plain symbols refer to propeller-off conditions. These data cover angles of attack

36

TABLE III

MODEL GEOMETRIC CHARACTERISTICS

REF. NO.	WING									PROPELLERS*	
	Area (Basic)	Span	Average Chord (Basic)	(with flap)	Flap Type	Airfoil Section	Aspect Ratio (Basic)	(with flap)	Taper Ratio	Dia.	Dir. of Rot. at Wing Tip
14	10.25	6.83	1.514	-	None	0015	4.55	-	0.714	2.00	Down
12	10.25	6.83	1.514	1.514	Plain	0015	4.55	4.55	0.714	2.00	Down
15	10.96	9.16	1.200	1.680	Fowler	4415	7.66	5.45	1.000	2.00	Down
4	47.24	13.84	3.420	4.780	Fowler	4415	4.05	2.90	1.000	5.67	Up
5	47.24	13.84	3.420	3.420	Slot'd	4415	4.05	4.05	1.000	5.67	Down

*Number of propellers: 4 for References 14, 12 and 15; 2 for References 4 and 5.

37
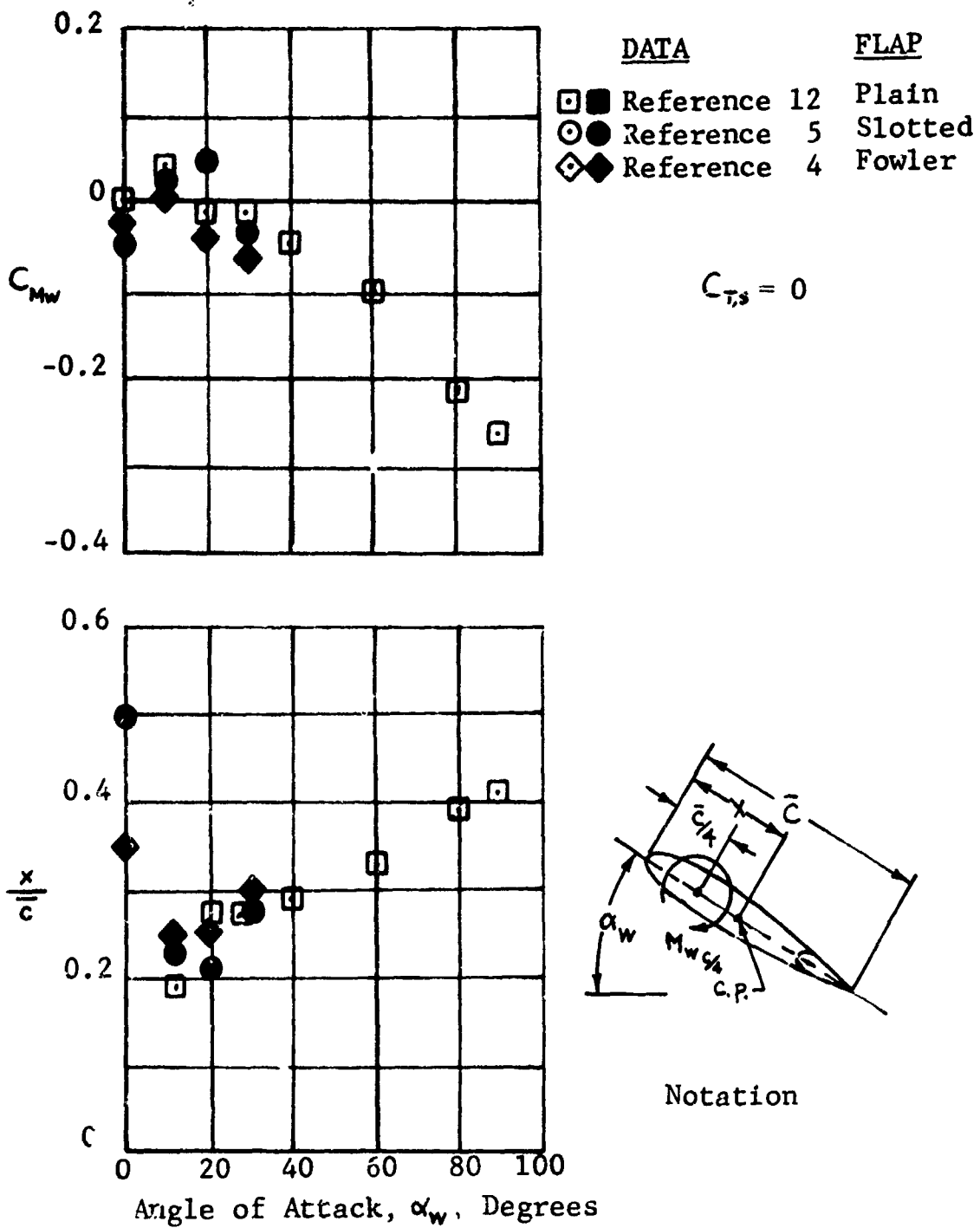
FIGURE 20. Wing Pitching Moment Coefficient and Center of Pressure Location as a Function of Angle of Attack, for $\delta_f = 0$.

	□ ■	Reference 12	Plain
$\delta_f = 20°$	⊙ ●	Reference 4	Slotted
	◇ ◆	Reference 5	Fowler
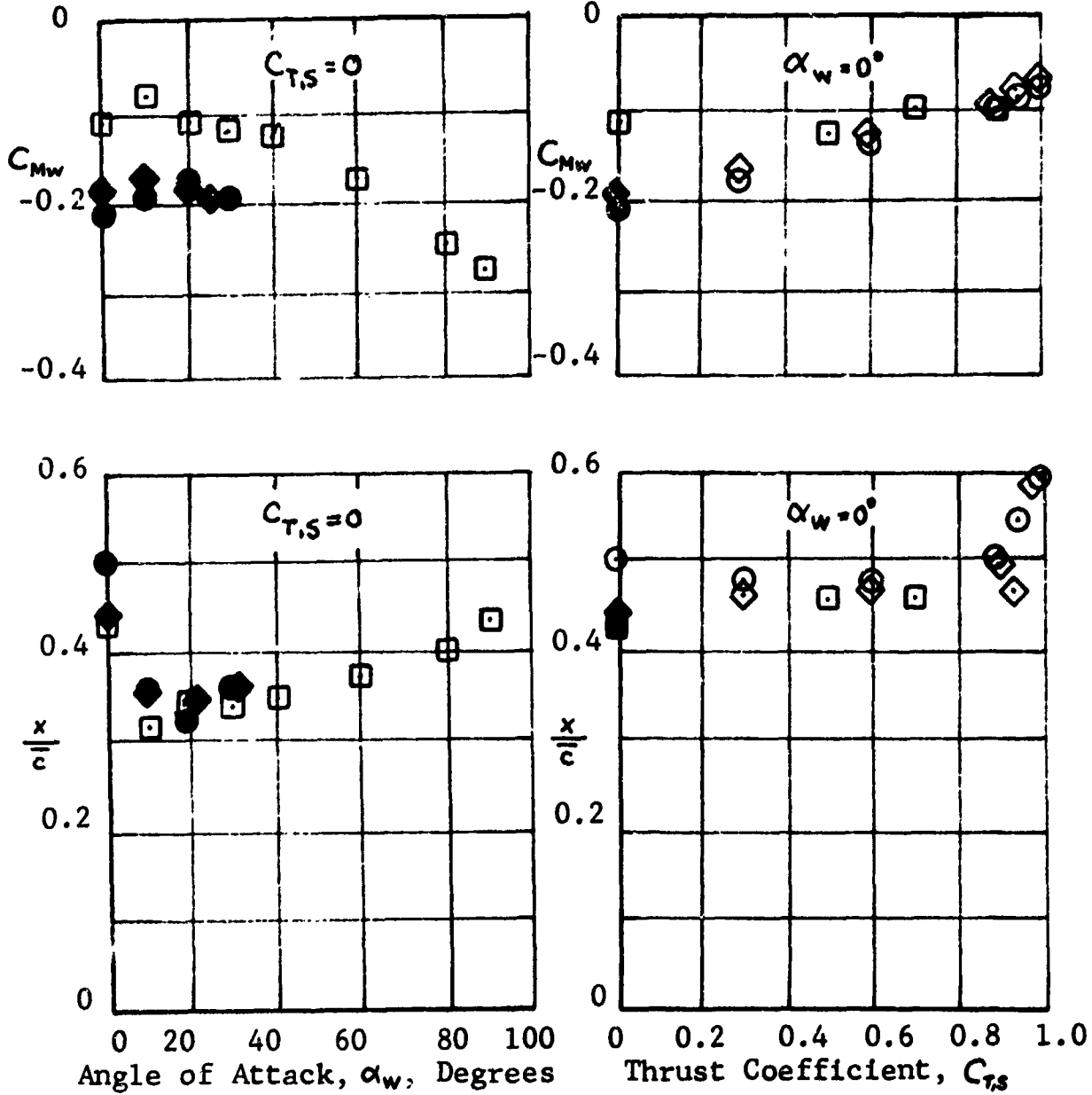
FIGURE 21. Wing Pitching Moment Coefficient and Center of Pressure Location as a Function of Angle of Attack and Thrust Coefficient, for $\delta_f = 20$ Degrees.

39
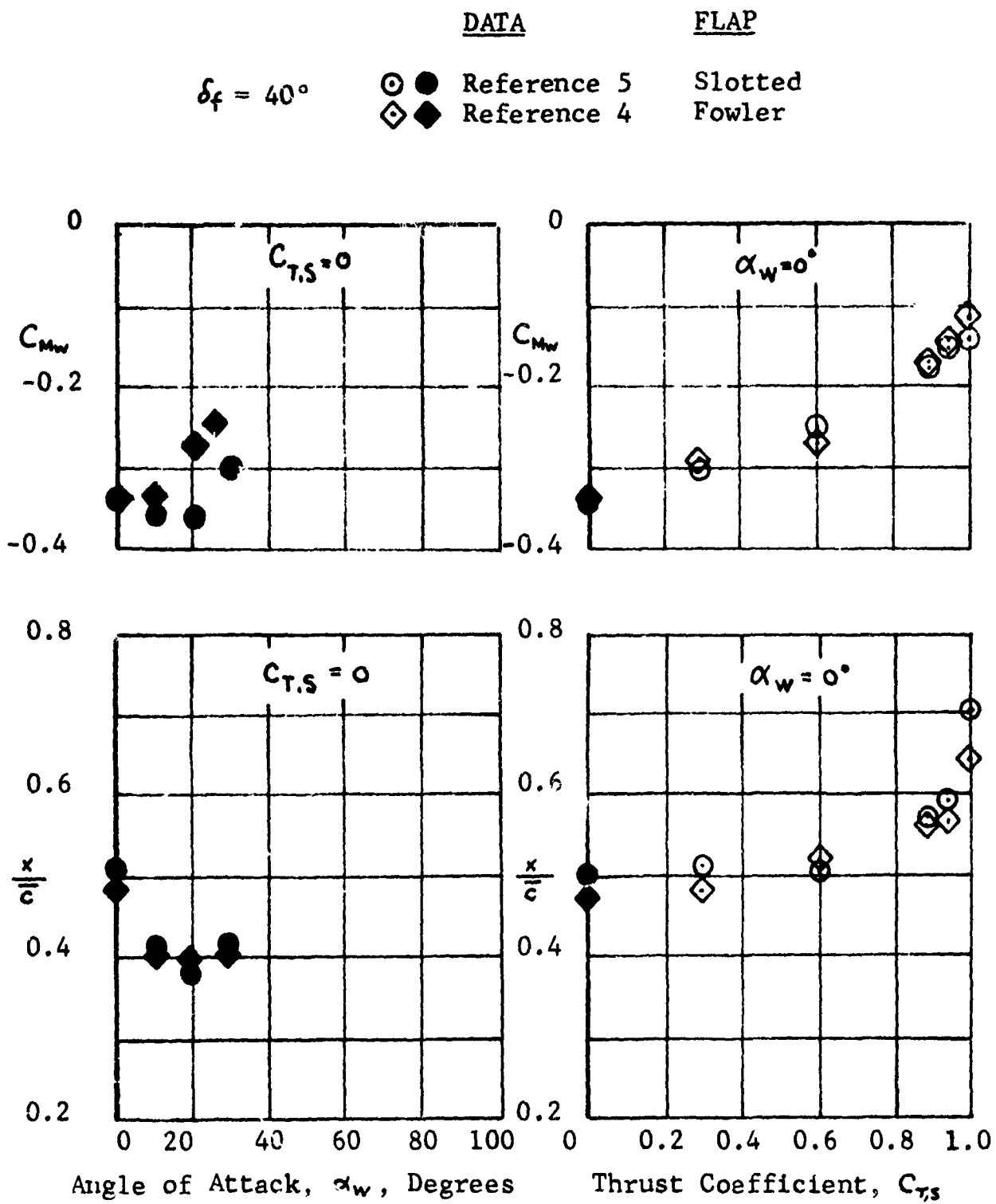
FIGURE 22. Wing Pitching Moment Coefficient and Center of Pressure Location as a Function of Angle of Attack and Thrust Coefficient, for δ_f = 40 Degrees.

40

□ ■   Reference 12   Plain

$\delta_f = 50°$ ⊙ ●   Reference   5   Slotted

◇ ◆   Reference   4   Fowler
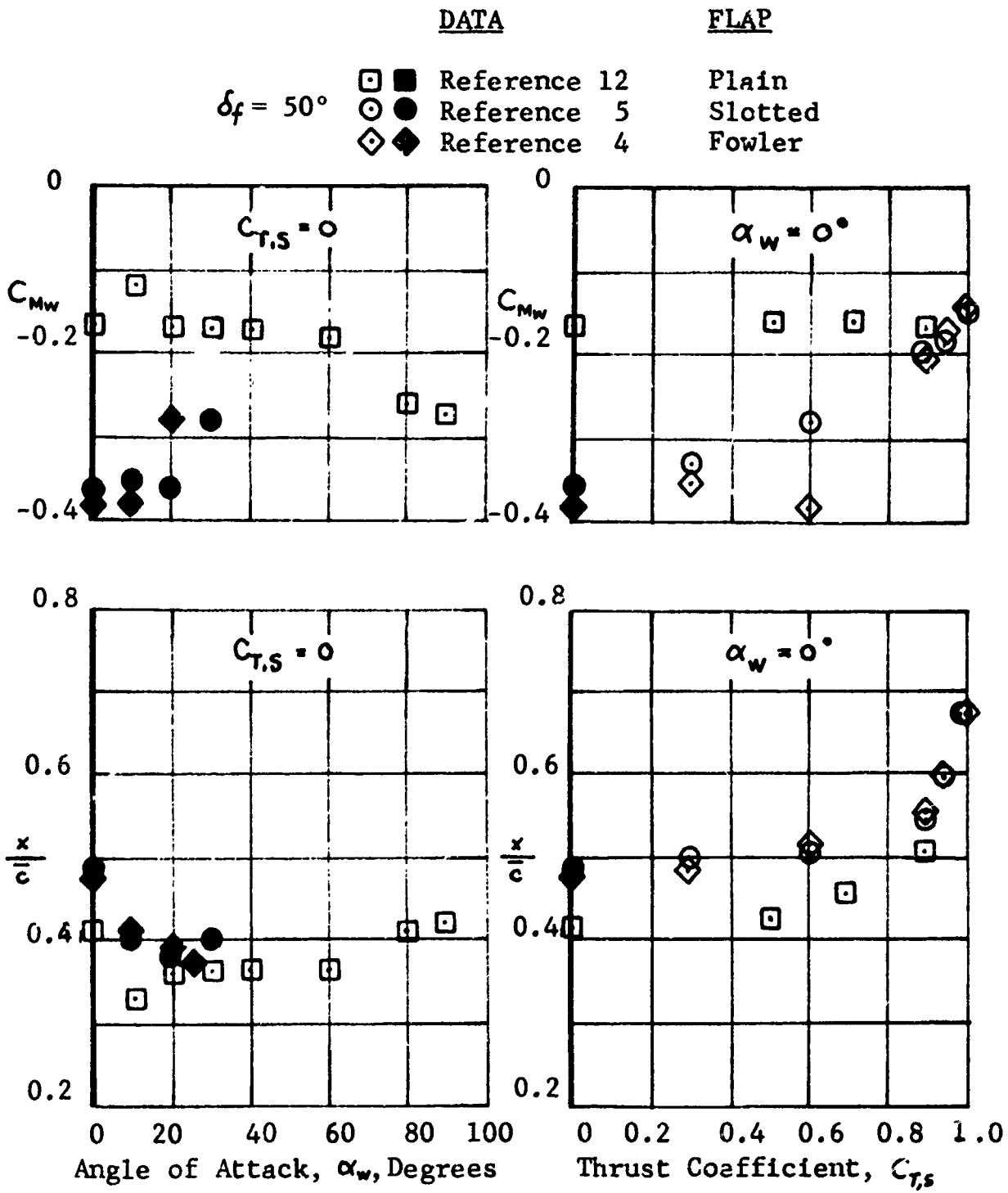
FIGURE 23. Wing Pitching Moment Coefficient and Center of Pressure Location as a Function of Angle of Attack and Thrust Coefficient, for δ_f = 50 Degrees.

41
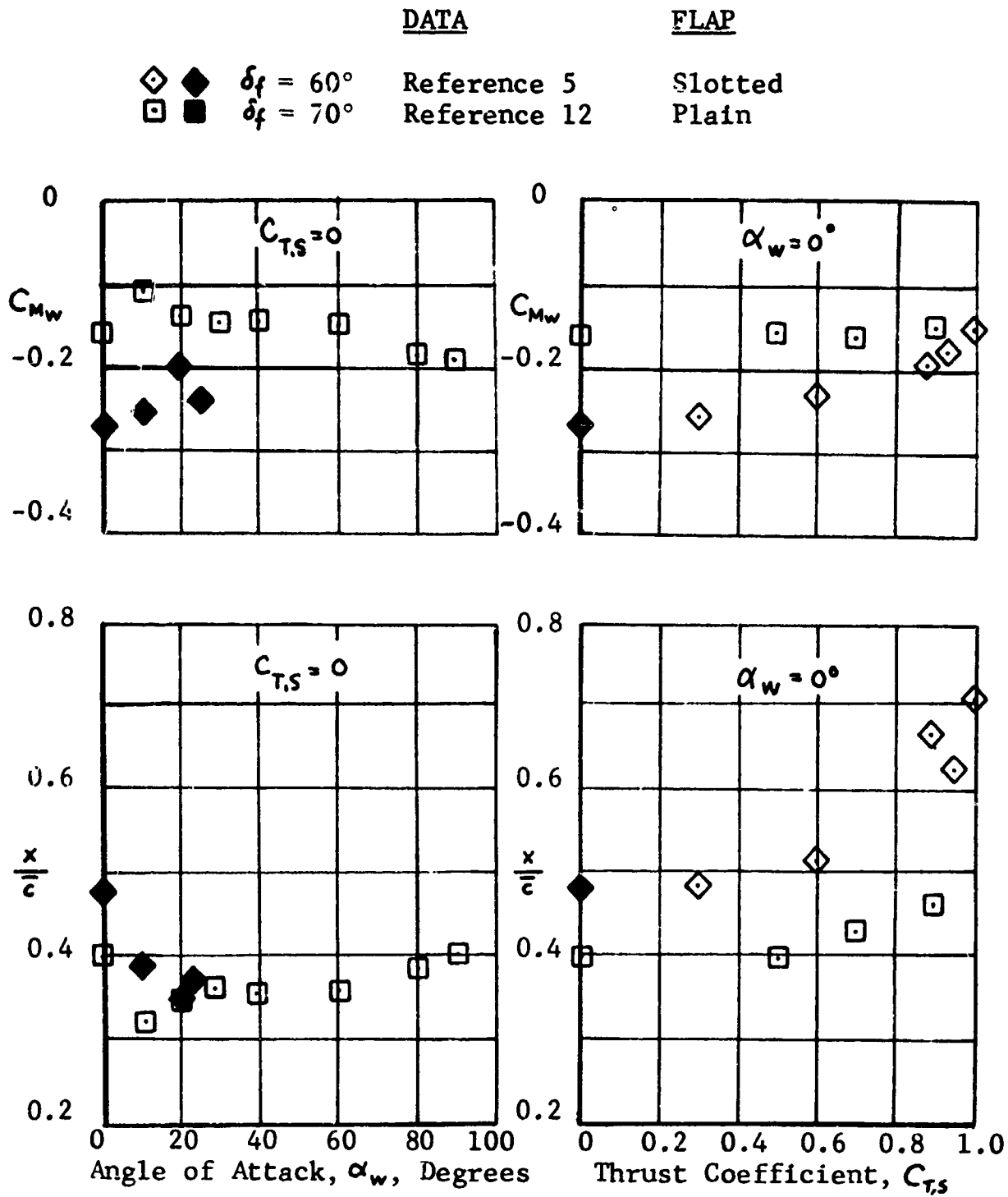
FIGURE 24. Wing Pitching Moment Coefficient and Center of Pressure Location as a Function of Angle of Attack and Thrust Coefficient, for $\delta_f = 60$ and 70 Degrees.

42

from 0 to 90 degrees and flap angles from 0 to 70 degrees. The data are presented versus α_w at $C_{T,s}$ = 0, and versus $C_{T,s}$ at α_w = 0. Data are not presented for simultaneously nonzero values of $C_{T,s}$ and α_w, since no direct measurements of the wing aerodynamic pitching moment were made for these conditions.

From the data presented it can be concluded that the effects of $C_{T,s}$ (which is a function of V_o and V_j) on center of pressure location are small for values of $C_{T,s}$ between 0 and 0.8. However, the data for $C_{T,s}$ = 0 show that the center of pressure location is affected by angle-of-attack changes. This implies that the data for $C_{T,s}$ = 0 are useful for approximating the center of pressure location and wing pitching moments in the $C_{T,s}$ range from 0 to 0.8. At values of $C_{T,s}$ above 0.8, however, there exists a sharp rearward shift in the center of pressure location to about the 70-percent chord point at $C_{T,s}$ = 1.0. Due to the predominant thrust effect at high values of $C_{T,s}$ (corresponding to a low speed and high tilt angle flight condition) the data from the α_w = 0, $C_{T,s} > 0$ curves may be used to approximate the actual center of pressure location and wing pitching moment.

The data also show that for models of the same geometric characteristics (the models of References 4 and 5) the Fowler and the slotted flaps produce equivalent wing pitching moments and center of pressure locations. The use of a plain flap results in lower negative values of C_{MW} than either the Fowler or the slotted flap. The effect of the slipstream (thrust) on the center of pressure location is about the same for all flap types analyzed.

The relative magnitude of the propeller and wing contributions to the total pitching moment is obtained by examining the data of Reference 14, which are reproduced in Figure 25. It is seen that for the specific conditions illustrated, the magnitude of the propeller pitching moment is two to three times that of the wing.
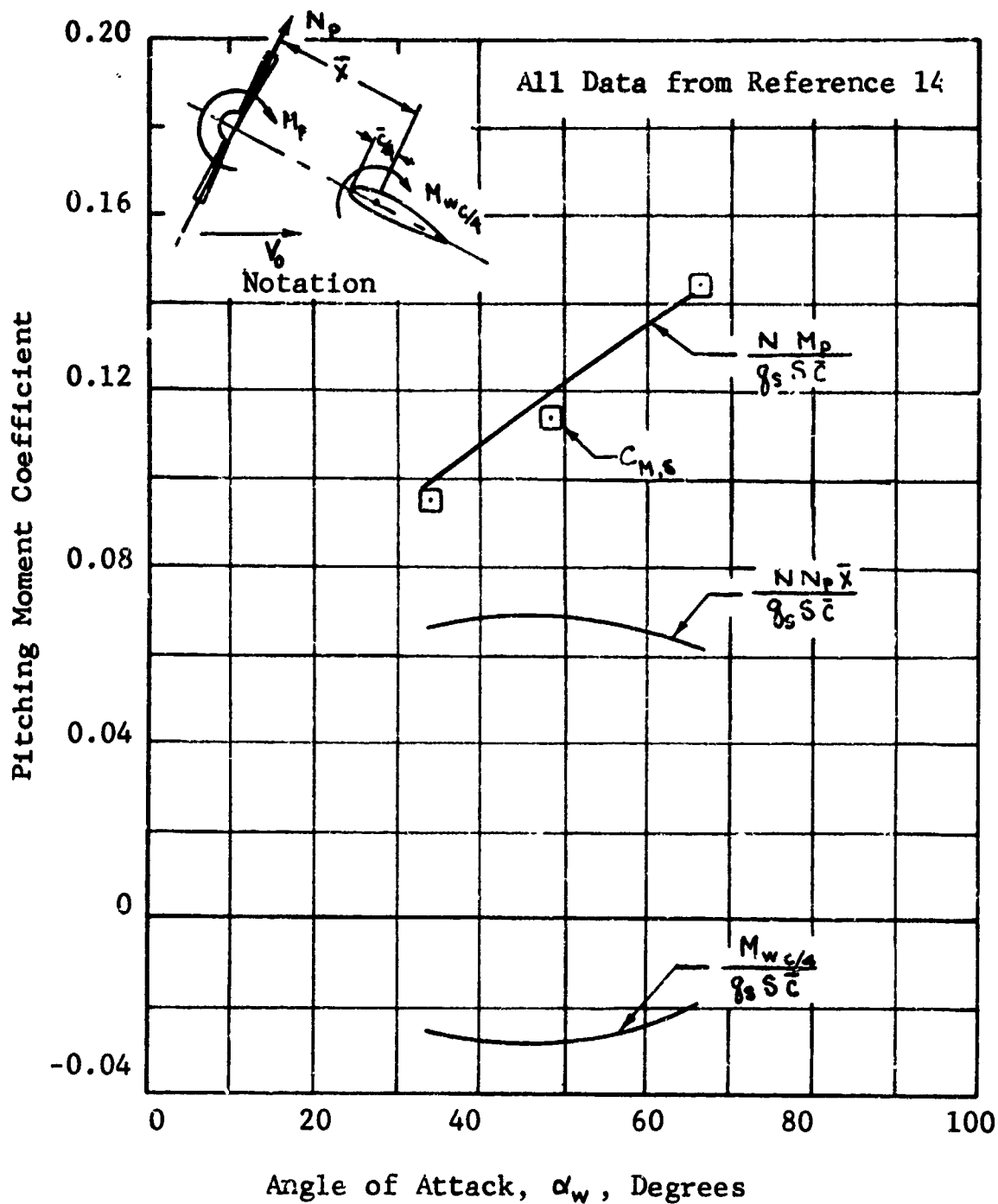
FIGURE 25. Pitching Moment Coefficient Breakdown for a Wing Immersed in Propeller Slipstreams.

44

SLIPSTREAM EFFECT ON THE HORIZONTAL TAIL

Data on the effects of propeller slipstreams on the flow in the vicinity of the horizontal tail of aircraft are presented in References 15, 25, 26 and 27. The data of Reference 25 are found to be the most applicable to the case of tilt-wing VTOL aircraft. These data are reproduced on Figures 26 and 27. Figure 26 presents the downwash angle at the tail, ϵ , as a function of C_{T_S} and α_w for several vertical positions of the tail above the wing quarter-chord line. For C_{T_S} = 0 the downwash angles are zero for locations $z/c > 0$. These angles remain relatively small for values of C_{T_S} up to 0.6. For larger values of C_{T_S} , i.e., where the slipstream effects are very large, the downwash angle, ϵ , increases rapidly with the angle of attack, α_w . As noted in the figure, a downwash angle of 40 degrees occurs for some of these conditions.

The effects of the slipstream on the velocities at the tail, V_t , are presented in Figure 27. It may be noted that in general V_t/V_o is less than unity. This implies that the tail is in a region of reduced dynamic pressure. The data indicate that an increase of slipstream velocity (an increase of C_{T_S}) results in decrease of velocity at the tail.

GROUND PROXIMITY

No general analytical method has been available for the determination of the effect of ground proximity on the aerodynamic characteristics of a wing immersed in a slipstream. However, a number of experimental investigations have been performed on this subject, and the results of these tests are now discussed. As reported in References 21, 22, and 28, buffeting, unsteadiness, and abrupt yaw disturbances were experienced during ground proximity tests of the Vertol V-76 aircraft. Similar results were obtained from model tests as reported in Reference 18. In the latter report, it is indicated that the unsteadiness may be the result of slipstream recirculation through the propeller. In general, the test data show that fuselage design has a pronounced effect on hovering stability in ground effect.
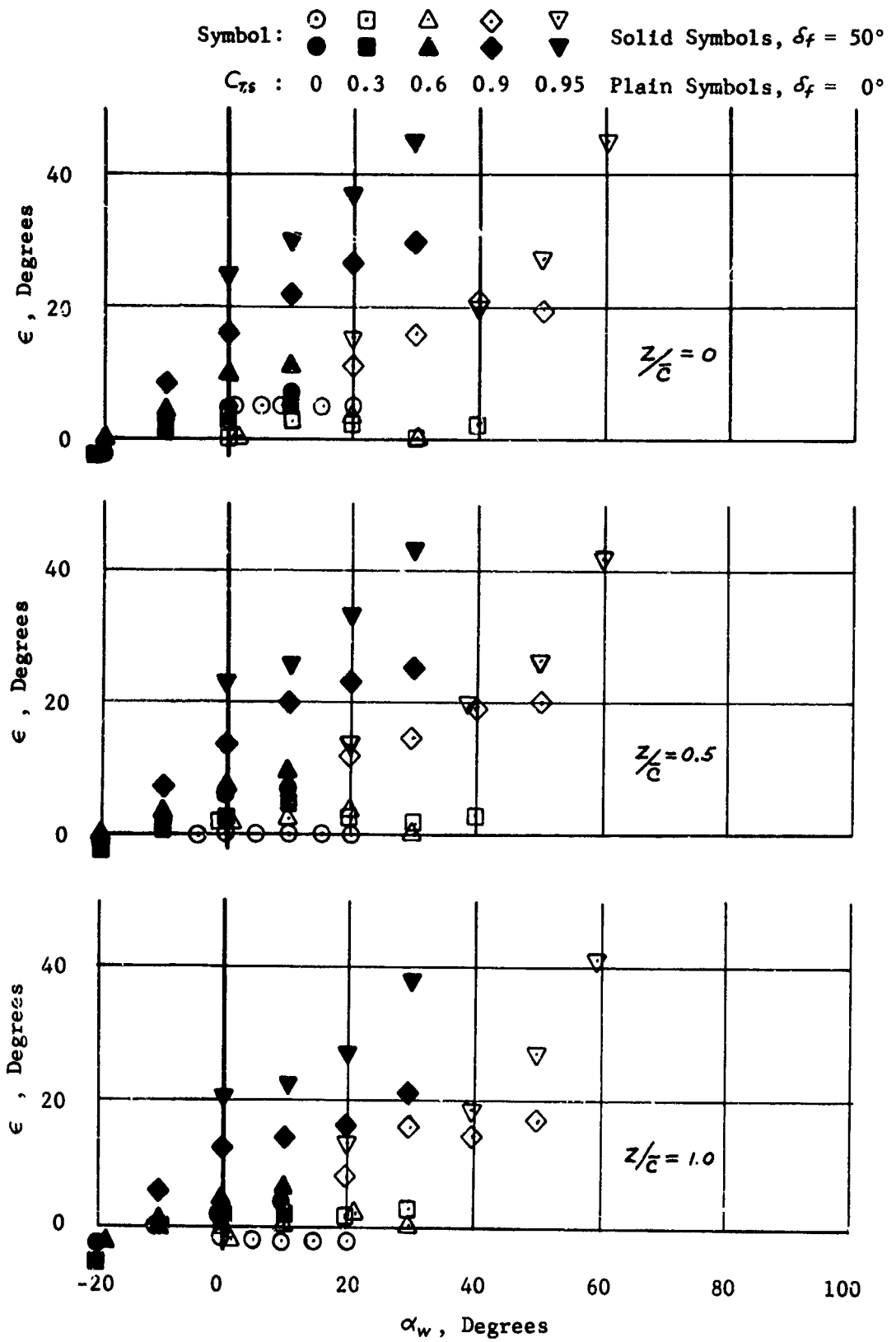
FIGURE 26. Slipstream Effects on Wing Downwash Angle (Data from Reference 15).

46
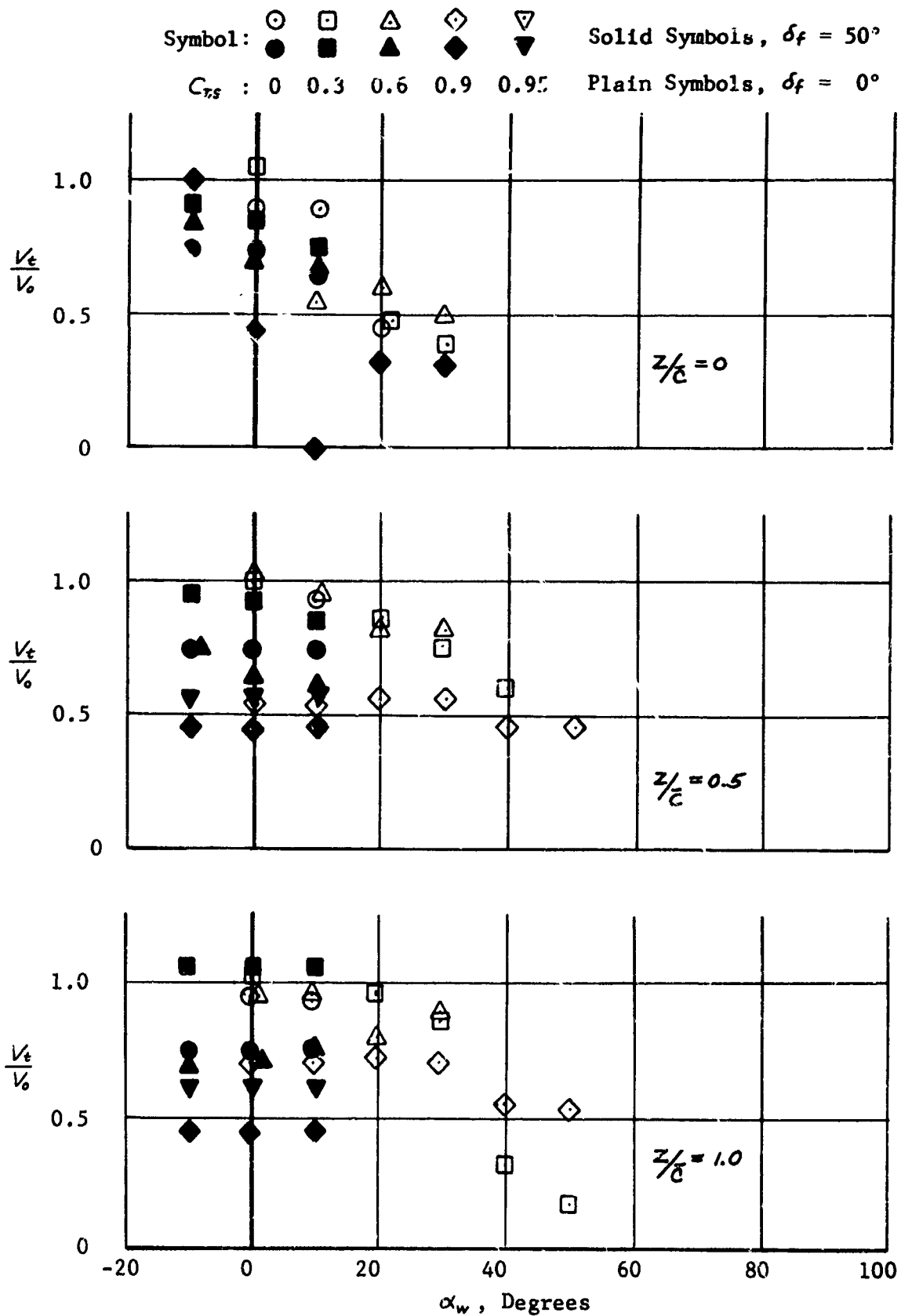
FIGURE 27. Slipstream Effects on Airflow Velocity in the Vicinity of a VTOL's Horizontal Tail (Data from Reference 15).

47

In particular, the shape of the fuselage bottom surface is of importance. In Reference 18, it is reported that the in-ground-effect flying qualities of a model of the Vertol V-76 aircraft were greatly improved by attaching deflector vanes to the bottom of the fuselage as shown in the sketch below.
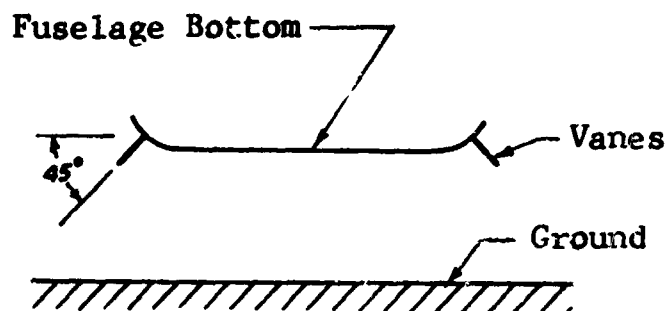
ENGINE FAILURE

Conditions of sudden power failure have been analyzed to determine the instantaneous aircraft response to power loss during the transition maneuver. The analysis was conducted for the Vertol V-76 aircraft operating at several transition trim conditions.

Partial engine failure effects are assumed to correspond to a reduction of propeller rotational speed to a value equal to $\sqrt[3]{1/2}\, n_o$, where n_o is the power-on trim value of the propeller speed. It is also assumed that the propeller speed is reduced instantaneously, and that V_o and α_w remain unchanged. The propeller advance ratio, J' , following power failure, is therefore a function of n only. Values of propeller thrust, power, and normal force coefficients are estimated at the new J' , using the data of Reference 30. Next, C_{T_S} is calculated as

$$C_{T_S} = \cfrac{1}{\left(1 + \cfrac{\pi\, q_o}{4\,\rho\, n^2 D^2 C_T'}\right)} \qquad (12)$$

48

Then the lift and longitudinal force coefficients are calculated for the power failure condition. Wing pitching moment coefficients, $C_{M,S}$, which include nacelle and propeller contributions, are estimated from data of Reference 5. These coefficients are utilized to determine the instantaneous change from the trim values of the forces and moments acting on the aircraft. The resulting longitudinal, normal, and pitching accelerations are presented in Figure 28. A change of $g/2$ of the normal acceleration occurs near the hovering condition. The maximum pitch acceleration (26 degrees per second per second) occurs at $\alpha_w = 30$ degrees.

In addition to aircraft trim changes, power failure can also cause the slipstream-immersed portion of the wing to stall. For example, before power failure, for a trim condition corresponding to $\alpha_w = 45$ degrees, $C_{T,S} = 0.74$ and $V_0 = 60$ feet per second, Figure 10 shows that the slipstream-immersed portion of the wing is unstalled. However, following power failure, $C_{T,S}$ decreases to 0.64, which results in a peak value of $C_{l,S} = 1.99$. The corresponding $C_{l_{max}}$ is 1.55, and hence wing stall is resulted.
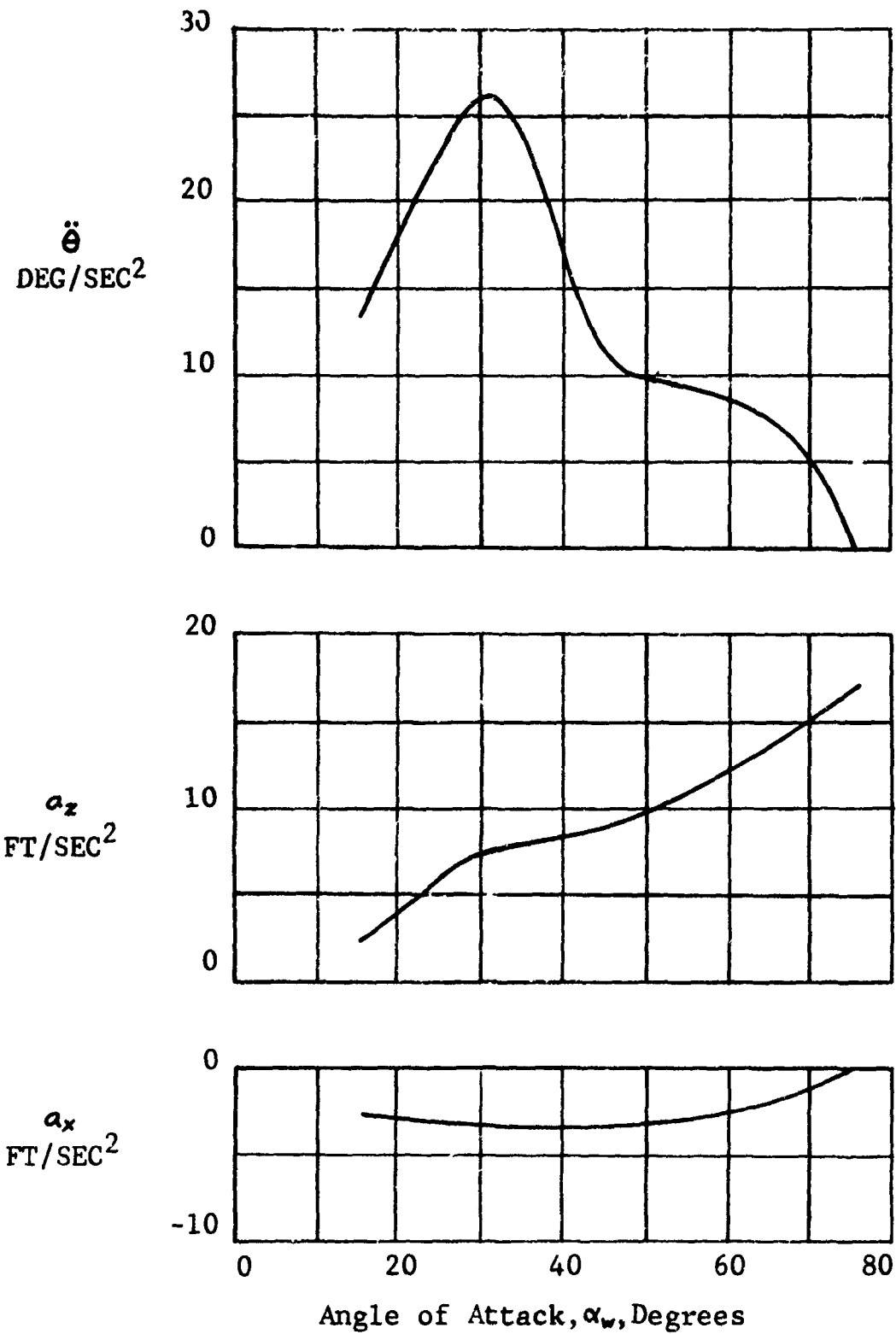
FIGURE 28. Aircraft Accelerations Following Partial
Engine Failure.

50

SLIPSTREAM EFFECTS ON VTOL AIRCRAFT STABILITY

   The primary objective of the analysis presented in this section is to evaluate the use of propeller slipstreams to augment the stability of a tilt-wing VTOL aircraft during transition. The stability analysis is conducted for a four-propeller tilt-wing VTOL transport aircraft similar in configuration to the XC-142 Tri-Service VTOL aircraft. Details of this aircraft are shown in Figure 29 and Table IV. The aircraft analyzed differs from the XC-142 in that it employs a full-span Fowler flap and has a wing area of 747 square feet when the flap is in the extended position. The analysis which is made for the longitudinal degrees of freedom at transition airspeeds of 30 to 70 knots is similar to that of References 31 and 32.

   A body axes coordinate system is used in the analysis. The body axes system refers to a right-handed, orthogonal system of axes fixed at the aircraft center of gravity, rotating and translating with the aircraft. As shown in Figure 30, the X-axis is aligned along a reference line (datum line) fixed to the fuselage (positive pointing forward). The Z-axis is perpendicular to the X-axis, positive towards the bottom of the fuselage, and the Y-axis is mutually perpendicular to the X- and Z-axes.

EQUATIONS OF MOTION

   The longitudinal equations of motion are as follows:

$$\Sigma X = \left[L_w \sin \alpha_F - D_w \cos \alpha_F \right] + \left[L_F \sin \alpha_F - D_F \cos \alpha_F \right]$$

$$+ \left[L_t \sin (\alpha_F - \epsilon) - D_t \cos (\alpha_F - \epsilon) \right]$$

$$+ \sum_{j=1}^{N} \left[T_{P_j} \cos i_{P_j} - N_{P_j} \sin i_{P_j} \right] - W \sin \theta - \frac{W}{g} (\dot{u} + w \dot{\theta}) = 0 \quad (13)$$

51
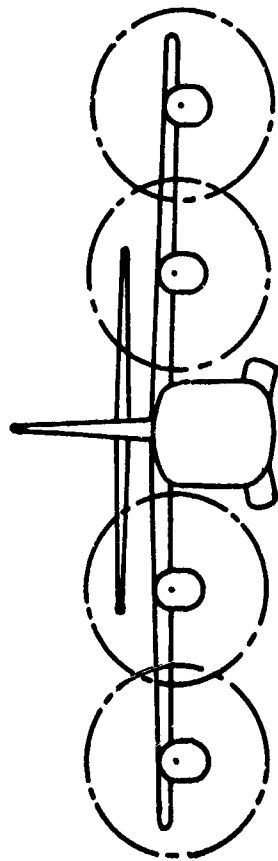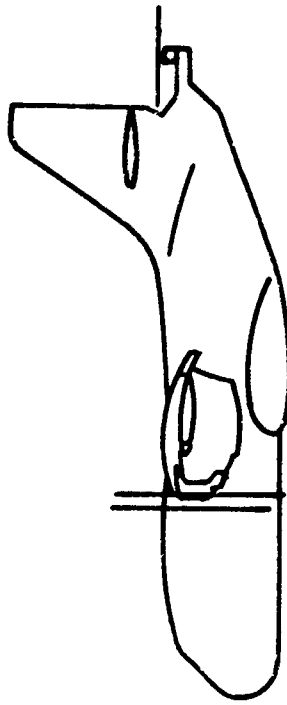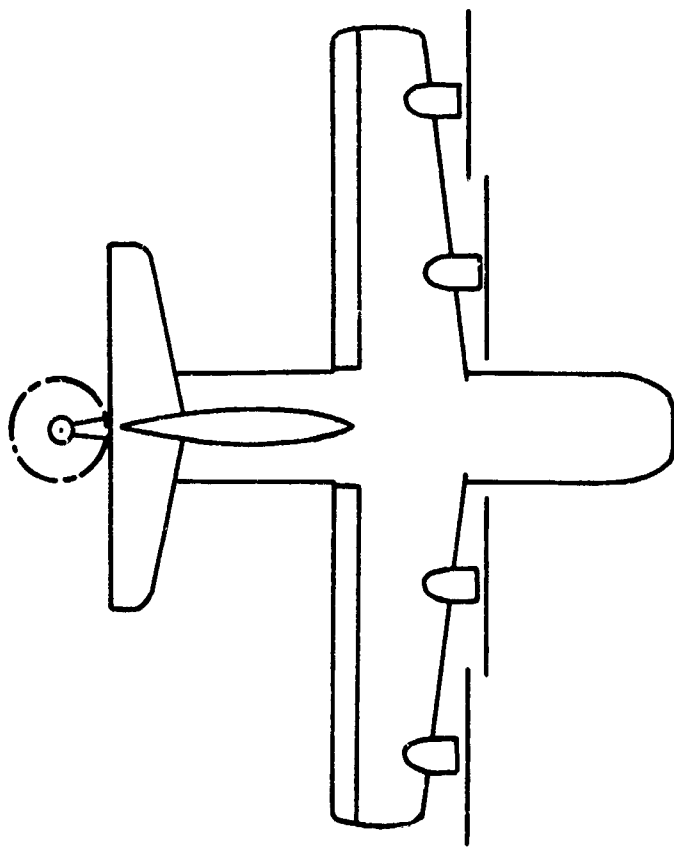
FIGURE 29. General Arrangement of a VTOL Transport Aircraft

52

TABLE IV
VTOL TRANSPORT CHARACTERISTICS

FUSELAGE:

Length, feet	50.0

WING:

Area (flap retracted), square feet	535
Area (flap extended), square feet	747
Span, feet	67.5
Aspect ratio (flap retracted)	8.53
Aspect ratio (flap extended)	6.42
Mean aerodynamic chord (flap retracted), feet	8.07
Mean aerodynamic chord (flap extended), feet	10.50
Taper ratio	0.61
Airfoil section	NACA 4415

FLAP:

Type	Fowler
Chord, percent of wing chord	39
Span	Full

HORIZONTAL TAIL:

Area, square feet	140
Aspect ratio	5.68
Span, feet	31.1
Mean aerodynamic chord, feet	5.5
Tail length, center of gravity to 0.25-max.,feet	25

PROPELLERS:

Main:	Number of blades	3
	Diameter, feet	15.5
Tail:	Number of blades	3
	Diameter, feet	8.0
	Moment arm, wing pivot to rotor center, feet	32.0
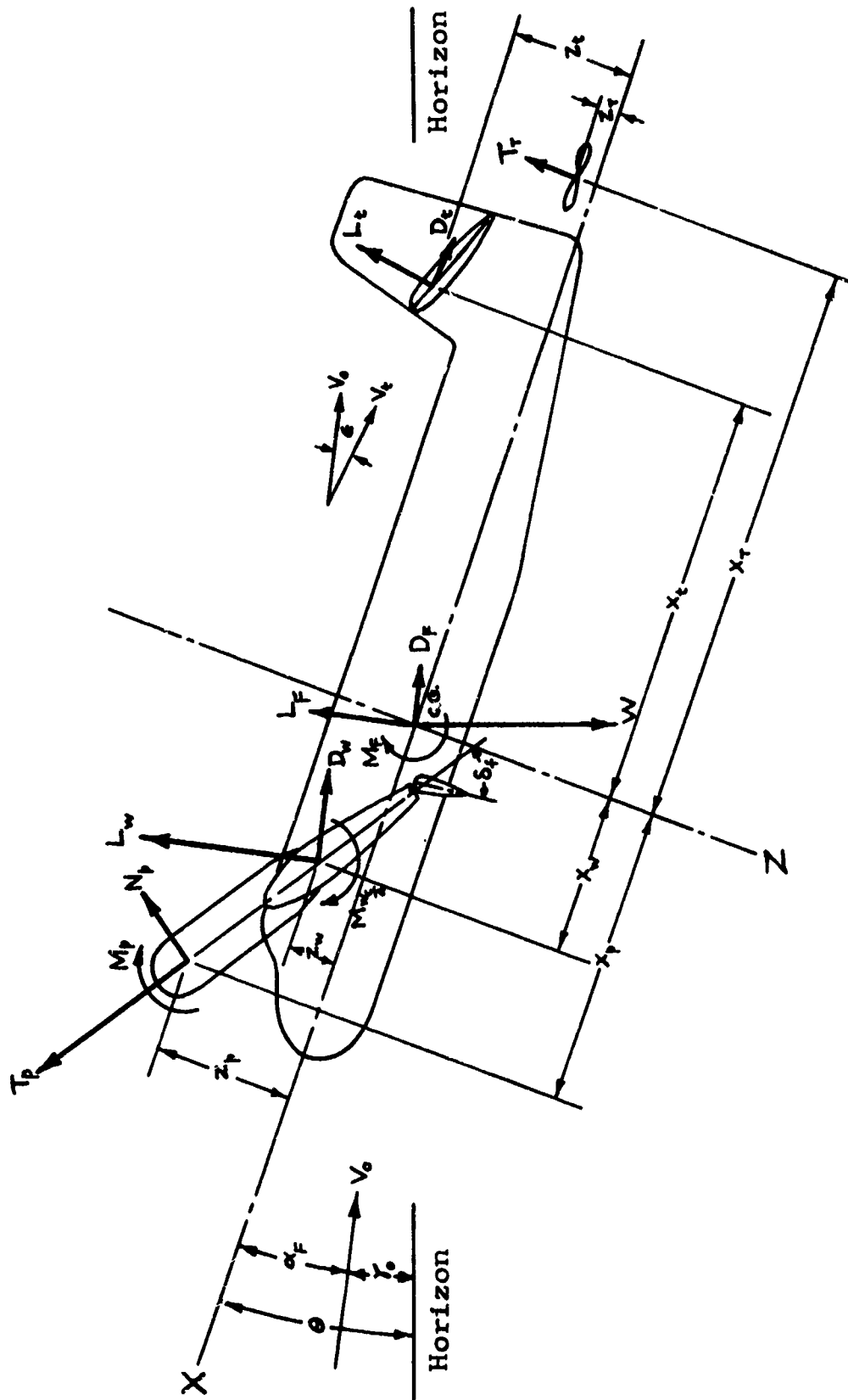
FIGURE 30. Force and Moment Notation.

54

$$\sum Z = -\left[L_w \cos \alpha_F + D_w \sin \alpha_F \right] - \left[L_F \cos \alpha_F + D_F \sin \alpha_F \right]$$

$$-\left[L_t \cos (\alpha_F - \epsilon) + D_t \sin (\alpha_F - \epsilon) \right] - T_T$$

$$-\sum_{j=1}^{N} \left[T_{P_j} \sin i_{P_j} + N_{P_j} \cos i_{P_j} \right] + W \cos \theta - \frac{W}{g} (\dot{w} - u \dot{\theta}) = 0 \qquad (14)$$

$$\sum M = M_{Wc/4} + \left[L_w \cos \alpha_F + D_w \sin \alpha_F \right] x_w$$

$$-\left[L_w \sin \alpha_F - D_w \cos \alpha_F \right] z_w + M_F$$

$$-\left[L_t \sin(\alpha_F - \epsilon) - D_t \cos (\alpha_F - \epsilon) \right] z_t$$

$$-\left[L_t \cos (\alpha_F - \epsilon) + D_t \sin (\alpha_F - \epsilon) \right] x_t - T_T x_T$$

$$-\sum_{j=1}^{N} \left[T_{P_j} \cos i_{P_j} - N_{P_j} \sin i_{P_j} \right] z_{P_j}$$

$$+\sum_{j=1}^{N} \left[T_{P_j} \sin i_{P_j} + N_{P_j} \cos i_{P_j} \right] x_{P_j} - I_{YY} \ddot{\theta} + \sum_{j=1}^{N} M_{P_j} = 0 \qquad (15)$$

The three independent variables in the above equations are the longitudinal component of the aircraft velocity, U, the normal velocity component, w, and the aircraft pitch attitude, θ.

Following the usual stability procedures, Reference 31, perturbation equations about the trim conditions can be obtained by linearizing Equations (13), (14), and (15). There results

55

$$X_u u + X_{\dot{u}} \dot{u} + X_w w + X_{\dot{w}} \dot{w} + X_\theta \theta + X_{\dot{\theta}} \dot{\theta} = 0 \qquad (16)$$

$$Z_u u + Z_{\dot{u}} \dot{u} + Z_w w + Z_{\dot{w}} \dot{w} + Z_\theta \theta + Z_{\dot{\theta}} \dot{\theta} = 0 \qquad (17)$$

$$M_u u + M_{\dot{u}} \dot{u} + M_w w + M_{\dot{w}} \dot{w} + M_\theta \theta + M_{\dot{\theta}} \dot{\theta} + M_{\ddot{\theta}} \ddot{\theta} = 0 \qquad (18)$$

In Equations (16), (17), and (18), u, w, and θ now represent perturbation variables; i.e., u is the change of the longitudinal component of velocity from the equilibrium value, etc. Also, X_u, Z_u, etc., are the total stability derivatives; that is, $X_u = \partial X / \partial u$, $Z_u = \partial Z / \partial u$. These derivatives, which are evaluated at the trim conditions, are obtained by performing the appropriate partial differentiation of Equations (13), (14), and (15).

The total stability derivatives are:

$$X_u = \frac{\partial X}{\partial u}$$

$$= \left[\frac{\partial L_w}{\partial u} \sin\alpha_F - \frac{\partial D_w}{\partial u} \cos\alpha_F \right] + \left[\frac{\partial L_F}{\partial u} \sin\alpha_F - \frac{\partial D_F}{\partial u} \cos\alpha_F \right]$$

$$+ \frac{\partial L_t}{\partial u} \sin(\alpha_F - \epsilon) - \frac{\partial D_t}{\partial u} \cos(\alpha_F - \epsilon)$$

$$- \frac{\partial \epsilon}{\partial u} \left[L_t \cos(\alpha_F - \epsilon) + D_t \sin(\alpha_F - \epsilon) \right]$$

$$+ \sum_{j=1}^{N} \left[\frac{\partial T_{P_j}}{\partial u} \cos i_{P_j} - \frac{\partial N_{P_j}}{\partial u} \sin i_{P_j} \right] \qquad (19)$$

$$X_{\dot{u}} = \frac{\partial X}{\partial \dot{u}} = -\frac{W}{g} \qquad (20)$$

$$X_w = \frac{\partial X}{\partial w} = \frac{1}{V_o} \frac{\partial X}{\partial \alpha_F}$$

$$= \frac{1}{V_o} \left\{ \left[\frac{\partial L_w}{\partial \alpha_F} + D_w \right] \sin \alpha_F + \left[L_w - \frac{\partial D_w}{\partial \alpha_F} \right] \cos \alpha_F \right.$$

$$+ \left[\frac{\partial L_F}{\partial \alpha_F} + D_F \right] \sin \alpha_F + \left[L_F - \frac{\partial D_F}{\partial \alpha_F} \right] \cos \alpha_F$$

$$+ \left[1 - \frac{\partial \epsilon}{\partial \alpha_F} \right] \left[\frac{\partial L_t}{\partial \alpha_t} \sin(\alpha_F - \epsilon) - \frac{\partial D_t}{\partial \alpha_t} \cos(\alpha_F - \epsilon) \right]$$

$$+ \left[1 - \frac{\partial \epsilon}{\partial \alpha_F} \right] \left[L_t \cos(\alpha_F - \epsilon) + D_t \sin(\alpha_F - \epsilon) \right]$$

$$\left. + \sum_{j=1}^{N} \left[\frac{\partial T_{P_j}}{\partial \alpha_F} \cos i_{P_j} - \frac{\partial N_{P_j}}{\partial \alpha_F} \sin i_{P_j} \right] \right\} \tag{21}$$

$$X_{\dot{w}} = \frac{\partial X}{\partial \dot{w}} = \frac{1}{V_o} \frac{\partial X}{\partial \dot{\alpha}_F}$$

$$= \frac{x_t}{V_o^2} \left[\frac{\partial L_t}{\partial \alpha_t} \sin(\alpha_F - \epsilon) - \frac{\partial D_t}{\partial \alpha_t} \cos(\alpha_F - \epsilon) \right.$$

$$\left. + L_t \cos(\alpha_F - \epsilon) + D_t \sin(\alpha_F - \epsilon) \right] \frac{\partial \epsilon}{\partial \alpha_F} \tag{22}$$

$$X_\theta = \frac{\partial X}{\partial \theta} = -W \cos \theta \tag{23}$$

$$X_{\dot{\theta}} = \frac{\partial X}{\partial \dot{\theta}}$$

$$= -z_w \left[\frac{\partial L_w}{\partial u} \sin \alpha_F - \frac{\partial D_w}{\partial u} \cos \alpha_F \right]$$

$$- \frac{x_w}{V_o} \left\{ \left[\frac{\partial L_w}{\partial \alpha_F} + D_w \right] \sin \alpha_F + \left[L_w - \frac{\partial D_w}{\partial \alpha_F} \right] \cos \alpha_F \right\}$$

57

$$-z_t \left[\frac{\partial L_t}{\partial u} sin(\alpha_F - \epsilon) - \frac{\partial D_t}{\partial u} cos(\alpha_F \cdot \epsilon) \right]$$

$$+ \frac{x_t}{V_o} \left[\frac{\partial L_t}{\partial \alpha_t} sin(\alpha_F - \epsilon) - \frac{\partial D_t}{\partial \alpha_t} cos(\alpha_F - \epsilon) \right.$$

$$\left. + L_t cos(\alpha_F - \epsilon) + D_t \; (\alpha_F - \epsilon) \right]$$

$$- \sum_{j=1}^{N} \left\{ z_{p_j} \left[\frac{\partial T_{p_j}}{\partial u} cos i_{p_j} - \frac{\partial N_{p_j}}{\partial u} sin i_{p_j} \right] \right.$$

$$\left. + \frac{x_{p_j}}{V_o} \left[\frac{\partial T_{p_j}}{\partial \alpha_F} cos i_{p_j} - \frac{\partial N_{p_j}}{\partial \alpha_F} sin i_{p_j} \right] \right\}$$

$$- \frac{W}{g} V_o sin \alpha_F \qquad\qquad (24)$$

$$Z_u = \frac{\partial Z}{\partial u}$$

$$= - \left[\frac{\partial L_W}{\partial u} cos \alpha_F - \frac{\partial D_W}{\partial u} sin \alpha_F \right] - \left[\frac{\partial L_F}{\partial u} cos \alpha_F + \frac{\partial D_F}{\partial u} sin \alpha_F \right]$$

$$- \left\{ \left[\frac{\partial L_t}{\partial u} cos(\alpha_F - \epsilon) + \frac{\partial D_t}{\partial u} sin(\alpha_F - \epsilon) \right] \right.$$

$$\left. + \left[L_t sin(\alpha_F - \epsilon) - D_t cos(\alpha_F - \epsilon) \right] \frac{\partial \epsilon}{\partial u} \right\}$$

$$- \frac{\partial T_T}{\partial u} - \sum_{j=1}^{N} \left[\frac{\partial T_{p_j}}{\partial u} sin i_{p_j} - \frac{\partial N_{p_j}}{\partial u} cos i_{p_j} \right] \qquad\qquad (25)$$

$$Z_{\dot{u}} = \frac{\partial Z}{\partial \dot{u}} = 0 \qquad\qquad (26)$$

$$Z_w = \frac{\partial Z}{\partial w} = \frac{1}{V_o} \frac{\partial Z}{\partial \alpha_F}$$

$$= -\frac{1}{V_o} \left\{ \left[\frac{\partial L_w}{\partial \alpha_F} + D_w \right] \cos \alpha_F - \left[L_w - \frac{\partial D_w}{\partial \alpha_F} \right] \sin \alpha_F \right.$$

$$+ \left[\frac{\partial L_F}{\partial \alpha_F} + D_F \right] \cos \alpha_F - \left[L_F - \frac{\partial D_F}{\partial \alpha_F} \right] \sin \alpha_F$$

$$+ \left[1 - \frac{\partial \epsilon}{\partial \alpha_F} \right] \left[\frac{\partial L_t}{\partial \alpha_t} \cos(\alpha_F - \epsilon) + \frac{\partial D_t}{\partial \alpha_t} \sin(\alpha_F - \epsilon) \right]$$

$$- \left[1 - \frac{\partial \epsilon}{\partial \alpha_F} \right] \left[L_t \sin(\alpha_F - \epsilon) - D_t \cos(\alpha_F - \epsilon) \right]$$

$$\left. + \frac{\partial T_T}{\partial \alpha_F} + \sum_{j=1}^{N} \left[\frac{\partial T_{P_i}}{\partial \alpha_F} \sin i_{P_j} + \frac{\partial N_{P_i}}{\partial \alpha_F} \cos i_{P_j} \right] \right\} \qquad (27)$$

$$Z_{\dot{w}} = \frac{\partial Z}{\partial \dot{w}} = \frac{1}{V_o} \frac{\partial Z}{\partial \dot{\alpha}_F}$$

$$= -\frac{x_t}{V_o^2} \left[-L_t \sin(\alpha_F - \epsilon) + D_t \cos(\alpha_F - \epsilon) \right.$$

$$\left. + \frac{\partial L_t}{\partial \alpha_t} \cos(\alpha_F - \epsilon) + \frac{\partial D_t}{\partial \alpha_t} \sin(\alpha_F - \epsilon) \right] \frac{\partial \epsilon}{\partial \alpha_F} - \frac{W}{g} \qquad (28)$$

$$Z_\theta = \frac{\partial Z}{\partial \theta} = -W \sin \theta \qquad (29)$$

$$Z_{\dot{\theta}} = \frac{\partial Z}{\partial \dot{\theta}}$$

$$= z_w \left[\frac{\partial L_w}{\partial u} \cos \alpha_F + \frac{\partial D_w}{\partial u} \sin \alpha_F \right]$$

$$+ \frac{x_w}{V_o} \left\{ \left[\frac{\partial L_w}{\partial \alpha_F} + D_w \right] \cos \alpha_F - \left[L_w - \frac{\partial D_w}{\partial \alpha_F} \right] \sin \alpha_F \right\}$$

59

$$+ z_t \left[\frac{\partial L_t}{\partial u} \cos(\alpha_F - \epsilon) + \frac{\partial D_t}{\partial u} \sin(\alpha_F - \epsilon) \right]$$

$$- \frac{x_t}{V_o} \left[\frac{\partial L_t}{\partial \alpha_t} \cos(\alpha_F - \epsilon) + \frac{\partial D_t}{\partial \alpha_t} \sin(\alpha_F - \epsilon) \right.$$

$$\left. - L_t \sin(\alpha_F - \epsilon) + D_t \cos(\alpha_F - \epsilon) \right]$$

$$+ \sum_{j=1}^{N} \left\{ \frac{x_{p_j}}{V_o} \left[\frac{\partial T_{p_j}}{\partial \alpha_F} \sin i_{p_j} + \frac{\partial N_{p_j}}{\partial \alpha_F} \cos i_{p_j} \right] \right.$$

$$\left. + z_{p_j} \left[\frac{\partial T_{p_j}}{\partial u} \sin i_{p_j} + \frac{\partial N_{p_j}}{\partial u} \cos i_{p_j} \right] \right\}$$

$$+ z_t \frac{\partial T_T}{\partial u} - \frac{x_r}{V_o} \frac{\partial T_T}{\partial \alpha_F} + \frac{W}{g} V_o \qquad\qquad (30)$$

$$M_u = \frac{\partial M}{\partial u}$$

$$= \left[\frac{\partial L_w}{\partial u} \cos \alpha_F + \frac{\partial D_w}{\partial u} \sin \alpha_F \right] x_w - \left[\frac{\partial L_w}{\partial u} \sin \alpha_F - \frac{\partial D_w}{\partial u} \cos \alpha_F \right] z_w$$

$$- x_t \left\{ \frac{\partial L_t}{\partial u} \cos(\alpha_F - \epsilon) + \frac{\partial D_t}{\partial u} \sin(\alpha_F - \epsilon) \right.$$

$$\left. + \left[L_t \sin(\alpha_F - \epsilon) - D_t \cos(\alpha_F - \epsilon) \right] \frac{\partial \epsilon}{\partial u} \right\}$$

$$- z_t \left\{ \frac{\partial L_t}{\partial u} \sin(\alpha_F - \epsilon) - \frac{\partial D_t}{\partial u} \cos(\alpha_F - \epsilon) \right.$$

$$\left. - \left[L_t \cos(\alpha_F - \epsilon) + D_t \sin(\alpha_F - \epsilon) \right] \frac{\partial \epsilon}{\partial u} \right\}$$

$$+ \sum_{j=1}^{N}\left[\frac{\partial T_{P_j}}{\partial u}\sin i_{p_j} + \frac{\partial N_{P_j}}{\partial u}\cos i_{p_j}\right]x_{p_j} - \sum_{j=1}^{N}\left[\frac{\partial T_{p_j}}{\partial u}\cos i_{p_j} - \frac{\partial N_{p_j}}{\partial u}\sin i_{p_j}\right]z_{p_j}$$

$$+ \sum_{j=1}^{N}\frac{\partial M_{P_j}}{\partial u} + \frac{\partial M_{wc_{44}}}{\partial u} + \frac{\partial M_F}{\partial u} - x_T\frac{\partial T_T}{\partial u} \tag{31}$$

$$M_{\dot{u}} = \frac{\partial M}{\partial \dot{u}} = 0 \tag{32}$$

$$M_{w} = \frac{\partial M}{\partial w} = \frac{1}{V_o}\frac{\partial M}{\partial \alpha_F}$$

$$= -\frac{z_w}{V_o}\left\{\left[\frac{\partial L_w}{\partial \alpha_F} + D_w\right]\sin\alpha_F + \left[L_w - \frac{\partial D_w}{\partial \alpha_F}\right]\cos\alpha_F\right\}$$

$$+ \frac{x_w}{V_o}\left\{\left[\frac{\partial L_w}{\partial \alpha_F} + D_w\right]\cos\alpha_F - \left[L_w - \frac{\partial D_w}{\partial \alpha_F}\right]\sin\alpha_F\right\}$$

$$- \frac{z_t}{V_o}\left\{\left[1 - \frac{\partial \epsilon}{\partial \alpha_F}\right]\left[\frac{\partial L_t}{\partial \alpha_t}\sin(\alpha_F - \epsilon) - \frac{\partial D_t}{\partial \alpha_t}\cos(\alpha_F - \epsilon)\right]\right.$$

$$\left. + \left[1 - \frac{\partial \epsilon}{\partial \alpha_F}\right]\left[L_t\cos(\alpha_F - \epsilon) + D_t\sin(\alpha_F - \epsilon)\right]\right\}$$

$$- \frac{x_t}{V_o}\left\{\left[1 - \frac{\partial \epsilon}{\partial \alpha_F}\right]\left[\frac{\partial L_t}{\partial \alpha_t}\cos(\alpha_F - \epsilon) + \frac{\partial D_t}{\partial \alpha_t}\sin(\alpha_F - \epsilon)\right]\right.$$

$$\left. - \left[1 - \frac{\partial \epsilon}{\partial \alpha_F}\right]\left[L_t\sin(\alpha_F - \epsilon) - D_t\cos(\alpha_F - \epsilon)\right]\right\}$$

$$- \frac{1}{V_o}\sum_{j=1}^{N}\left[\frac{\partial T_{p_j}}{\partial \alpha_F}\cos i_{p_j} - \frac{\partial N_{p_j}}{\partial \alpha_F}\sin i_{p_j}\right]z_{p_j}$$

$$+ \frac{1}{V_o}\sum_{j=1}^{N}\left[\frac{\partial T_{p_j}}{\partial \alpha_F}\sin i_{p_j} + \frac{\partial N_{p_j}}{\partial \alpha_F}\cos i_{p_j}\right]x_{p_j}$$

$$+ \frac{1}{V_o}\sum_{j=1}^{N}\frac{\partial M_{P_j}}{\partial \alpha_F} + \frac{1}{V_o}\frac{\partial M_{wc_{44}}}{\partial \alpha_F} - \frac{x_T}{V_o}\frac{\partial T_T}{\partial \alpha_F} \tag{33}$$

61

$$M_{\dot{w}} = \frac{\partial M}{\partial \dot{w}} = \frac{1}{V_o} \frac{\partial M}{\partial \dot{\alpha}_F}$$

$$= -\frac{x_t z_t}{V_o^2}\left[\frac{\partial L_t}{\partial \alpha_t} \sin(\alpha_F - \epsilon) - \frac{\partial D_t}{\partial \alpha_t}\cos(\alpha_F - \epsilon)\right.$$

$$\left. + L_t \cos(\alpha_F - \epsilon) - D_t \sin(\alpha_F - \epsilon)\right]\frac{\partial \epsilon}{\partial \alpha_F}$$

$$- \frac{x_t^2}{V_o^2}\left[\frac{\partial L_t}{\partial \alpha_t}\cos(\alpha_F - \epsilon) + \frac{\partial D_t}{\partial \alpha_t}\sin(\alpha_F - \epsilon)\right.$$

$$\left. - L_t \sin(\alpha_F - \epsilon) + D_t \cos(\alpha_F - \epsilon)\right]\frac{\partial \epsilon}{\partial \alpha_F} \qquad (34)$$

$$M_\theta = \frac{\partial M}{\partial \theta} = 0 \qquad (35)$$

$$M_{\dot{\theta}} = \frac{\partial M}{\partial \dot{\theta}}$$

$$= z_w^2\left[\frac{\partial L_w}{\partial u}\sin\alpha_F - \frac{\partial D_w}{\partial u}\cos\alpha_F\right]$$

$$- x_w z_w\left[\frac{\partial L_w}{\partial u}\cos\alpha_F + \frac{\partial L_w}{\partial u}\sin\alpha_F\right]$$

$$+ \frac{x_w z_w}{V_o}\left\{\left[\frac{\partial L_w}{\partial \alpha_F} + D_w\right]\sin\alpha_F + \left[L_w - \frac{\partial D_w}{\partial \alpha_F}\right]\cos\alpha_F\right\}$$

$$- \frac{x_w^2}{V_o}\left\{\left[\frac{\partial L_w}{\partial \alpha_F} + D_w\right]\cos\alpha_F - \left[L_w - \frac{\partial D_w}{\partial \alpha_F}\right]\sin\alpha_F\right\}$$

$$- z_t^2\left[\frac{\partial L_t}{\partial u}\sin(\alpha_F - \epsilon) - \frac{\partial D_t}{\partial u}\cos(\alpha_F - \epsilon)\right]$$

$$+ x_t z_t\left[\frac{\partial L_t}{\partial u}\cos(\alpha_F - \epsilon) + \frac{\partial D_t}{\partial u}\sin(\alpha_F - \epsilon)\right]$$

$$- \frac{x_t z_t}{V_o} \left[\frac{\partial L_t}{\partial \alpha_t} \sin(\alpha_F - \epsilon) - \frac{\partial D_t}{\partial \alpha_t} \cos(\alpha_F - \epsilon) \right.$$

$$\left. + L_t \cos(\alpha_F - \epsilon) + D_t \sin(\alpha_F - \epsilon) \right]$$

$$- \frac{x_t^2}{V_o} \left[\frac{\partial L_t}{\partial \alpha_t} \cos(\alpha_F - \epsilon) + \frac{\partial D_t}{\partial \alpha_t} \sin(\alpha_F - \epsilon) \right.$$

$$\left. - L_t \sin(\alpha_F - \epsilon) + D_t \cos(\alpha_F - \epsilon) \right]$$

$$- x_T z_T \frac{\partial T_T}{\partial u}$$

$$- \sum_{j=1}^{N} \left\{ z_{p_j}^2 \left[\frac{\partial T_{p_j}}{\partial u} \cos i_{p_j} - \frac{\partial N_{p_j}}{\partial u} \sin i_{p_j} \right] \right.$$

$$+ \frac{x_{p_j} z_{p_j}}{V_o} \left[\frac{\partial T_{p_j}}{\partial \alpha_F} \cos i_{p_j} - \frac{\partial N_{p_j}}{\partial \alpha_F} \sin i_{p_j} \right]$$

$$- x_{p_j} z_{p_j} \left[\frac{\partial T_{p_j}}{\partial u} \sin i_{p_j} + \frac{\partial N_{p_j}}{\partial u} \cos i_{p_j} \right]$$

$$\left. - \frac{x_{p_j}^2}{V_o} \left[\frac{\partial T_{p_j}}{\partial \alpha_F} \sin i_{p_j} + \frac{\partial N_{p_j}}{\partial \alpha_F} \cos i_{p_j} \right] \right\}$$

$$- \frac{x_T^2}{V_o} \frac{\partial T_T}{\partial \alpha_F} + \frac{\partial M_{wc_b}}{\partial \dot{\theta}} + \frac{\partial M_F}{\partial \dot{\theta}} + \sum_{j=1}^{N} \frac{\partial M_{p_j}}{\partial \dot{\theta}} \tag{36}$$

$$M_{\ddot{\theta}} = \frac{\partial M}{\partial \ddot{\theta}} = -I_{YY} \tag{37}$$

Using the assumptions that

$$\alpha_F = 0 \ , \quad \frac{\partial \epsilon}{\partial u} = 0 \ , \quad \frac{\partial D_t}{\partial u} = 0, \quad D_t = 0$$

the total stability derivatives become

$$X_u = \frac{\partial X}{\partial u}$$

$$= -\frac{\partial D_w}{\partial u} - \frac{\partial D_F}{\partial u} - \frac{\partial L_t}{\partial u}\sin\epsilon + \sum_{j=1}^{N}\left[\frac{\partial T_{p_j}}{\partial u}\cos i_{p_j} - \frac{\partial N_{p_j}}{\partial u}\sin i_{p_j}\right] \tag{38}$$

$$X_{\dot{u}} = \frac{\partial X}{\partial \dot{u}} = -\frac{W}{g} \tag{39}$$

$$X_w = \frac{\partial X}{\partial w} = \frac{1}{V_o}\frac{\partial X}{\partial \alpha_F}$$

$$= \frac{1}{V_o}\left\{\left[L_w - \frac{\partial D_w}{\partial \alpha_F}\right] + \left[L_F - \frac{\partial D_F}{\partial \alpha_F}\right]\right.$$

$$- \left[1 - \frac{\partial \epsilon}{\partial \alpha_F}\right]\left[\frac{\partial L_t}{\partial \alpha_t}\sin\epsilon + \frac{\partial D_t}{\partial \alpha_t}\cos\epsilon\right] + \left[1 - \frac{\partial \epsilon}{\partial \alpha_F}\right]L_t\cos\epsilon$$

$$\left. + \sum_{j=1}^{N}\left[\frac{\partial T_{p_j}}{\partial \alpha_F}\cos i_{p_j} - \frac{\partial N_{p_j}}{\partial \alpha_F}\sin i_{p_j}\right]\right\} \tag{40}$$

$$X_{\dot{w}} = \frac{\partial X}{\partial \dot{w}} = \frac{1}{V_o}\frac{\partial X}{\partial \dot{\alpha}_F}$$

$$= -\frac{x_t}{V_o^2}\left[\frac{\partial L_t}{\partial \alpha_t}\sin\epsilon + \frac{\partial D_t}{\partial \alpha_t}\cos\epsilon - L_t\cos\epsilon\right]\frac{\partial \epsilon}{\partial \alpha_F} \tag{41}$$

$$X_\theta = \frac{\partial X}{\partial \theta} = -W\cos\theta \tag{42}$$

$$X_{\dot{\theta}} = \frac{\partial X}{\partial \dot{\theta}}$$

$$= z_w\frac{\partial D_w}{\partial u} - \frac{x_w}{V_o}\left[L_w - \frac{\partial D_w}{\partial \alpha_F}\right] + z_t\frac{\partial L_t}{\partial u}\sin\epsilon$$

64

$$-\sum_{j=1}^{N}\left\{\left[\frac{\partial T_{p_i}}{\partial u}\cos i_{p_j}-\frac{\partial N_{p_i}}{\partial u}\sin i_{p_j}\right]z_{p_j}\right.$$

$$\left.+\frac{x_{p_j}}{V_o}\left[\frac{\partial T_{p_j}}{\partial \alpha_F}\cos i_{p_j}-\frac{\partial N_{p_j}}{\partial \alpha_F}\sin i_{p_j}\right]\right\} \tag{43}$$

$$Z_u=\frac{\partial Z}{\partial u}$$

$$=-\frac{\partial L_w}{\partial u}-\frac{\partial L_F}{\partial u}-\frac{\partial L_t}{\partial u}\cos\epsilon-\frac{\partial T_T}{\partial u}$$

$$-\sum_{j=1}^{N}\left[\frac{\partial T_{p_j}}{\partial u}\sin i_{p_j}+\frac{\partial N_{p_j}}{\partial u}\cos i_{p_j}\right] \tag{44}$$

$$Z_{\dot{u}}=\frac{\partial Z}{\partial \dot{u}}=0 \tag{45}$$

$$Z_w=\frac{\partial Z}{\partial w}=\frac{1}{V_o}\frac{\partial Z}{\partial \alpha_F}$$

$$=-\frac{1}{V_o}\left\{\left[\frac{\partial L_w}{\partial \alpha_F}+D_w\right]+\left[\frac{\partial L_F}{\partial \alpha_F}+D_F\right]\right.$$

$$+\left[1-\frac{\partial \epsilon}{\partial \alpha_F}\right]\left[\frac{\partial L_t}{\partial \alpha_t}\cos\epsilon-\frac{\partial D_t}{\partial \alpha_t}\sin\epsilon\right]+\left[1-\frac{\partial \epsilon}{\partial \alpha_F}\right]L_t\sin\epsilon$$

$$\left.-\frac{\partial T_T}{\partial \alpha_F}-\sum_{j=1}^{N}\left[\frac{\partial T_{p_j}}{\partial \alpha_F}\sin i_{p_j}-\frac{\partial N_{p_j}}{\partial \alpha_F}\cos i_{p_j}\right]\right\} \tag{46}$$

$$Z_{\dot{w}}=\frac{\partial Z}{\partial \dot{w}}=\frac{1}{V_o}\frac{\partial Z}{\partial \dot{\alpha}_F}$$

$$=-\frac{x_t}{V_o^2}\left[\frac{\partial L_t}{\partial \alpha_t}\cos\epsilon-\frac{\partial D_t}{\partial \alpha_t}\sin\epsilon+L_t\sin\epsilon\right]\frac{\partial \epsilon}{\partial \alpha_F}-\frac{W}{g} \tag{47}$$

$$Z_\theta = \frac{\partial Z}{\partial \theta} = -W \sin\theta \tag{48}$$

$$Z_{\dot{\theta}} = \frac{\partial Z}{\partial \dot{\theta}}$$

$$= z_w \frac{\partial L_w}{\partial u} + \frac{x_w}{V_o}\left[\frac{\partial L_w}{\partial \alpha_F} + D_w\right] + z_t \frac{\partial L_t}{\partial u} \cos\epsilon$$

$$- \frac{x_t}{V_o}\left[\frac{\partial L_t}{\partial \alpha_t} \cos\epsilon - \frac{\partial D_t}{\partial \alpha_t} \sin\epsilon + L_t \sin\epsilon\right]$$

$$+ z_T \frac{\partial T_T}{\partial u} - \frac{x_T}{V_o} \frac{\partial T_T}{\partial \alpha_F} + \frac{W}{g} V_o$$

$$+ \sum_{j=1}^{N}\left\{ z_{p_j}\left[\frac{\partial T_{p_j}}{\partial u} \sin i_{p_j} + \frac{\partial N_{p_j}}{\partial u} \cos i_{p_j}\right]\right.$$

$$\left. + \frac{x_{p_j}}{V_o}\left[\frac{\partial T_{p_j}}{\partial \alpha_F} \sin i_{p_j} + \frac{\partial N_{p_j}}{\partial \alpha_F} \cos i_{p_j}\right]\right\} \tag{49}$$

$$M_u = \frac{\partial M}{\partial u}$$

$$= x_w \frac{\partial L_w}{\partial u} + z_w \frac{\partial D_w}{\partial u} - x_t\left[\frac{\partial L_t}{\partial u} \cos\epsilon - \frac{\partial D_t}{\partial u} \sin\epsilon\right]$$

$$+ z_t\left[\frac{\partial L_t}{\partial u} \sin\epsilon + \frac{\partial D_t}{\partial u} \cos\epsilon\right] - x_T \frac{\partial T_T}{\partial u}$$

$$+ \sum_{j=1}^{N}\left\{ x_{p_j}\left[\frac{\partial T_{p_j}}{\partial u} \sin i_{p_j} + \frac{\partial N_{p_j}}{\partial u} \cos i_{p_j}\right]\right.$$

$$\left. - z_{p_j}\left[\frac{\partial T_{p_j}}{\partial u} \cos i_{p_j} - \frac{\partial N_{p_j}}{\partial u} \sin i_{p_j}\right]\right\}$$

$$+ \frac{\partial M_{w_{c.H}}}{\partial u} + \frac{\partial M_F}{\partial u} + \sum_{j=1}^{N} \frac{\partial M_{p_j}}{\partial u} \tag{50}$$

66

$$M_{\dot{u}} = \frac{\partial M}{\partial \dot{u}} = 0 \tag{51}$$

$$M_w = \frac{\partial M}{\partial w} = \frac{1}{V_o}\frac{\partial M}{\partial \alpha_F}$$

$$= -\frac{z_w}{V_o}\left[L_w - \frac{\partial D_w}{\partial \alpha_F}\right] + \frac{x_w}{V_o}\left[\frac{\partial L_w}{\partial \alpha_F} + D_w\right]$$

$$+ \frac{z_t}{V_o}\left[1 - \frac{\partial \epsilon}{\partial \alpha_F}\right]\left[\frac{\partial L_t}{\partial \alpha_t}\sin\epsilon + \frac{\partial D_t}{\partial \alpha_t}\cos\epsilon - L_t\cos\epsilon\right]$$

$$- \frac{x_t}{V_o}\left[1 - \frac{\partial \epsilon}{\partial \alpha_F}\right]\left[\frac{\partial L_t}{\partial \alpha_t}\cos\epsilon - \frac{\partial D_t}{\partial \alpha_t}\sin\epsilon + L_t\sin\epsilon\right] - \frac{x_T}{V_o}\frac{\partial T_T}{\partial \alpha_F}$$

$$- \frac{1}{V_o}\sum_{j=1}^{N}\left\{\left[\frac{\partial T_{p_j}}{\partial \alpha_F}\cos i_{p_j} - \frac{\partial N_{p_j}}{\partial \alpha_F}\sin i_{p_j}\right]z_{p_j}\right.$$

$$\left. - \left[\frac{\partial T_{p_j}}{\partial \alpha_F}\sin i_{p_j} + \frac{\partial N_{p_j}}{\partial \alpha_F}\cos i_{p_j}\right]x_{p_j} - \frac{\partial M_{p_j}}{\partial \alpha_F}\right\}$$

$$+ \frac{1}{V_o}\frac{\partial M_{w_{c.g.}}}{\partial \alpha_F} \tag{52}$$

$$M_{\dot{w}} = \frac{\partial M}{\partial \dot{w}} = \frac{1}{V_o}\frac{\partial M}{\partial \dot{\alpha}_F}$$

$$= \frac{x_t z_t}{V_o^2}\left[\frac{\partial L_t}{\partial \alpha_t}\sin\epsilon + \frac{\partial D_t}{\partial \alpha_t}\cos\epsilon - L_t\cos\epsilon\right]\frac{\partial \epsilon}{\partial \alpha_F}$$

$$- \frac{x_t^2}{V_o^2}\left[\frac{\partial L_t}{\partial \alpha_t}\cos\epsilon - \frac{\partial D_t}{\partial \alpha_t}\sin\epsilon + L_t\sin\epsilon\right]\frac{\partial \epsilon}{\partial \alpha_F} \tag{53}$$

$$M_\theta = \frac{\partial M}{\partial \theta} = 0 \tag{54}$$

$$M_{\dot{\theta}} = \frac{\partial M}{\partial \dot{\theta}}$$

$$= -z_w^2 \frac{\partial D_w}{\partial u} - \frac{x_w z_w}{V_o}\left[L_w - \frac{\partial D_w}{\partial \alpha_F}\right]$$

$$-x_w z_w \frac{\partial L_w}{\partial u} - \frac{x_w^2}{V_o}\left[\frac{\partial L_w}{\partial \alpha_F} + D_w\right]$$

$$-z_t^2\left[\frac{\partial L_t}{\partial u}\sin\epsilon + \frac{\partial D_t}{\partial u}\cos\epsilon\right]$$

$$+\frac{x_t z_t}{V_o}\left[\frac{\partial L_t}{\partial \alpha_t}\sin\epsilon + \frac{\partial D_t}{\partial \alpha_t}\cos\epsilon - L_t\cos\epsilon\right]$$

$$+x_t z_t\left[\frac{\partial L_t}{\partial u}\cos\epsilon - \frac{\partial D_t}{\partial u}\sin\epsilon\right]$$

$$-\frac{x_t^2}{V_o}\left[\frac{\partial L_t}{\partial \alpha_t}\cos\epsilon - \frac{\partial D_t}{\partial x_t}\sin\epsilon + L_t\sin\epsilon\right]$$

$$+x_T z_T \frac{\partial T_T}{\partial u} - \frac{x_T^2}{V_o}\frac{\partial T_T}{\partial \alpha_F}$$

$$+\sum_{j=1}^{N}\left\{ z_{p_j}^2\left[\frac{\partial T_{p_j}}{\partial u}\cos i_{p_j} - \frac{\partial N_{p_j}}{\partial u}\sin i_{p_j}\right]\right.$$

$$+\frac{x_{p_j} z_{p_j}}{V_o}\left[\frac{\partial T_{p_j}}{\partial \alpha_F}\cos i_{p_j} - \frac{\partial N_{p_j}}{\partial \alpha_F}\sin i_{p_j}\right]$$

$$-x_{p_j} z_{p_j}\left[\frac{\partial T_{p_j}}{\partial u}\sin i_{p_j} + \frac{\partial N_{p_j}}{\partial u}\cos i_{p_j}\right]$$

$$\left. -\frac{x_{p_j}^2}{V_o}\left[\frac{\partial T_{p_j}}{\partial \alpha_F}\sin i_{p_j} + \frac{\partial N_{p_j}}{\partial \alpha_F}\cos i_{p_j}\right]\right\}$$

$$+\frac{\partial M_{wst}}{\partial \dot\theta} + \frac{\partial M_F}{\partial \dot\theta} + \sum_{j=1}^{N}\frac{\partial M_{p_j}}{\partial \dot\theta} \tag{55}$$

$$M_{\ddot\theta} = \frac{\partial M}{\partial \ddot\theta} = -I_{yy} \tag{56}$$

68

INCORPORATION OF SLIPSTREAM EFFECTS INTO THE VTOL STABILITY DERIVATIVES

The derivatives X_u, Z_u, M_u, etc., defined in the preceding section consist of contributions from propeller forces and moments, wing forces and moments, and horizontal tail and tail rotor forces. The methods used to determine the contributions of each of these items to the derivatives are now discussed.

Wing Derivatives

The wing X and Z stability derivatives are estimated by using the lift and drag analysis of Reference 3 for wings immersed in slipstreams. The wing moment derivatives are estimated from the test data of Reference 15.

The slipstream lift and drag analysis is summarized by the following equations. Wing lift and drag are expressed as

$$L_w = C_{Lw}\, q_s S \tag{57}$$

and

$$D_w = C_{Dw}\, q_s S \tag{58}$$

The lift and drag coefficients, C_{Lw} and C_{Dw}, based on slipstream dynamic pressure, are

$$C_{Lw} = (1 - C_{T,s})\, a\alpha + 3.74\,(1 - \mu^2)\left(\frac{r_s}{D}\right)^2 \frac{ND^2}{S}\, \alpha_s \cos(\alpha_p - \phi)$$

$$- \left[\frac{S_s}{S} C_{D_{0,s}} + 1.113\,(1 - \mu^2)^2 \left(\frac{r_s}{D}\right)^2 \frac{ND^2}{S}\, \alpha_s^2 \right] \sin(\alpha_p - \phi) \tag{59}$$

$$C_{Dw} = (1 - C_{T,s})\left[\left(1 - \frac{S_s}{S}\right)C_{D_0} + \frac{(a\alpha)^2}{\pi R}\right] + \frac{S_s}{S} C_{D_{0,s}} \cos(\alpha_p - \phi)$$

69

$$+ 1.113 (1-\mu^2)^2 \left(\frac{r_s}{D}\right)^2 \frac{ND^2}{S} \alpha_s^2 \cos(\alpha_p - \phi)$$

$$+ 3.74 (1-\mu^2) \left(\frac{r_s}{D}\right)^2 \frac{ND^2}{S} \alpha_s \sin(\alpha_p - \phi) \qquad (60)$$

The wing stability derivatives can be obtained by differentiating Equations (59) and (60) with respect to u and α_F. Since

$$\frac{\partial \alpha_w}{\partial \alpha_F} = \frac{\partial \alpha_p}{\partial \alpha_F} = 1$$

there follows

$$\frac{\partial C_{L_W}}{\partial u} = -a\alpha' \frac{\partial C_{T,S}}{\partial u}$$

$$+ 3.74 \frac{ND^2}{S} \left[(1-\mu^2) \left(\frac{r_s}{D}\right)^2 \frac{\partial \phi}{\partial u} \cos(\alpha_p - \phi) \right.$$

$$+ 2 (1-\mu^2) \frac{r_s}{D^2} \alpha_s \frac{\partial r_s}{\partial u} \cos(\alpha_p - \phi)$$

$$- 2\mu \left(\frac{r_s}{D}\right)^2 \alpha_s \frac{\partial \mu}{\partial u} \cos(\alpha_p - \phi)$$

$$+ (1-\mu^2) \left(\frac{r_s}{D}\right)^2 \alpha_s \frac{\partial \phi}{\partial u} \sin(\alpha_p - \phi) \Big]$$

$$- \frac{2Nc}{S} C_{D_0,s} \frac{\partial r_s}{\partial u} \sin(\alpha_p - \phi) + \frac{2Nc}{S} r_s C_{D_0,s} \frac{\partial \phi}{\partial u} \cos(\alpha_p - \phi)$$

$$- 1.113 \frac{ND^2}{S} \left[2(1-\mu^2)^2 \left(\frac{r_s}{D}\right)^2 \alpha_s \frac{\partial \phi}{\partial u} \sin(\alpha_p - \phi) \right.$$

70

$$+ 2(1-\mu^2)^2 \frac{r_s}{D^3} \alpha_s^2 \frac{\partial r_s}{\partial u} \sin(\alpha_p - \phi)$$

$$- 4\mu(1-\mu^2)\left(\frac{r_s}{D}\right)^2 \alpha_s^2 \frac{\partial \mu}{\partial u} \sin(\alpha_p - \phi)$$

$$- (1-\mu^2)^2\left(\frac{r_s}{D}\right)^2 \alpha_s^2 \frac{\partial \phi}{\partial u} \cos(\alpha_p - \phi)\Bigg] \tag{61}$$

$$\frac{\partial C_{D_N}}{\partial u} = -2(1-C_{T,s})\frac{Nc}{S}C_{D_o}\frac{\partial r_s}{\partial u} - \left[1 - \frac{2Ncr_s}{S}\right]C_{D_o}\frac{\partial C_{T,s}}{\partial u} - \frac{(a\alpha)^2}{\pi R}\frac{\partial C_{T,s}}{\partial u}$$

$$+ \frac{2Nc}{S}C_{D_o}\left[\frac{\partial r_s}{\partial u}\cos(\alpha_p - \phi) + r_s\frac{\partial \phi}{\partial u}\sin(\alpha_p - \phi)\right]$$

$$+ 1.113\frac{ND^2}{S}\left[2(1-\mu^2)^2\left(\frac{r_s}{D}\right)^2 \alpha_s \frac{\partial \phi}{\partial u}\cos(\alpha_p - \phi)\right.$$

$$+ 2(1-\mu^2)^2 \frac{r_s}{D^3} \alpha_s^2 \frac{\partial r_s}{\partial u}\cos(\alpha_p - \phi)$$

$$- 4\mu(1-\mu^2)\left(\frac{r_s}{D}\right)^2 \alpha_s^2 \frac{\partial \mu}{\partial u}\cos(\alpha_p - \phi)$$

$$+ (1-\mu^2)^2\left(\frac{r_s}{D}\right)^2 \alpha_s^2 \frac{\partial \phi}{\partial u}\sin(\alpha_p - \phi)\Bigg]$$

$$+ 3.74\frac{ND^2}{S}\left[(1-\mu^2)\left(\frac{r_s}{D}\right)^2 \frac{\partial \phi}{\partial u}\sin(\alpha_p - \phi)\right.$$

$$+ 2(1-\mu^2)\frac{r_s}{D^3}\alpha_s \frac{\partial r_s}{\partial u}\sin(\alpha_p - \phi)$$

$$- 2\mu\left(\frac{r_s}{D}\right)^2 \alpha_s \frac{\partial \mu}{\partial u}\sin(\alpha_p - \phi)$$

$$- (1-\mu^2)\left(\frac{r_s}{D}\right)^2 \alpha_s \frac{\partial \phi}{\partial u}\cos(\alpha_p - \phi)\Bigg] \tag{62}$$

71

$$\frac{\partial C_{LW}}{\partial \alpha_F} = \frac{\partial C_{LW}}{\partial \alpha_W}$$

$$= a(1 - C_{T,S}) - a\alpha \frac{\partial C_{T,S}}{\partial \alpha_p}$$

$$+ 3.74 \frac{ND^2}{S}\left[(1-\mu^2)\left(\frac{r_S}{D}\right)^2 \frac{\partial \phi}{\partial \alpha_p} \cos(\alpha_p - \phi)\right.$$

$$+ 2(1-\mu^2)\frac{r_S}{D^2}\alpha_S \frac{\partial r_S}{\partial \alpha_p} \cos(\alpha_p - \phi)$$

$$- 2\mu\left(\frac{r_S}{D}\right)^2 \alpha_S \frac{\partial \mu}{\partial \alpha_p} \cos(\alpha_p - \phi)$$

$$\left. - (1-\mu^2)\left(\frac{r_S}{D}\right)^2 \alpha_S \left(1 - \frac{\partial \phi}{\partial \alpha_p}\right) \sin(\alpha_p - \phi)\right]$$

$$- \frac{2Nc}{S}C_{D_0,S} \frac{\partial r_S}{\partial \alpha_p} \sin(\alpha_p - \phi)$$

$$- \frac{2Ncr_S}{S}\frac{\partial C_{D_0,S}}{\partial \alpha_W} \sin(\alpha_p - \phi)$$

$$+ \frac{2Ncr_S}{S}C_{D_0,S}\frac{\partial \phi}{\partial \alpha_p} \cos(\alpha_p - \phi)$$

$$- 1.113 \frac{ND^2}{S}\left[2(1-\mu^2)^2\left(\frac{r_S}{D}\right)^2 \alpha_S \frac{\partial \phi}{\partial \alpha_p} \sin(\alpha_p - \phi)\right.$$

$$+ 2(1-\mu^2)^2 \frac{r_S}{D^2}\alpha_S^2 \frac{\partial r_S}{\partial \alpha_p} \sin(\alpha_p - \phi)$$

$$- 4\mu(1-\mu^2)\left(\frac{r_S}{D}\right)^2 \alpha_S^2 \frac{\partial \mu}{\partial \alpha_p} \sin(\alpha_p - \phi)$$

$$\left. + (1-\mu^2)^2\left(\frac{r_S}{D}\right)^2 \alpha_S^2 \left(1 - \frac{\partial \phi}{\partial \alpha_p}\right) \cos(\alpha_p - \phi)\right] \tag{63}$$

$$\frac{\partial C_{DW}}{\partial \alpha_F} = \frac{\partial C_{DW}}{\partial \alpha_w}$$

$$= -2\left(1-C_{T,s}\right)\frac{Nc}{S}C_{Do}\frac{\partial r_s}{\partial \alpha_p} - 2\left(1-C_{T,s}\right)\frac{Nc\,r_s}{S}\frac{\partial C_{Do}}{\partial \alpha_w}$$

$$-\left[1-\frac{2Nc\,r_s}{S}\right]C_{Do}\frac{\partial C_{T,s}}{\partial \alpha_p} - \frac{(a\alpha)^2}{\pi R}\frac{\partial C_{T,s}}{\partial \alpha_p}$$

$$+\frac{2Nc}{S}C_{Do,s}\frac{\partial r_s}{\partial \alpha_p}\cos(\alpha_p-\phi) + \frac{2Nc\,r_s}{S}\frac{\partial C_{Do,s}}{\partial \alpha_w}\cos(\alpha_p-\phi)$$

$$-\frac{2Nc\,r_s}{S}C_{Do,s}\left(1-\frac{\partial \phi}{\partial \alpha_p}\right)\sin(\alpha_p-\phi)$$

$$+1.113\frac{ND^2}{S}\left[2\left(1-\mu^2\right)^2\left(\frac{r_s}{D}\right)^2\alpha_s\frac{\partial \phi}{\partial \alpha_p}\cos(\alpha_p-\phi)\right.$$

$$+2\left(1-\mu^2\right)^2\frac{r_s}{D}\alpha_s^2\frac{\partial r_s}{\partial \alpha_p}\cos(\alpha_p-\phi)$$

$$-4\mu\left(1-\mu^2\right)\left(\frac{r_s}{D}\right)^2\alpha_s^s\frac{\partial \mu}{\partial \alpha_p}\cos(\alpha_p-\phi)$$

$$\left.-\left(1-\mu^2\right)^2\left(\frac{r_s}{D}\right)^2\alpha_s^2\left(1-\frac{\partial \phi}{\partial \alpha_p}\right)\sin(\alpha_p-\phi)\right]$$

$$+3.74\frac{ND^2}{S}\left[\left(1-\mu^2\right)\left(\frac{r_s}{D}\right)^2\frac{\partial \phi}{\partial \alpha_p}\sin(\alpha_p-\phi)\right.$$

$$+2\left(1-\mu^2\right)\frac{r_s}{D}\alpha_s\frac{\partial r_s}{\partial \alpha_p}\sin(\alpha_p-\phi)$$

$$-2\mu\left(\frac{r_s}{D}\right)^2\alpha_s\frac{\partial \mu}{\partial u}\sin(\alpha_p-\phi)$$

$$\left.+\left(1-\mu^2\right)\left(\frac{r_s}{D}\right)^2\alpha_s\left(1-\frac{\partial \phi}{\partial \alpha_p}\right)\cos(\alpha_p-\phi)\right] \qquad (64)$$

In the above equations,

$$C_{T,s} = \frac{T_p}{q_s \frac{\pi D^2}{4}} \tag{65}$$

$$\frac{\partial C_{T,s}}{\partial u} = C_{T,s}(1 - C_{T,s})\left[\frac{1}{T_p}\frac{\partial T_p}{\partial u} - \frac{2}{V_0}\right] \tag{66}$$

$$\frac{\partial C_{T,s}}{\partial \alpha_p} = \frac{C_{T,s}}{T_p}(1 - C_{T,s})\frac{\partial T_p}{\partial \alpha_p} \tag{67}$$

$$q_s = \frac{q_o}{1 - C_{T,s}} \tag{68}$$

$$\frac{\partial q_s}{\partial u} = q_s\left[\frac{2}{V_0} + \frac{1}{1 - C_{T,s}}\frac{\partial C_{T,s}}{\partial u}\right] \tag{69}$$

$$\frac{\partial q_s}{\partial \alpha_p} = \frac{q_s}{1 - C_{T,s}}\frac{\partial C_{T,s}}{\partial \alpha_p} \tag{70}$$

$$r_s = D\sqrt{\frac{1}{8}\left[\frac{\tan\phi}{\tan\alpha_p} + 1\right]} \qquad (\alpha_p \neq 0) \tag{71}$$

$$\frac{\partial r_s}{\partial u} = \frac{D^2}{16\, r_s \cos^2\phi\, \tan\alpha_p}\frac{\partial \phi}{\partial u} \tag{72}$$

$$\frac{\partial r_s}{\partial \alpha_p} = \frac{D^2}{16\, r_s \cos\phi\, \sin\alpha_p}\left[\frac{\cos\alpha_p}{\cos\phi}\frac{\partial \phi}{\partial \alpha_p} - \frac{\sin\phi}{\sin\alpha_p}\right] \tag{73}$$

$$\phi = \tan^{-1}\left[\frac{\sin\alpha_p}{\sqrt{\cos^2\alpha_p + \frac{C_{T,s}}{1 - C_{T,s}}}}\right] \tag{74}$$

$$\frac{\partial \phi}{\partial u} = -\frac{\sin\alpha_p\,\cos^2\phi}{2\sqrt{(1 - C_{T,s})\left[(1 - C_{T,s})\cos^2\alpha_p + C_{T,s}\right]^3}}\frac{\partial C_{T,s}}{\partial u} \tag{75}$$

74

$$\frac{\partial \phi}{\partial \alpha_p} = \frac{1}{2} \sin 2\phi \left\{ \frac{1}{\tan \alpha_p} + \frac{(1-C_{T,s})^2 \sin 2\alpha_p - \frac{\partial C_{T,s}}{\partial \alpha_p}}{2(1-C_{T,s})\left[(1-C_{T,s})\cos \alpha_p + C_{T,s}\right]} \right\} \tag{76}$$

$$\mu = \sqrt{1-C_{T,s}} \, \cos(\alpha_p - \phi) \tag{77}$$

$$\frac{\partial \mu}{\partial u} = -\frac{\cos(\alpha_p - \phi)}{2\sqrt{1-C_{T,s}}} \frac{\partial C_{T,s}}{\partial u} + \sqrt{1-C_{T,s}} \, \frac{\partial \phi}{\partial u} \, \sin(\alpha_p - \phi) \tag{78}$$

$$\frac{\partial \mu}{\partial \alpha_p} = -\frac{\cos(\alpha_p - \phi)}{2\sqrt{1-C_{T,s}}} \frac{\partial C_{T,s}}{\partial \alpha_p} + \sqrt{1-C_{T,s}} \left[1 - \frac{\partial \phi}{\partial \alpha_p}\right] \sin(\alpha_p - \phi) \tag{79}$$

The drag coefficients, C_{D_o} and $C_{D_o,s}$, are esti-mated by making use of Figure 31 which presents profile drag coefficients of a wing equipped with a Fowler type flap. These data are derived from Reference 4 by sub-tracting the wing induced drag contribution from mea-sured values of the longitudinal force coefficient. It should be noted that the profile drag coefficients of Figure 31 are based on the total wing area including that resulting from the extension of the flap, i.e.,

$$S = b(\bar{c} + c_f) \tag{80}$$

The wing pitching moment, $M_{w_{c/4}}$, and the derivatives, M_{w_u} and M_{w_α} , are based on the data of References 4 and 15.

Propeller Derivatives

The propeller derivatives, T_{p_u} , T_{p_α} , M_{p_u} , M_{p_α} , N_{p_u} , and N_{p_v} , are based on propeller test data such as those of Reference 30. These data are adjusted to account for the effect of wing proximity as indicated by the data of Reference 15.

75
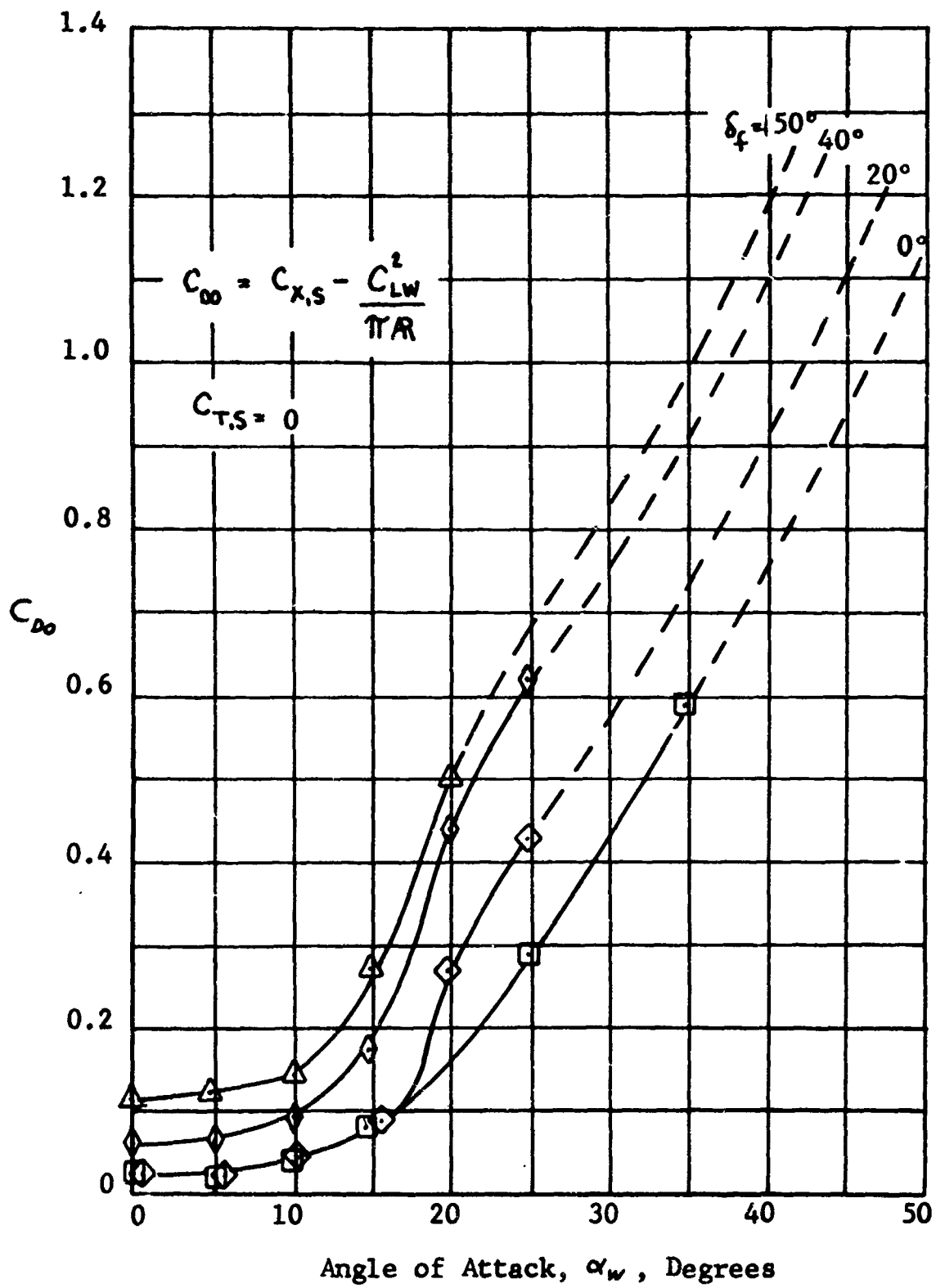
FIGURE 31. Profile Drag Coefficients of a Wing Equipped with a Fowler Type Flap.

76

Horizontal Tail Derivatives

The numerical evaluation of the horizontal tail derivatives is based on the data of Reference 15. These data are reproduced, in part, as Figures 26 and 27. Tail rotor derivatives are obtained from the data of Reference 29 using a tail rotor advance ratio and a tail rotor angle of attack, based on values of ϵ and V_t from Reference 15. In the analysis, consideration was given to the fact that at 30 knots control moments are generated by means of a horizontal tail rotor, and at 70 knots by means of a horizontal tail surface.

Slipstream Stabilizer Derivatives

From Equation (5) it is seen that the angle of attack in the slipstream, α_s , is affected by flap deflection, δ_f . It follows that the lift and drag derivatives of the wing can be readily varied provided that a means for changing α_s is incorporated into the aircraft control system. Accordingly, the use of a wing trailing-edge flap for stability augmentation is investigated. The general flap stabilizer characteristics are described by the following equation:

$$k_4 \delta + k_1 \theta + k_2 \dot{\theta} + k_3 w = 0 \tag{81}$$

Equation (81) includes pitch attitude and rate feedback, $k_1 \theta + k_2 \dot{\theta}$, and vertical velocity feedback, k_3. The appropriate stabilizer derivatives for the three aircraft equations of motion are:

$$\frac{1}{m} \frac{\partial X}{\partial \delta} = \frac{1}{m} \left[-\frac{\partial D_w}{\partial \delta} \right] \tag{82}$$

$$\frac{1}{m} \frac{\partial Z}{\partial \delta} = \frac{1}{m} \left[-\frac{\partial L_w}{\partial \delta} \right] \tag{83}$$

$$\frac{1}{I_{yy}} \frac{\partial M}{\partial \delta} = \frac{1}{I_{yy}} \left[\frac{\partial M_w}{\partial \delta} - \frac{\partial Z}{\partial \delta} x_w - \frac{\partial X}{\partial \delta} z_w \right] \tag{84}$$

77

Values of $\partial L_w/\partial\delta$, $\partial D_w/\partial\delta$ and $\partial M/\partial\delta$ are obtained from the test data of Reference 12.

NUMERICAL VALUES OF DERIVATIVES

The trim conditions for 30 and 60 knots are as follows:

30 Knots

$$
\begin{aligned}
C_{T,S} &= 0.9275 \\
\alpha_w &= \alpha_p = 40 \text{ degrees} \\
\delta_f &= 50 \text{ degrees} \\
W &= 35{,}288 \text{ pounds} \\
T_T &= -650 \text{ pounds } (\text{for } \Sigma M_{c.g.} = 0) \\
C_{L_w} &= 0.516 \\
C_{D_w} &= 0.718 \\
C_{D_o} &= 1.22 \\
C_{\Delta c,s} &= 0.15
\end{aligned}
$$

70 Knots

$$
\begin{aligned}
C_{T,S} &= 0.35 \\
\alpha_w &= \alpha_p = 8 \text{ degrees} \\
\delta_f &= 50 \text{ degrees} \\
W &= 34{,}200 \text{ pounds} \\
L_t &= -2070 \text{ pounds } (\text{for } \Sigma M_{c.g.} = 0) \\
C_{L_w} &= 1.85 \\
C_{D_w} &= 0.313 \\
C_{D_o} &= 0.13 \\
C_{\Delta a,s} &= 0.11
\end{aligned}
$$

The numerical values of the derivatives are summarized in Table V.

TABLE   V
DERIVATIVE SUMMARY

DERIVATIVE	AIRSPEED	
	V_O =30 Knots	V_O=70 Knots
L_{w_u}	220	329
L_{w_α}	-19,966	64,208
D_{w_u}	102	19.18
D_{w_α}	21,108	19,833
T_{p_u}	-10	-41
T_{p_α}	420	620
N_{p_u}	3.5	0
N_{p_α}	160	935
M_{p_u}	60	0
M_{p_α}	8,150	9,980
X_u/m	-0.1293	-0.1677
$X_{\dot u}/m$	-1	-1
X_w/m	-0.0717	0.1186
$X_{\dot w}/m$	0	0
X_θ/m	-32.2	-32.2
$X_{\dot\theta}/m$	0.3936	-0.2070
Z_u/m	-0.1872	-0.2506
$Z_{\dot u}/m$	0	0
Z_w/m	-0.0783	-0.6475
$Z_{\dot w}/m$	-1	-1
Z_θ/m	0	0
$Z_{\dot\theta}/m$	51.38	117.16
M_u/I_{yy}	-0.0027	0.0112
$M_{\dot u}/I_{yy}$	0	0
M_w/I_{yy}	0.0089	-0.0145
$M_{\dot w}/I_{yy}$	0	-0.0006
M_θ/I_{yy}	0	0
$M_{\dot\theta}/I_{yy}$	-0.0260	-0.4345
$M_{\ddot\theta}/I_{yy}$	-1	-1
X_δ/m	-10.62	-16.85
Z_δ/m	-2.32	-17.75
M_δ/I_{yy}	-0.483	-0.948

ANALOG COMPUTER STUDY

The equations utilized in the analog computer study are as follows:

$$\dot{u} - \frac{X_u}{m}u - \frac{X_w}{m}w - \frac{X_{\dot{w}}}{m}\dot{w} - \frac{X_\theta}{m}\theta - \frac{X_{\dot{\theta}}}{m}\dot{\theta} - \frac{X_\delta}{m}\delta = 0 \tag{85}$$

$$\dot{w} - \frac{Z_u}{m}u - \frac{Z_{\dot{u}}}{m}\dot{u} - \frac{Z_w}{m}w - \frac{Z_\theta}{m}\theta - \frac{Z_{\dot{\theta}}}{m}\dot{\theta} - \frac{Z_\delta}{m}\delta = 0 \tag{86}$$

$$\ddot{\theta} - \frac{M_u}{I_{yy}}u - \frac{M_{\dot{u}}}{I_{yy}}\dot{u} - \frac{M_w}{I_{yy}}w - \frac{M_{\dot{w}}}{I_{yy}}\dot{w} - \frac{M_\theta}{I_{yy}}\theta - \frac{M_{\dot{\theta}}}{I_{yy}}\dot{\theta} - \frac{M_\delta}{I_{yy}}\delta = 0 \tag{87}$$

$$k_4\,\delta + k_1\,\theta + k_3\,w = 0 \tag{88}$$

The corresponding machine equations for the 30- and 70-knot conditions are:

30 Knots

$$\left(\frac{\dot{u}}{25}\right) + 0.1293\left(\frac{u}{25}\right) + 0.0717\left(\frac{w}{25}\right) + 0.1288\left(\frac{\theta}{0.4}\right) - 0.00629\left(\frac{\dot{\theta}}{0.4}\right) + 0.425\left(\frac{\delta}{1}\right) = 0 \tag{89}$$

$$\left(\frac{\dot{w}}{25}\right) + 0.1872\left(\frac{u}{25}\right) + 0.0783\left(\frac{w}{25}\right) - 0.8221\left(\frac{\dot{\theta}}{0.4}\right) + 0.0927\left(\frac{\delta}{1}\right) = 0 \tag{90}$$

$$\left(\frac{\ddot{\theta}}{0.4}\right) + 0.1689\left(\frac{u}{25}\right) - 0.5560\left(\frac{w}{25}\right) + 0.0260\left(\frac{\dot{\theta}}{0.4}\right) + 1.207\left(\frac{\delta}{1}\right) = 0 \tag{91}$$

$$k_4\left(\frac{\delta}{1}\right) + 0.4\,k_1\left(\frac{\theta}{0.4}\right) + 25\,k_3\left(\frac{w}{25}\right) = 0 \tag{92}$$

80

70 Knots

$$\left(\frac{\dot{u}}{59}\right)+0.1677\left(\frac{u}{59}\right)-0.1186\left(\frac{w}{59}\right)+0.2183\left(\frac{\theta}{0.4}\right)+0.0014\left(\frac{\dot{\theta}}{0.4}\right)+0.2856\left(\frac{\delta}{1}\right)=0 \qquad (93)$$

$$\left(\frac{\dot{w}}{59}\right)+0.2506\left(\frac{u}{59}\right)+0.6475\left(\frac{w}{59}\right)-0.7943\left(\frac{\dot{\theta}}{0.4}\right)+0.3008\left(\frac{\delta}{1}\right)=0 \qquad (94)$$

$$\left(\frac{\ddot{\theta}}{0.4}\right)-1.648\left(\frac{u}{59}\right)+2.145\left(\frac{w}{59}\right)+0.6981\left(\frac{w}{59}\right)+0.4345\left(\frac{\dot{\theta}}{0.4}\right)+2.37\left(\frac{\delta}{1}\right)=0 \qquad (95)$$

$$k_4\left(\frac{\delta}{1}\right)+0.4\,k_1\left(\frac{\theta}{0.4}\right)+59\,k_3\left(\frac{w}{59}\right)=0 \qquad (96)$$

The computer schematic, applicable to both the 30- and 70-knot conditions is presented in Figure 32. The values of the potentiometer settings are shown in Table VI.

Computer Solution at 30 Knots

The response of the unstabilized aircraft to a pulse disturbance, δ , is shown in Figure 33. It is noted that the response consists of an unstable aperiodic mode with a time to double of 0.9 seconds.

The effect of a number of combinations of stabilizer settings is now discussed.

The stabilizer system investigated is described by the following equation:

$$\delta + k_1\theta + k_3 w = 0 \qquad (97)$$

The effectiveness of the various stabilizers analyzed was determined by examining the aircraft transient response to a pulse input of the flap deflection, δ .

The use of only vertical velocity feedback, i.e., $k_1 = 0$, in Equation (97), results in the responses presented in Figures 34 and 35 for two values of k_3. For $k_3 = -0.08$, Figure 34, the predominant mode is an unstable oscillation having a period of 13 seconds and a time to double amplitude of 4 seconds. For $k_3 = -0.16$, Figure 35, the aircraft exhibits a stable oscillatory mode having a period of 4 seconds and a time to half amplitude of 2.8 seconds. Hence, a vertical velocity feedback with suitable gain, which for forward flight conditions is equivalent to an angle of attack feedback, can be used to obtain positive dynamic stability at 30 knots.
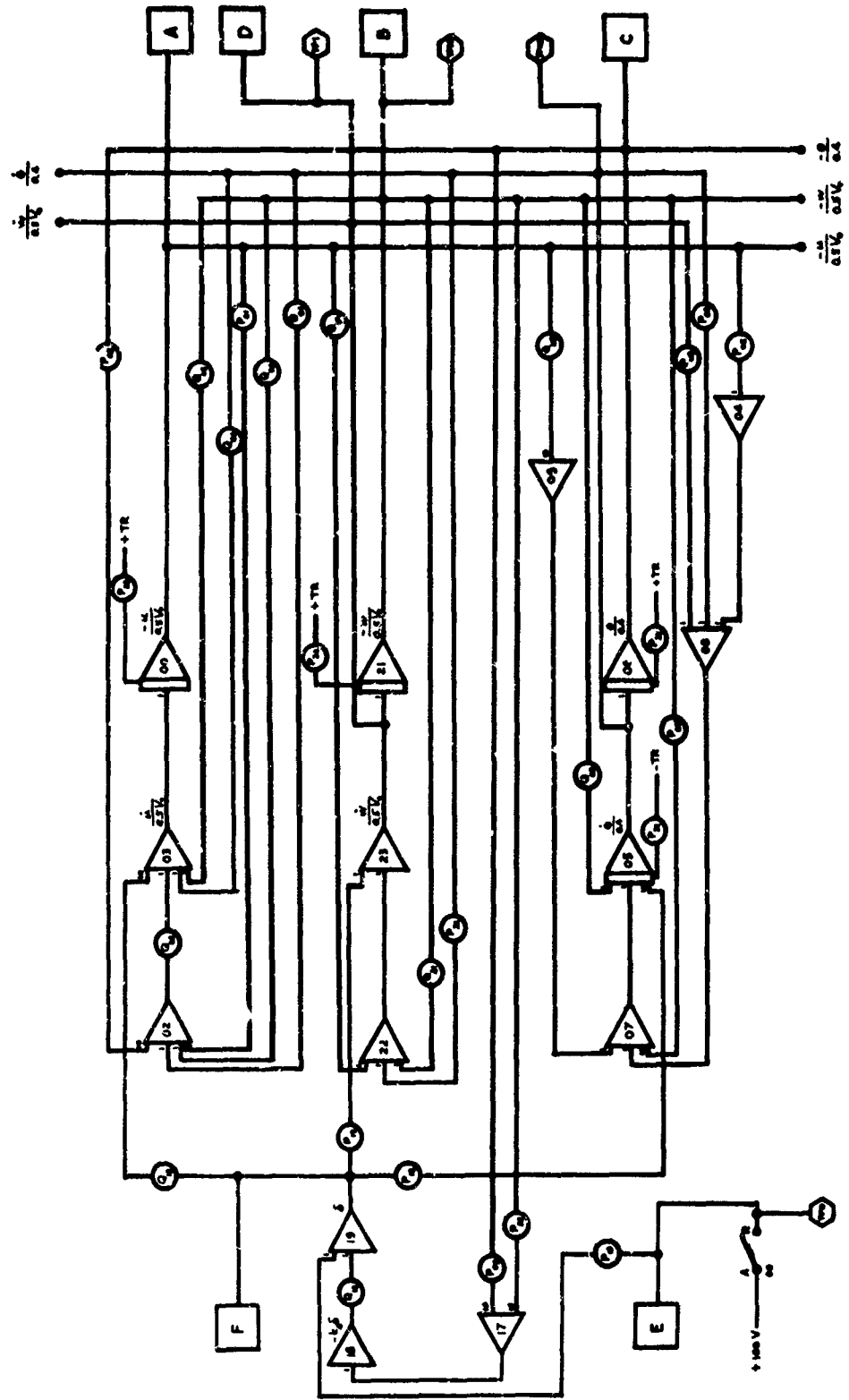
FIGURE 32. Analog Computer Schematic for VTOL Longitudinal Stability

TABLE   VI
ANALOG COMPUTER POTENTIOMETER SETTINGS
FOR VTOL LONGITUDINAL STABILITY ANALYSIS
(WITHOUT STABILIZER)

| POTENTIOMETER | POTENTIOMETER SETTING* | |
NUMBER	30-Knot Airspeed	70-Knot Airspeed
Q_{00}	0.7170	0
P_{01}	0.1293	0.1677
Q_{01}	0.0629	0
P_{02}	0.5152	0.2183
Q_{02}	0.1000	0.1000
Q_{03}	0	0.1186
Q_{04}	0	0.0014
P_{05}	0.1689	0
Q_{05}	0.5560	0
P_{07}	0	0.2145
Q_{07}	0	0.1648
P_{08}	0.0260	0.4345
Q_{08}	0	0.0881
P_{13}	0.0100	0.0100
P_{18}	0.1207	0.2370
P_{19}	0.0927	0.3008
Q_{19}	0.0425	0.0286
P_{21}	0.8221	0.7943
Q_{21}	0.0783	0.6475
Q_{22}	0.1872	0.2506

*The remaining potentiometers shown in Figure 32 were
used to simulate the stabilizer or for static check.
Hence, they were set at zero for the unstabilized flight
conditions.
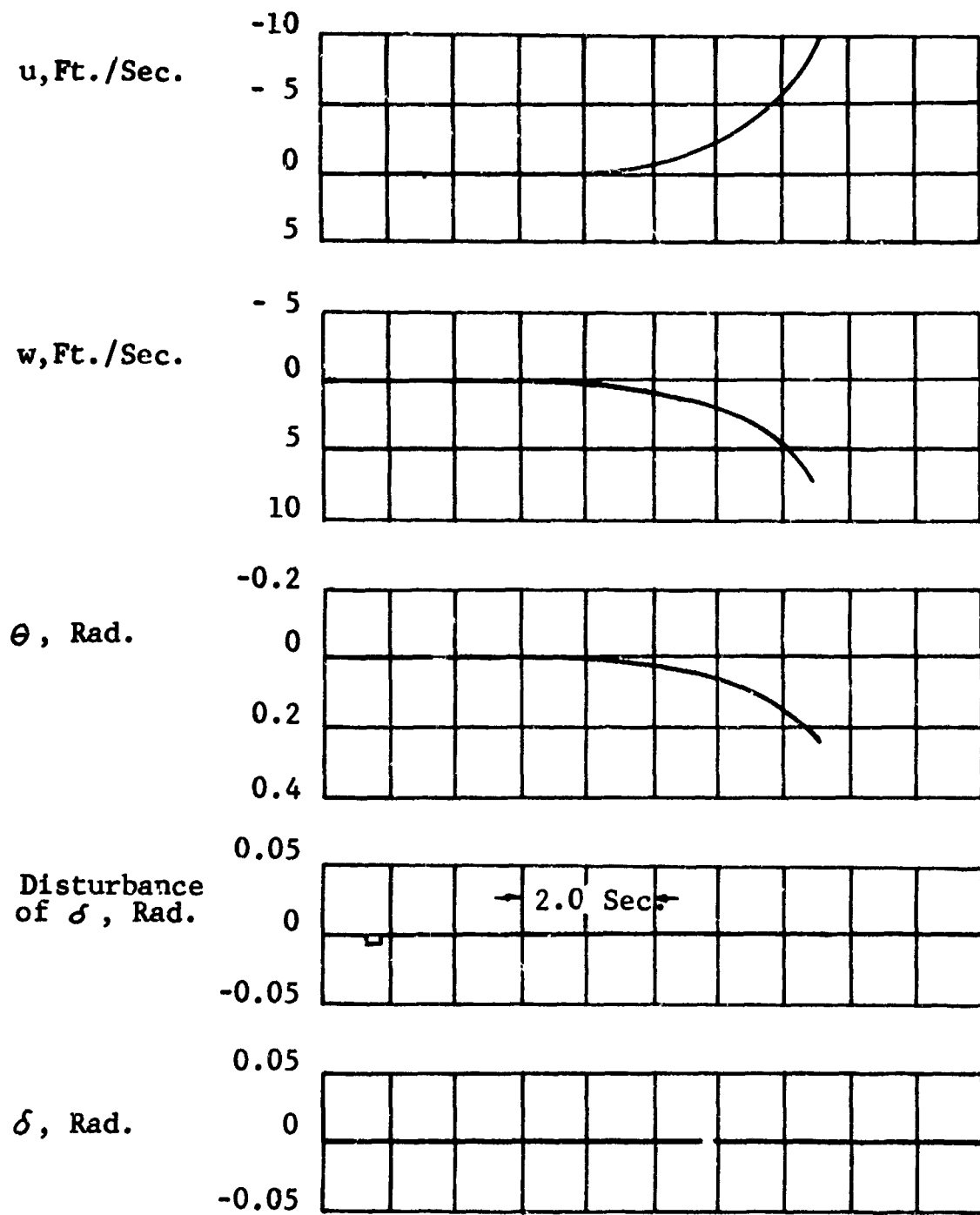
FIGURE 33. Transient Response of Unstabilized Aircraft
to a Pulse Disturbance (V_o = 30 Knots).

84
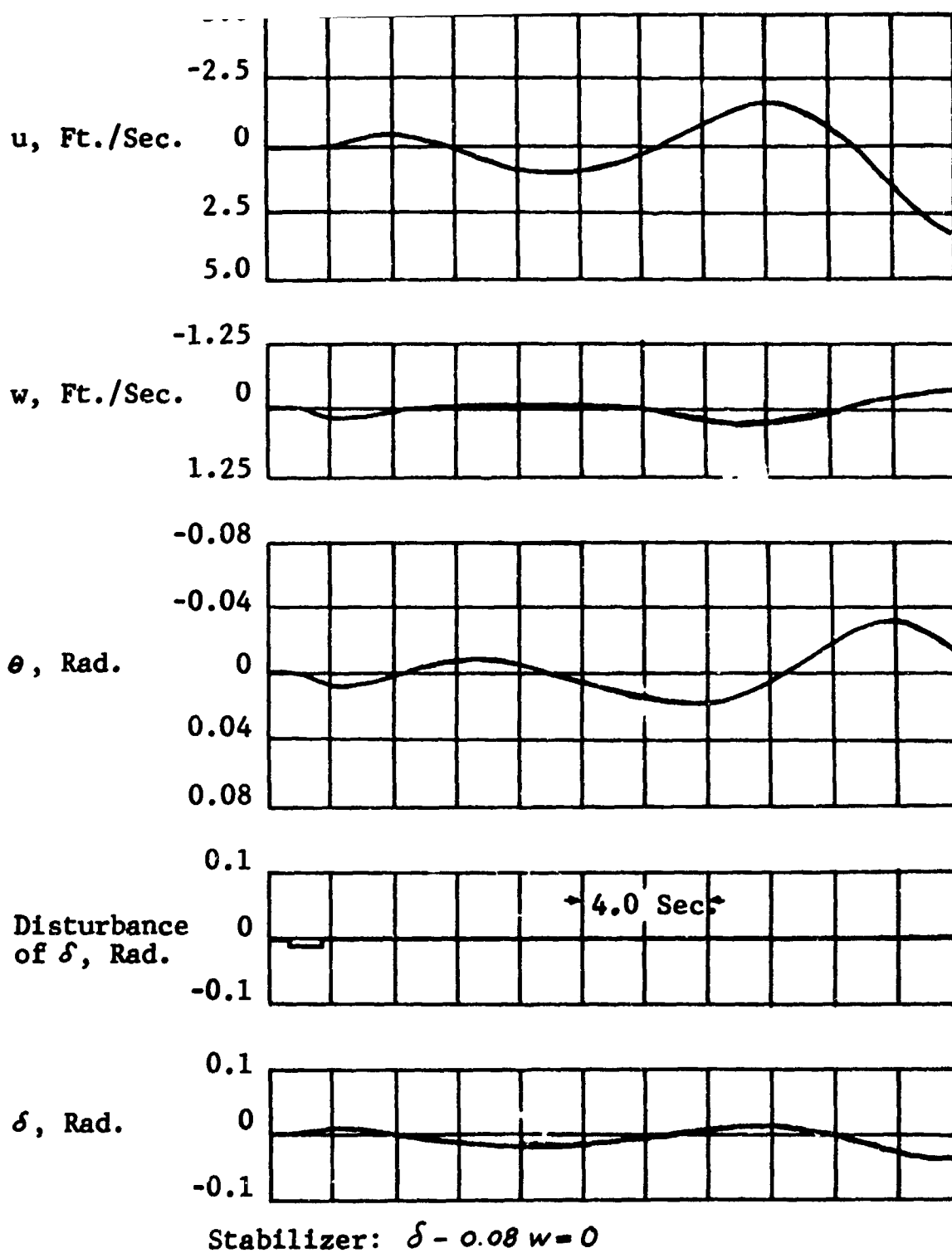
FIGURE 34. Transient Response with Vertical Velocity Feedback Stabilization (V_o = 30 Knots).

85
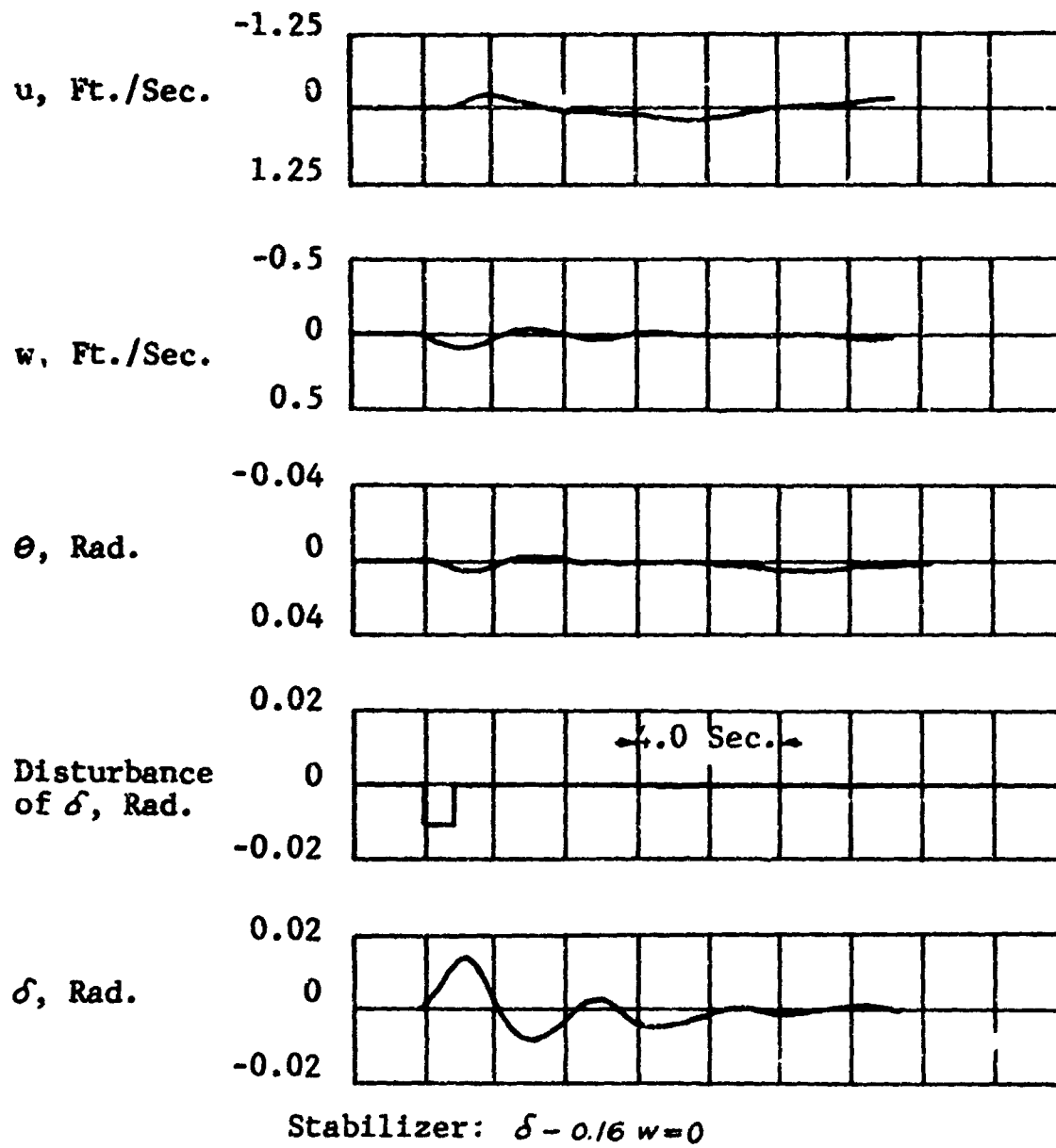
FIGURE 35. Transient Response with Vertical Velocity Feedback Stabilization (V_o = 30 Knots).

86

The effect of using attitude stabilization, i.e., $k_3 = 0$ in Equation (97), can be seen from Figures 36, 37, and 38 for $k_1 = -3.75, -7.5,$ and -15, respectively.

Figure 36, the aircraft longitudinal motion consists of a slightly stable oscillatory mode with a period of 3.5 seconds and an aperiodic mode with a time to double amplitude of about 3 seconds.

An increase in the gain of the attitude stabilization to $k_1 = -7.5$ as shown in Figure 37, results in a decrease in the instability of the aperiodic mode which now has a time to double amplitude of 4.5 seconds. The period of oscillation is reduced to 2.4 seconds.

A further increase in the gain of the attitude stabilization to $k_1 = -15$ as shown in Figure 38, results in the aircraft neutral stability with an oscillatory mode having a period of 1.6 seconds. The stabilizer equation for this case is given by

$$\delta - 15\theta = 0 \qquad\qquad (98)$$

Thus, it can be inferred that an attitude feedback stabilizer with a gain ($k_1 < -15$) could be used to obtain positive dynamic stability at aircraft transition speed of $V_0 = 30$ knots. It can be noted however, comparing Figures 35 and 38, that the vertical velocity feedback ($k_1 = -0.08$ and $k_3 = 0$) provides a more effective means of stabilization with lower gains required.

The transient response of the aircraft with both "w" and "θ" feedback is shown in Figure 39. The stabilizer for this case is given by

$$\delta - 15\theta - 0.32w = 0 \qquad\qquad (99)$$

It can be seen that the aircraft becomes very stable with this type of stabilization.

The effect of propeller normal force and pitching moment derivatives $N_{p\alpha}$ and $M_{p\alpha}$ is seen in Figure 40. The aircraft response is similar to that of the basic aircraft, Figure 33. However, the use of reduced values of $N_{p\alpha}$ and $M_{p\alpha}$ results in slightly less instability of aircraft response, i.e., the time to double amplitude in this case is 1.2 seconds as compared with 0.9 seconds for the basic aircraft.

87

Stabilizer: $\delta - 375 \, \theta = 0$
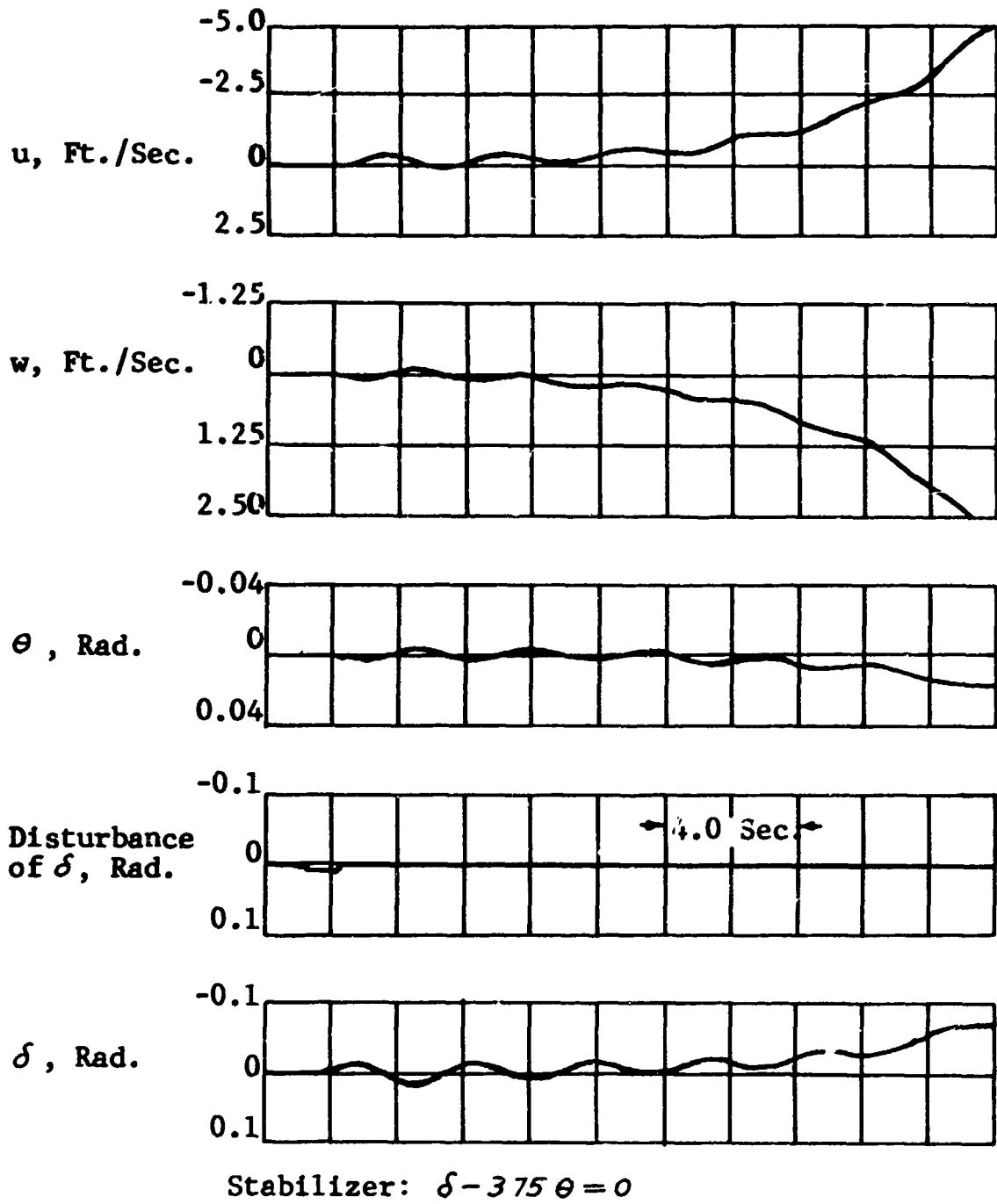
FIGURE 36. Transient Response with Attitude Feedback
Stabilization (V_o = 30 Knots).

88

FIGURE 37. Transient Response with Attitude Feedback Stabilization (V_0 = 30 Knots).
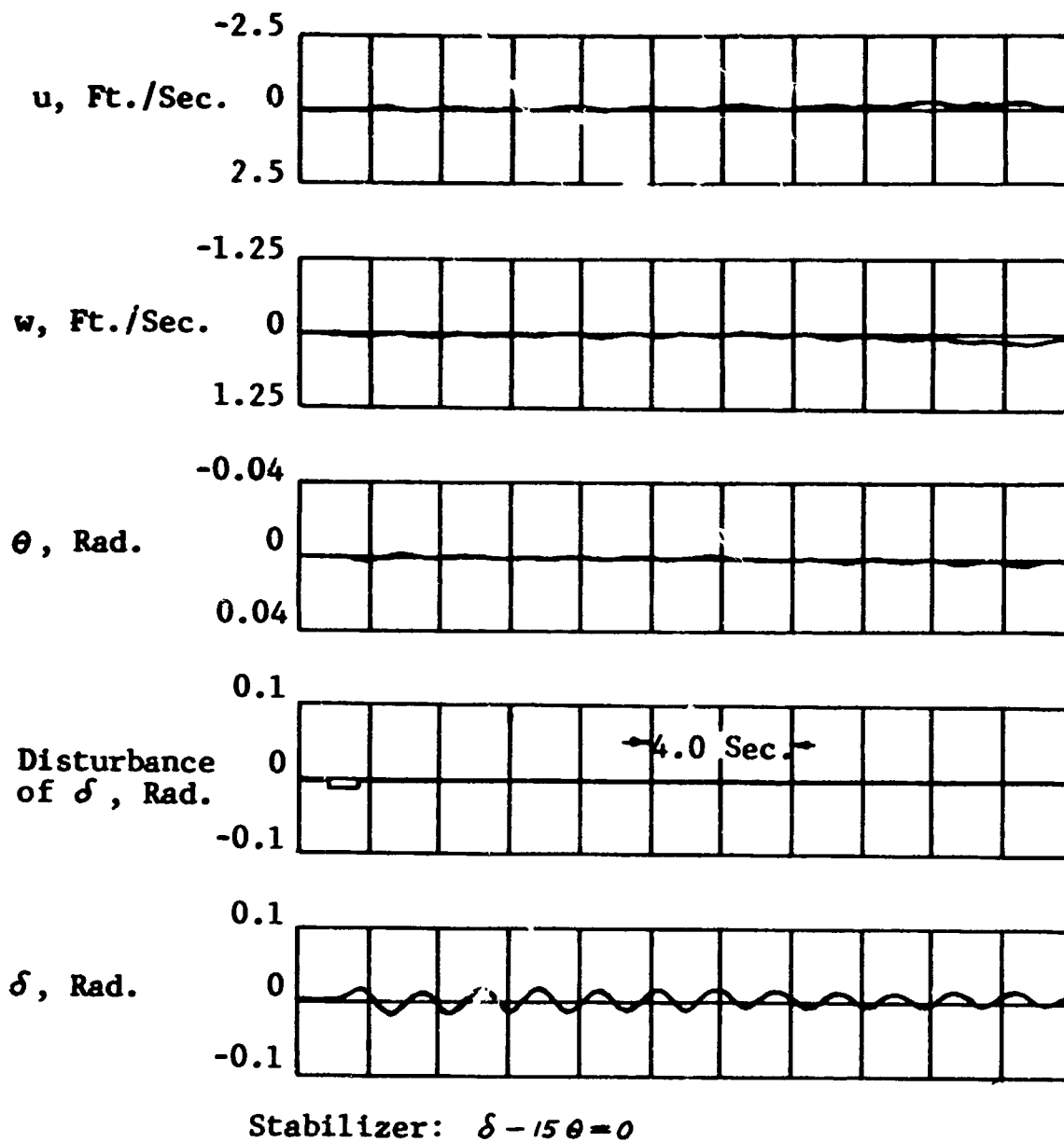
Stabilizer: $\delta - 15\theta = 0$

FIGURE 38. Transient Response with Attitude Feedback
Stabilization (V_O = 30 Knots).

Stabilizer: $\delta - 15\theta - 0.32w = 0$
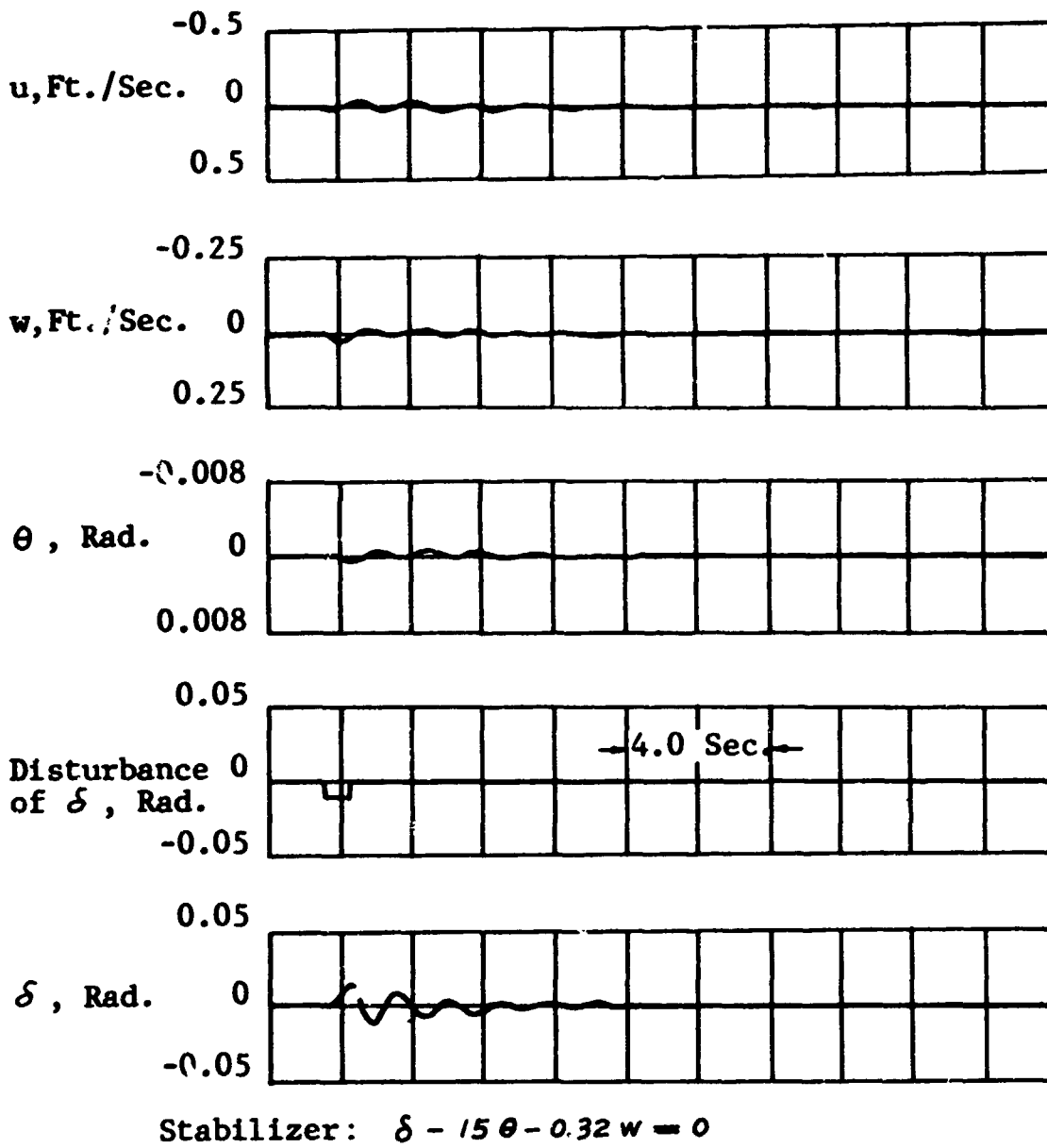
FIGURE 39. Transient Response with Vertical Velocity and Attitude Feedback Stabilization (V_o = 30 Knots).

u, Ft./Sec.

-1.5
-1.0
-0.5
0

w, Ft./Sec.

0
0.25
0.50
0.75

Θ, Rad.

0
0.008
0.016
0.024

Disturbance of δ, Rad.

0.05
0
-0.05

$\vdash$-2.0Sec.$\vdash$

δ, Rad.

0.05
0
-0.05
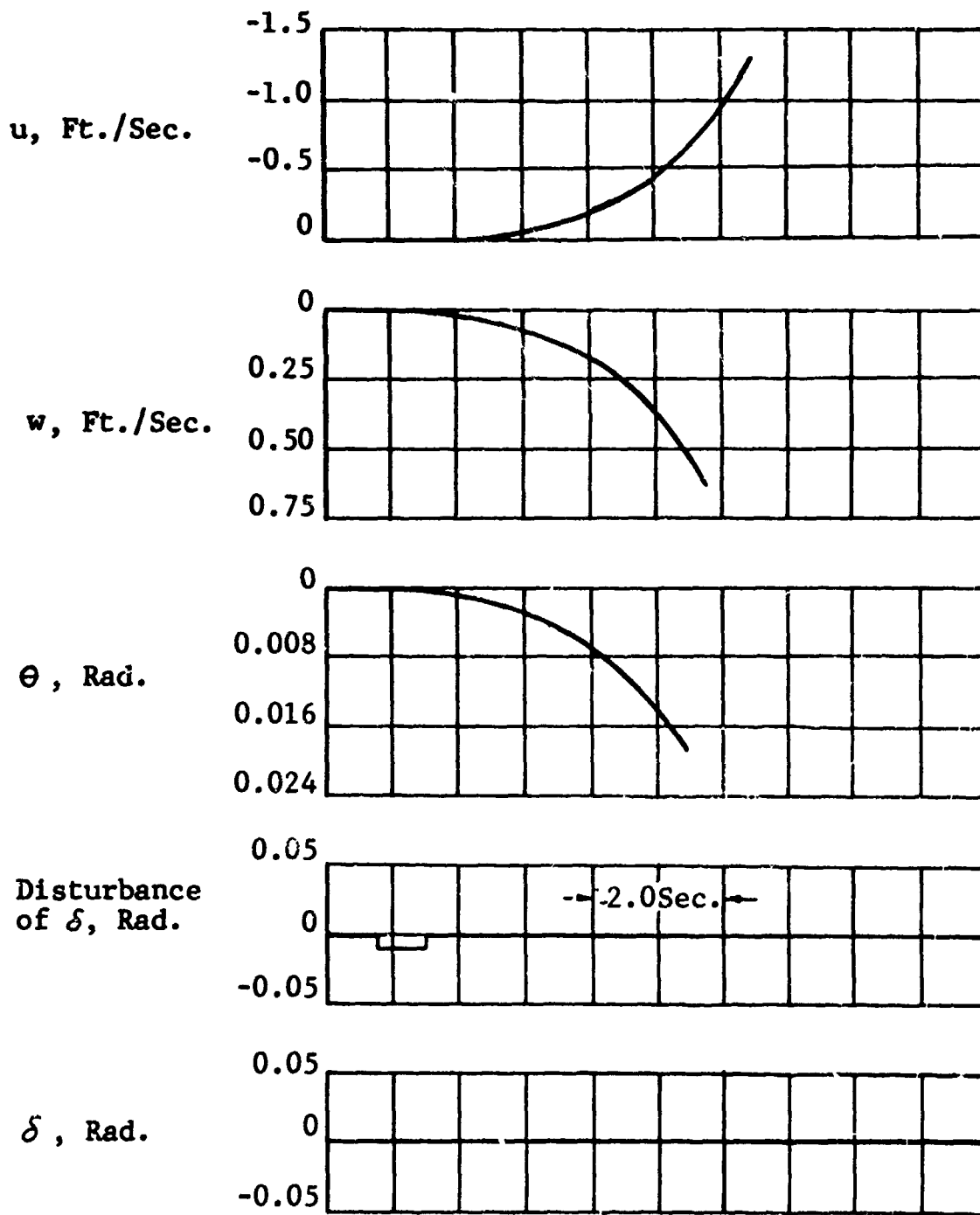
FIGURE 40. Transient Response of the Unstabilized Aircraft with Reduced Values of N_{p_α} and M_{p_α} (V_o= 30 Knots).

Computer Solution at 70 Knots

The basic, unstabilized, aircraft response to a pulse disturbance is shown in Figure 41. As expected, the response for this flight condition is similar to that of a typical fixed-wing aircraft. The aircraft response consists of a long period oscillation (phugoid mode) with a period of 10 seconds and a time to half amplitude of 9 seconds.

The use of a stabilizer corresponding to

$$\delta - 15\theta - 0.169\, w = 0 \qquad\qquad (100)$$

results in the response shown in Figure 42. As noted from this Figure, the response is very rapid and stable.

Correlation with Experimental Data

The calculations made herein can be compared only qualitatively with existing test data. Available data, such as those of Reference 17, and still unpublished data obtained from the Princeton University long track facility, are for model aircraft with scaled-up gross weights and moments of inertia which substantially exceed the design values utilized herein. However, the trend shown in the present calculations agrees with the experimental data, in that the instability exhibited at low speeds is gradually reduced as the speed increases.

Conclusions

From the above analog computer study, it may be concluded that propeller slipstream can be used to augment the dynamic stability of a tilt-wing VTOL aircraft throughout the entire transition flight regime. This includes the hovering condition as reported in Reference 3. It is noted that a combination of attitude and angle-of-attack feedback results in stable responses both at 30 and 70 knots.
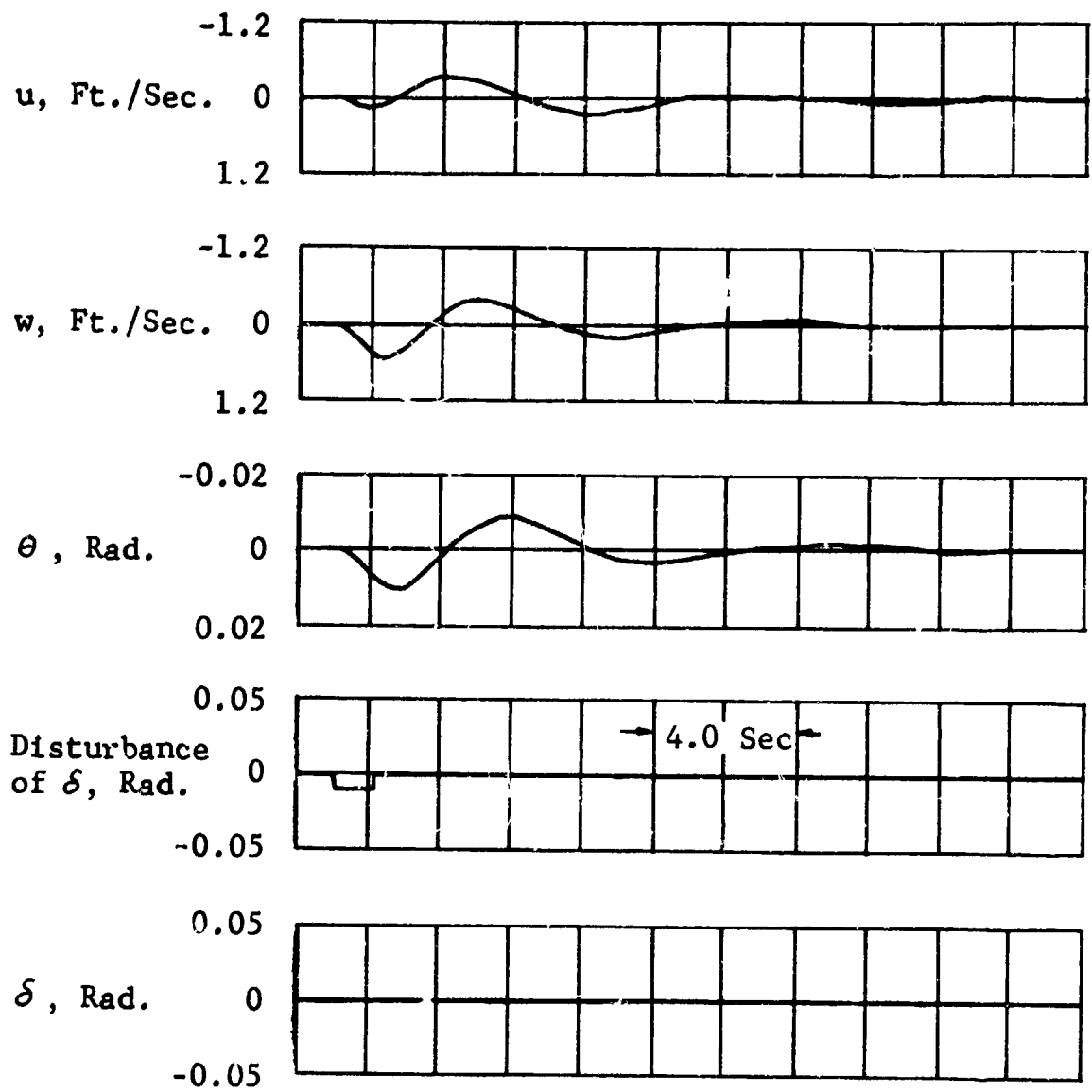
FIGURE 41. Transient Response of the Unstabilized Aircraft to a Pulse Disturbance (V_o = 70 Knots).

94
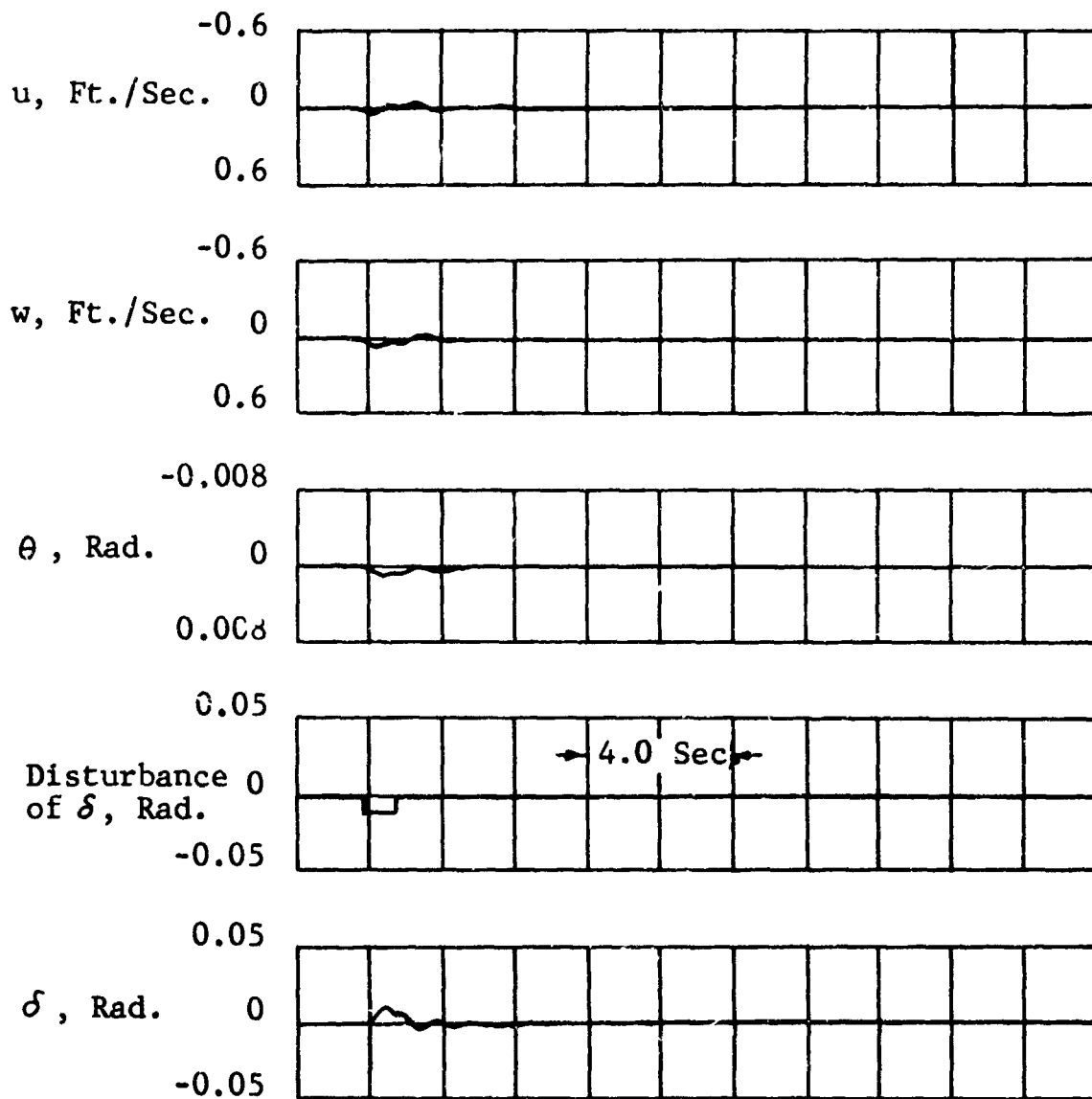
FIGURE 42. Transient Response with Vertical Velocity and Attitude Feedback Stabilization (V_o = 70 Knots).

95

This section presents the results of an analytical study of the effect of the nonuniformity of the velocity of a jet o.. the lift coefficient of an immersed wing.

The equation of the lift coefficient for a rectangular wing totally immersed in a circular jet, as presented in Reference 3, is

$$C_{L_w} = \frac{8\, r_s\, \alpha}{\pi\, c}\left[1 + \frac{1}{2\mu}\left(\frac{\pi^2}{4} - 1\right)\right] \qquad (101)$$

where α = angle of attack, radians
  r_s = radius of the jet, feet
  c = chord of the wing, feet
  μ = ratio of free-stream to jet velocity

This equation has been derived with the assumption that the velocity of the jet is uniform throughout any cross section perpendicular to the direction of flow. In that case there exists a single velocity potential in the jet, Φ_j , which satisfies Laplace's equation and is also subject to the jet boundary conditions.

In extending the theory to cover a jet with non-uniform velocity distribution, it is necessary that the velocity pattern is such that tne jet flow is still a potential one. A flow with a number of concentric velocity zones in each of which the velocity is uniform, such as illustrated in Figure 43, meets this requirement.

In this particular case, the whole jet is considered to consist of four separate concentric "sub-jets", in each of which there exists a velocity potential. Each potential has to satisfy its own boundary conditions.

Velocity Zones

Velocity Pattern
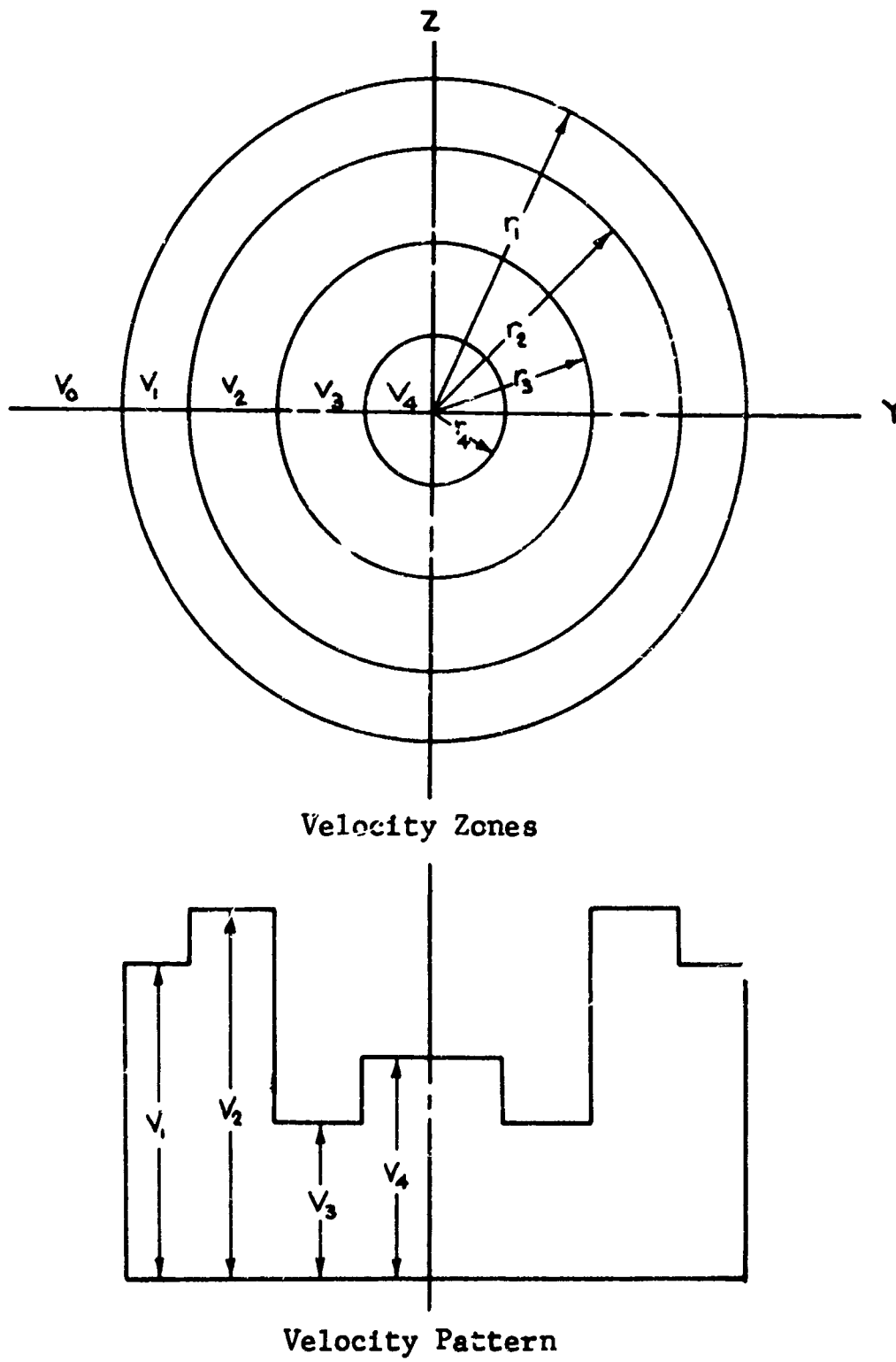
FIGURE 43 . Circular Jet with Four Concentric Velocity Zones.

As can be expected, the velocity potentials of the various concentric "sub-jets" will by no means be in a simple form similar to that presented in Reference 3. This is due to the fact that far more complex boundary conditions are involved. It is thus preferable to consider first the simplest case, where only two velocity zones exist, as shown in Figure 44.

In this case the jet consists of two separate concentric "sub-jets", having velocity potentials Φ_1 and Φ_2, due to which resultant velocities V_1 and V_2 occur respectively.

Before going further, it will be necessary to determine the resultant flow velocity pattern of such a jet from a given induced velocity pattern. As it is desired to determine the effect of the nonuniformity of the jet velocity distribution on the wing lift coefficient, a uniform jet with the same thrust and outside radius is taken for comparison. From Reference 3, it is seen that the thrust of a jet is

$$T = \frac{\rho}{2}\left(V_j^2 - V_0^2\right)A_j$$

$$= \frac{\rho}{2}\left[\left(V_0 + U\right)^2 - V_0^2\right]A_j \tag{102}$$

where
ρ = mass density of air, slugs per cubic foot
V_j = jet velocity, feet per second
V_0 = free-stream velocity, feet per second
A_j = cross sectional area of the jet, square feet
U = induced velocity of the jet, feet per second

Hence, if the thrust remains unchanged,

$$\left(V_0 U + \frac{U^2}{2}\right)A_j = \text{constant} \tag{103}$$
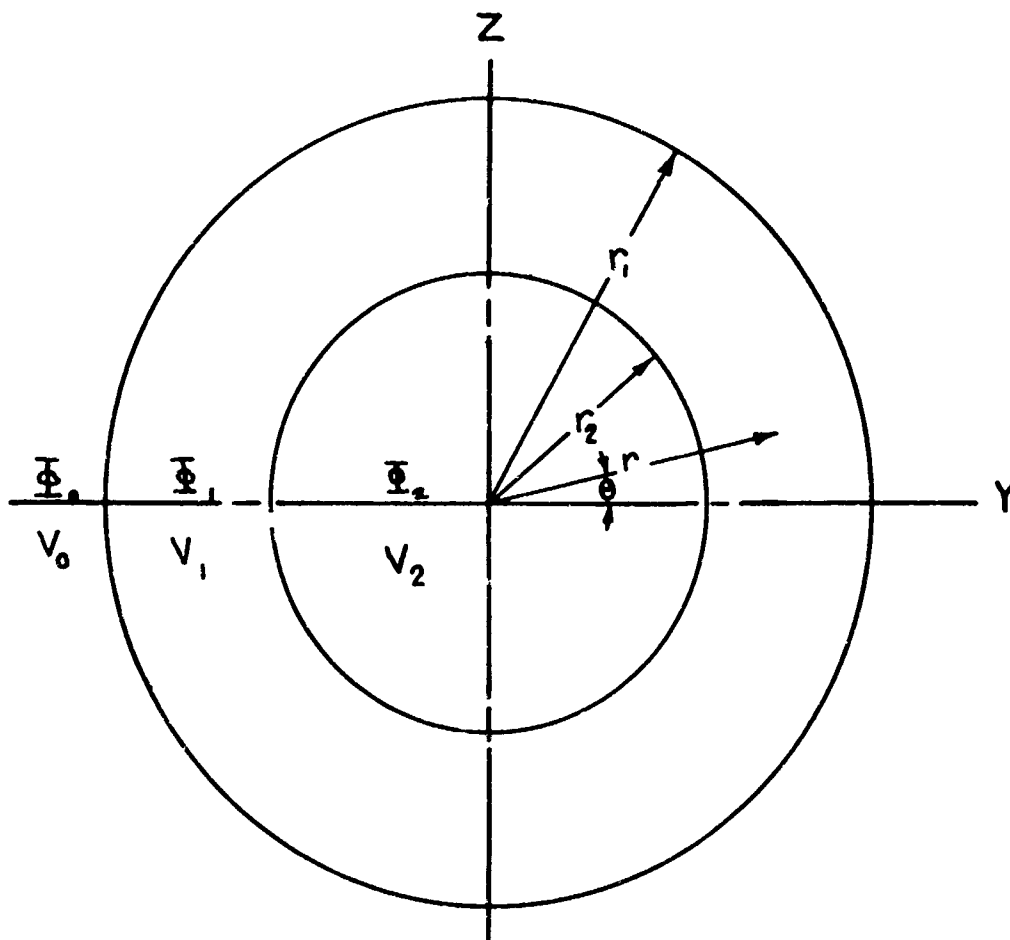
Velocity Zones
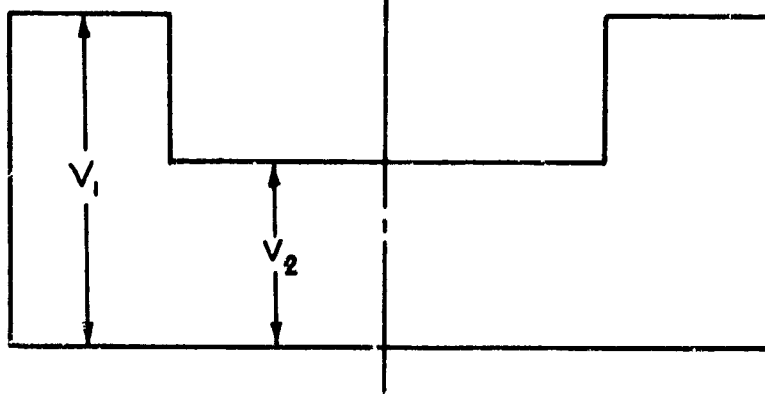
Velocity Pattern

FIGURE 44. Circular Jet with Two Concentric Velocity Zones.

99

By defining

$\overline{U}$ = induced velocity of the uniform jet, feet per second

U_1 = induced velocity in the outer velocity zone of the nonuniform jet, feet per second

U_2 = induced velocity in the inner velocity zone of the nonuniform jet, feet per second

r_1 = radius of the uniform jet and also radius of the nonuniform jet, feet per second

r_2 = radius at the common boundary of the two velocity zones of the nonuniform jet, feet per second

it follows that

$$\left(V_0 U_1 + \frac{U_1^2}{2}\right)\pi\left(r_1^2 - r_2^2\right) + \left(V_0 U_2 + \frac{U_2^2}{2}\right)\pi r_2^2 = \left(V_0 \overline{U} + \frac{\overline{U}^2}{2}\right)\pi r_1^2 \qquad (104)$$

This equation can be rewritten as

$$\left(V_0 U_1 + \frac{U_1^2}{2}\right)\pi\left[r_1^2 - (\eta r_1)^2\right] + \left[V_0 (\gamma U_1) + \frac{(\gamma U_1)^2}{2}\right]\pi(\eta r_1)^2 = \left(V_0 \overline{U} + \frac{\overline{U}^2}{2}\right)\pi r_1^2 \qquad (105)$$

where

$$\eta = \frac{r_2}{r_1}$$

$$\gamma = \frac{U_2}{U_1}$$

100

Upon introducing the following nondimensionalized variables,

$$\bar{U}' = \frac{U}{V_0}$$

$$U_1' = \frac{U_1}{V_0}$$

$$U_2' = \frac{U_2}{V_0}$$

Equation (105) is transformed into

$$U_1'^2 + \frac{2[1-\eta^2(1-\gamma)]}{1-\eta^2(1-\gamma^2)} U_1' - \frac{\bar{U}'(2+\bar{U}')}{1-\eta^2(1-\gamma^2)} = 0 \tag{106}$$

The solution of Equation (106) is

$$U_1' = -\frac{1-\eta^2(1-\gamma)}{1-\eta^2(1-\gamma^2)} + \sqrt{\left[\frac{1-\eta^2(1-\gamma)}{1-\eta^2(1-\gamma^2)}\right]^2 + \frac{\bar{U}_1'(2+\bar{U}')}{1-\eta^2(1-\gamma^2)}} \tag{107}$$

and it follows that

$$U_2' = \gamma \left\{ -\frac{1-\eta^2(1-\gamma)}{1-\eta^2(1-\gamma^2)} - \sqrt{\left[\frac{1-\eta^2(1-\gamma)}{1-\eta^2(1-\gamma^2)}\right]^2 - \frac{\bar{U}'(2+\bar{U}')}{1-\eta^2(1-\gamma^2)}} \right\} \tag{108}$$

Furthermore, by defining

$$\mu = \frac{V_0}{V_0 + \bar{U}} = \frac{1}{1+\bar{U}'} \tag{109}$$

$$\mu_1 = \frac{V_0}{V_0 + U_1} = \frac{1}{1+U_1'} \tag{110}$$

$$\mu_2 = \frac{V_0}{V_0 + U_2} = \frac{1}{1+U_2'} \tag{111}$$

101

it is possible to evaluate μ_1 and μ_2 in terms of $\bar{\mu}$, η and γ as a result of the use of Equations (107) and (108), as follows:

$$\mu_1 = \cfrac{1}{1 + \left\{ -\cfrac{1-\eta^2(1-\gamma)}{1-\eta^2(1-\gamma^2)} + \sqrt{\left[\cfrac{1-\eta^2(1-\gamma)}{1-\eta^2(1-\gamma^2)}\right]^2 + \cfrac{1-\bar{\mu}^2}{\bar{\mu}^2\left[1-\eta^2(1-\gamma^2)\right]}} \right\}} \qquad (112)$$

$$\mu_2 = \cfrac{1}{1 + \gamma\left\{ -\cfrac{1-\eta^2(1-\gamma)}{1-\eta^2(1-\gamma^2)} + \sqrt{\left[\cfrac{1-\eta^2(1-\gamma)}{1-\eta^2(1-\gamma^2)}\right]^2 + \cfrac{1-\bar{\mu}^2}{\bar{\mu}^2\left[1-\eta^2(1-\gamma^2)\right]}} \right\}} \qquad (113)$$

The new boundary conditions for the jet with two velocity zones are as follows:

$$\frac{\partial \Phi_1}{\partial z} = -V_1\alpha \quad \text{at} \quad z = 0 \text{ and } r_2 \le y \le r_1 \qquad (114)$$

$$\frac{\partial \Phi_2}{\partial z} = -V_2\alpha \quad \text{at} \quad z = 0 \text{ and } 0 \le y \le r_2 \qquad (115)$$

$$V_1 \frac{\partial \Phi_0}{\partial r} = V_0 \frac{\partial \Phi_1}{\partial r} \quad \text{at} \quad r = r_1 \qquad (116)$$

$$V_1 \Phi_1 = V_0 \Phi_0 \quad \text{at} \quad r = r_1 \qquad (117)$$

$$V_2 \frac{\partial \Phi_1}{\partial r} = V_1 \frac{\partial \Phi_2}{\partial r} \quad \text{at} \quad r = r_2 \qquad (118)$$

$$V_2 \Phi_2 = V_1 \Phi_1 \quad \text{at} \quad r = r_2 \qquad (119)$$

102

$$\Phi_0 = 0 \text{ as } r \rightarrow \infty \tag{120}$$

$$\Phi_2 \text{ finite at } r = 0 \tag{121}$$

The general solution of Laplace's equation in polar coordinates, i.e.,

$$\frac{\partial^2 \Phi}{\partial r^2} + \frac{1}{r}\frac{\partial \Phi}{\partial \theta} + \frac{1}{r^2}\frac{\partial^2 \Phi}{\partial \theta^2} = 0 \tag{122}$$

is

$$\Phi = \sum_{m=0}^{\infty}\left[a_m r^m \cos m\theta + b_m r^m \sin m\theta + c_m r^{-m}\cos m\theta + d_m r^{-m}\sin m\theta \right] \tag{123}$$

It can be shown that by satisfying the above boundary conditions, the respective velocity potentials of the two zones at the wing surface are

$$\Phi_{I_s} = \frac{2(1+\mu_1^2)V_0 r_1 \alpha}{\pi \mu_1}$$

$$+ \frac{4V_0 r_1 \alpha}{\pi \mu_1}\sum_{m=2,4,\cdots}^{\infty}\left[\frac{(1-\mu_1^2)(\mu_1^2-\mu_2^2)\left(\frac{r_1}{r_1}\right)^m - (1+\mu_1^2)(\mu_1^2+\mu_2^2)\left(\frac{r_1}{r_1}\right)}{(1+\mu_1^2)(\mu_1^2+\mu_2^2)+(1-\mu_1^2)(\mu_1^2-\mu_2^2)\left(\frac{r_1}{r_1}\right)^{2m}} \right]\frac{\bar{y}^m}{m^2-1}$$

$$+ \frac{4V_0 r_1 \alpha}{\pi \mu_1}\sum_{m=2,4,\cdots}^{\infty}\left[\frac{(1+\mu_1^2)(\mu_1^2-\mu_2^2)\left(\frac{r_1}{r_1}\right)^m + (1+\mu_1^2)(\mu_2^2-\mu_1^2)\left(\frac{r_1}{r_1}\right)\left(\frac{r_1}{r_1}\right)^{2m}}{(1+\mu_1^2)(\mu_1^2+\mu_2^2)+(1-\mu_1^2)(\mu_1^2-\mu_2^2)\left(\frac{r_1}{r_1}\right)^{2m}} \right]\frac{1}{(m^2-1)\bar{y}^m} \tag{124}$$

where

$$\bar{y} = \frac{r}{r_1}$$

and

$$\frac{r_2}{r_1} \leq \bar{y} \leq 1$$

$$\Phi_{d_5} = \frac{2V_0\alpha}{\pi}\left[\frac{\mu_2}{\mu_1^2}(1+\mu_1^2)r_1 + \frac{1}{\mu_1^2\mu_2}(\mu_1^2-\mu_2^2)r_2\right]$$

$$+ \frac{4V_0 r_2 \alpha}{\pi\mu_2}\sum_{m=2,4\cdots}^{\infty}\left[\frac{(1+\mu_1^2)(\mu_2^2-\mu_1^2)\left(\frac{r_1}{r_2}\right)^m + (1-\mu_1^2)(\mu_2^2-\mu_1^2)\left(\frac{r_2}{r_1}\right)^m - 2(1+\mu_1^2)\mu_2^2\left(\frac{r_1}{r_2}\right)}{(1+\mu_1^2)(\mu_1^2+\mu_2^2) + (1-\mu_1^2)(\mu_1^2-\mu_2^2)\left(\frac{r_2}{r_1}\right)^{2m}}\right]\frac{\bar{y}^m}{m^2-1} \qquad (125)$$

where

$$0 \leq \bar{y} \leq \frac{r_2}{r_1}$$

It is seen that the second item in the denominator of the general expression of the infinite series appearing in Equations (124) and (125), viz. $(1-\mu_1^2)(\mu_1^2-\mu_2^2)(r_2/r_1)^{2m}$, is in most cases of a higher order and can be neglected. Also, an approximation of Equations (124) and (125) can be achieved by taking m = 2, 4, 6, and 8, and disregarding the remaining terms of the infinite series which converge fast. There follows:

104

$$\Phi_{1S} = \frac{2(1+\mu_1^2)V_0 r_1 \alpha}{\pi \mu_1}$$

$$+ \frac{2(1-\mu_1^2)(\mu_2^2-\mu_1^2)V_0 r_2 \alpha}{\pi \mu_1 (1+\mu_1^2)(\mu_1^2+\mu_2^2)}\left\{1+\frac{1}{2}\left[\left(\frac{r_2}{r_1}\right)\bar{y}-\frac{1}{\left(\frac{r_2}{r_1}\right)\bar{y}}\right]\ell_n\left[\frac{1+\left(\frac{r_2}{r_1}\right)\bar{y}}{1-\left(\frac{r_2}{r_1}\right)\bar{y}}\right]\right\}$$

$$- \frac{2V_0 r_1 \alpha}{\pi \mu_1}\left\{1+\frac{1}{2}\left[\bar{y}-\frac{1}{\bar{y}}\right]\ell_n\left[\frac{1+\bar{y}}{1-\bar{y}}\right]\right\}$$

$$+ \frac{2(\mu_1^2-\mu_2^2)V_0 r_2 \alpha}{\pi \mu_1 (\mu_1^2+\mu_2^2)}\left\{1+\frac{1}{2}\left[\frac{\left(\frac{r_2}{r_1}\right)}{\bar{y}}-\frac{\bar{y}}{\left(\frac{r_2}{r_1}\right)}\right]\hat{\ell}_n\left[\frac{1+\left(\frac{r_2}{r_1}\right)\frac{1}{\bar{y}}}{1-\left(\frac{r_2}{r_1}\right)\frac{1}{\bar{y}}}\right]\right\}$$

$$+ \frac{2(\mu_2^2-\mu_1^2)V_0 r_1 \alpha}{\pi \mu_1 (\mu_1^2+\mu_2^2)}\left\{1+\frac{1}{2}\left[\left(\frac{r_2}{r_1}\right)^2\frac{1}{\bar{y}}-\frac{\bar{y}}{\left(\frac{r_2}{r_1}\right)^2}\right]\ell_n\left[\frac{1+\left(\frac{r_2}{r_1}\right)^2\frac{1}{\bar{y}}}{1-\left(\frac{r_2}{r_1}\right)^2\frac{1}{\bar{y}}}\right]\right\} \tag{126}$$

$$\Phi_{2S} = \frac{2V_0 \alpha}{\pi}\left[\frac{\mu_2}{\mu_1}(1+\mu_1^2)r_1+\frac{1}{\mu_1^2\mu_2}(\mu_1^2-\mu_2^2)r_2\right]$$

$$+ \frac{2(\mu_2^2-\mu_1^2)V_0 r_2 \alpha}{\pi \mu_2 (\mu_1^2+\mu_2^2)}\left\{1+\frac{1}{2}\left[\left(\frac{r_1}{r_2}\right)\bar{y}-\frac{1}{\left(\frac{r_1}{r_2}\right)\bar{y}}\right]\ell_n\left[\frac{1+\left(\frac{r_1}{r_2}\right)\bar{y}}{1-\left(\frac{r_1}{r_2}\right)\bar{y}}\right]\right\}$$

$$+ \frac{2(1-\mu_1^2)(\mu_2^2-\mu_1^2)V_0 r_2 \alpha}{\pi \mu_2 (1+\mu_1^2)(\mu_1^2+\mu_2^2)}\left\{1+\frac{1}{2}\left[\left(\frac{r_2}{r_1}\right)\bar{y}-\frac{1}{\left(\frac{r_2}{r_1}\right)\bar{y}}\right]\ell_n\left[\frac{1+\left(\frac{r_2}{r_1}\right)\bar{y}}{1-\left(\frac{r_2}{r_1}\right)\bar{y}}\right]\right\}$$

$$- \frac{2\mu_2 V_0 r_1 \alpha}{\pi (\mu_1^2+\mu_2^2)}\left\{1+\frac{1}{2}\left[\bar{y}-\frac{1}{\bar{y}}\right]\ell_n\left[\frac{1+\bar{y}}{1-\bar{y}}\right]\right\} \tag{127}$$

105

The lift coefficient of the totally immersed wing, based on free-stream dynamic pressure, q_o , is

$$C_{L_w} = \frac{4}{\mu_1 V_o c} \int_{\frac{r_2}{r_1}}^{1} \Phi_{1s} \, d\bar{y} + \frac{4}{\mu_2 V_o c} \int_0^{\frac{r_2}{r_1}} \Phi_{2s} \, d\bar{y} \qquad (128)$$

where Φ_{1s} and Φ_{2s} are the functions of $\bar{y}$ given in Equations (126) and (127).

Two sample calculations are now made using the following velocity patterns:

(1) $\eta = \frac{r_2}{r_1} = \frac{1}{2}$

$\gamma = \frac{U_2}{U_1} = \frac{1}{2}$

$\bar{U} = V_o$, i.e., $\bar{\mu} = 0.5$

(2) $\eta = \frac{r_2}{r_1} = \frac{1}{2}$

$\gamma = \frac{U_2}{U_1} = 2$

$\bar{U} = V_o$, i.e., $\bar{\mu} = 0.5$

The lift coefficient of the wing has been calculated for the two cases as follows:

(1) $C_{L_w} = 9.82 \frac{r_1 \alpha}{c}$ \qquad (129)

(2) $C_{L_w} = 10.31 \frac{r_1 \alpha}{c}$ \qquad (130)

106

Also, by setting

$$r_s = r_i$$

$$\mu = \bar{\mu} = 0.5$$

In Equation (101), there results that the lift coefficient of a wing immersed in a uniform jet with the same thrust as that in each of the two nonuniform jets is

$$C_{L_w} = 10.02 \frac{r_i \alpha}{c} \tag{131}$$

It is seen from the above that a jet with an induced velocity in the outer zone double that in the inner zone gives a lift coefficient about 2 percent less than a uniform jet having the same thrust. On the other hand, a jet with an induced velocity in the inner zone double that in the outer zone gives a lift coefficient about 3 percent more than a uniform jet having the same thrust.

The velocity pattern of an actual slipstream is usually very nonuniform. However, this can be well approximated by a jet consisting of a number of concentric "sub-jets", by means of which an analysis similar to that performed above for the case of two "sub-jets" can be worked out. Without finding the solution in detail, it can be concluded qualitatively at this stage that by shifting the peak velocity at any cross section of the jet toward the center, the lift on the wing will increase.

The result of the above analysis is substantiated by the test data of References 2 and 13. As reported therein, the propeller with a blade angle, $\beta_{0.75}$, of 3.7 degrees gives a higher lift coefficient than the one with a blade angle of 8.0 degrees. As can be seen from the dynamic pressure survey diagram (see Figure 45, reproduced from Reference 2), for $\beta_{0.75}$ = 3.7 degrees the velocity pattern is such that the peak is closer to the slipstream center.
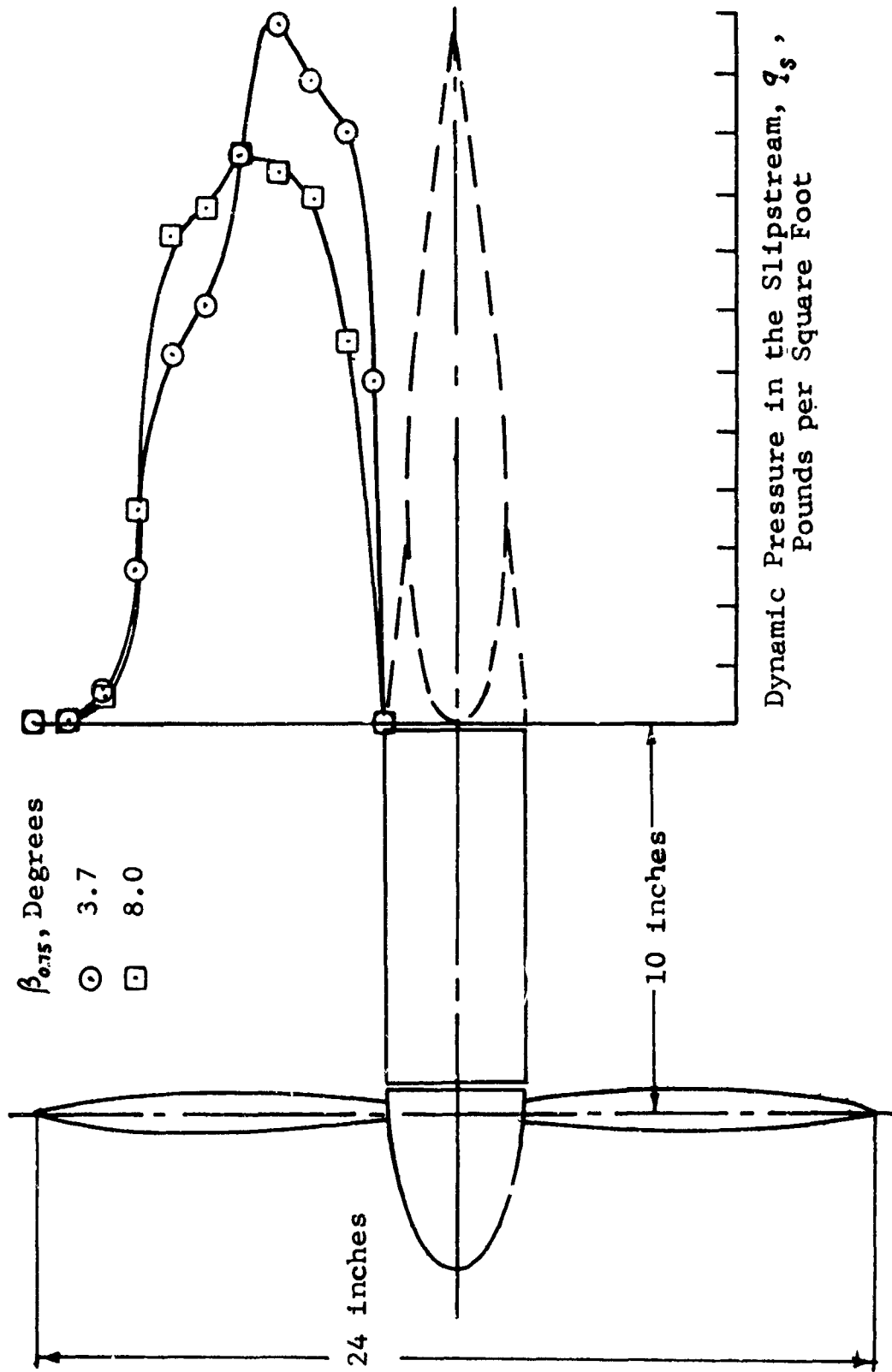
FIGURE 45. Dynamic Pressure Survey Behind Propeller (Reference 2, Figure 7; Wing Removed, $C_{T,s} = 1.0$, $T = 25$ Pounds).

It should also be noted that an increase of lift corresponds to an increase of pitching moment about the aircraft center of gravity. Hence, increased wing performance, at constant propeller thrust, can be utilized to increase the controllability of the aircraft.

THE EFFECT OF WING GEOMETRY ON LIFT

TRAILING EDGE FLAPS

This section presents the result of an investigation of the effect of large flap deflections on the lift coefficient of a wing immersed in a propeller slipstream.

The effective angle of attack, α_s , of the portion of the wing immersed in the propeller slipstream, as indicated in Reference 3, is

$$\alpha_s = i_T + \phi - \alpha_{L_o} + \delta_f \tag{132}$$

The above equation indicates that a change in flap deflection angle is equal to an equal change of angle of attack of the wing. This relationship gives quite satisfactory results when compared with test data for small flap deflection angles, i.e., less than 15 to 20 degrees. However, for larger deflection angles the use of Equation (132) often results in values of lift which exceed the experimental values.

This region of higher flap deflections is of particular interest for V/STOL aircraft which utilize flap deflections up to 60 degrees. No theoretical analysis has been found to determine the wing lift for very high flap deflections, and hence the determination of the lift must be accomplished by use of experimental data.

Existing experimental data for the special case of zero forward speed, μ = 0, have been used here to formulate empirical correction factors to the basic theory of Reference 3. Under this condition, the increment lift coefficient accounts for the entire wing lift and can be written as follows:

$$\Delta C_{L_s} = 1.87 \frac{r_s}{c} \left(i_T - \alpha_{L_o} + K \delta_f \right) \tag{133}$$

110

where K is an empirically derived correction factor.

The experimental data utilized for this purpose are obtained from References 2, 4, 12, and 13 for plain, single-slotted, and Fowler flaps. The data are compared in Figures 46 through 49 with values calculated using Equation (130) with different values of K . It is noted that the test data can be approximately reproduced by use of a correction factor $K = \cos K_1 \delta_f$. In particular, by comparing the test data with the curves plotted on Figures 46 and 47 , it is noted that for $c_f/c = 0.3$, K_1 ranges between 0.75 and 0.85, whereas for $c_f/c = 0.6$, $K_1 = 0.75$ provides reasonably accurate results. Similarly for the single-slotted flaps, the data on Figure 48 indicate values of K_1 of 0.7 and 0.6 for c_f/c of 0.3 and 0.6, respectively. Also, Figure 49 indicates that for Fowler flaps with $c_f/c = 0.4$, a value of $K_1 = 0.875$ is appropriate.

WING TWIST

The theory presented in Reference 3 for the lift increment of a wing immersed in a slipstream was developed for a rectangular, untwisted wing. To a first-order approximation, twist can be introduced into the equations as a local change of angle of attack. There follows that for a linear twist distribution, the lift coefficient increment due to the slipstream can be written as

$$\Delta C_L = \frac{2(1-\mu^2)\Gamma_s \alpha_{sc}}{\pi \mu^2 c} \int_{-1}^{1} \left(1 + \frac{\epsilon_s}{\alpha_{s_c}}\bar{y}\right)\left(\frac{1}{\bar{y}} - \bar{y}\right)\ln\left(\frac{1+\bar{y}}{1-\bar{y}}\right)d\bar{y} \tag{134}$$

where ϵ_s is the wing twist between slipstream center and periphery. Since it can be shown that

$$\frac{\epsilon_s}{\alpha_{s_c}}\int_{-1}^{1} \bar{y}\left(\frac{1}{\bar{y}} - \bar{y}\right)\ln\left(\frac{1+\bar{y}}{1-\bar{y}}\right)d\bar{y} = 0 \tag{135}$$

111
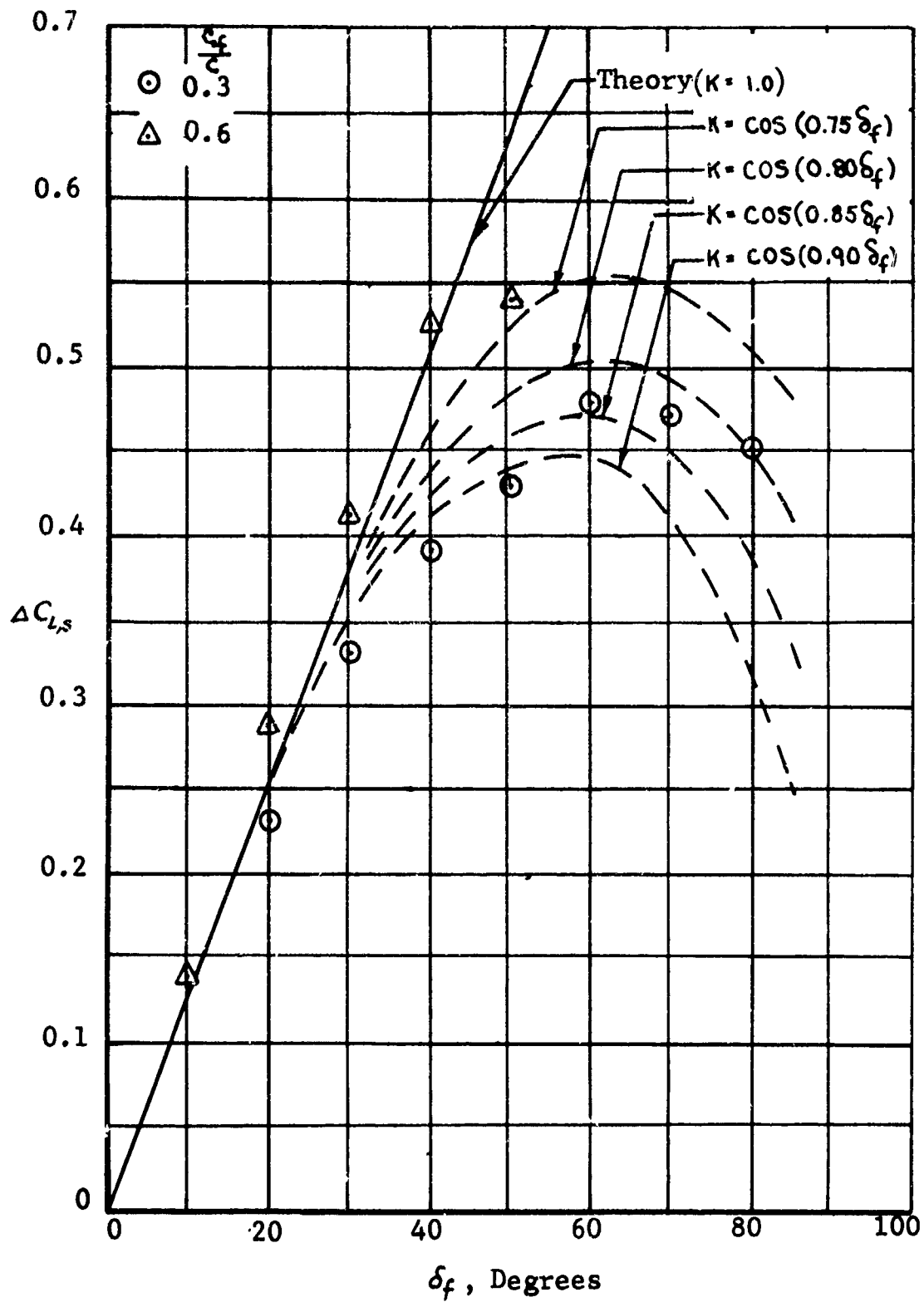
FIGURE 46. Variation of Lift Coefficient Increment with Flap
Deflection Angle (Test Data from Reference 12, Figure 9a;
Plain Flap, $C_{T,s} = 1.0$).

112
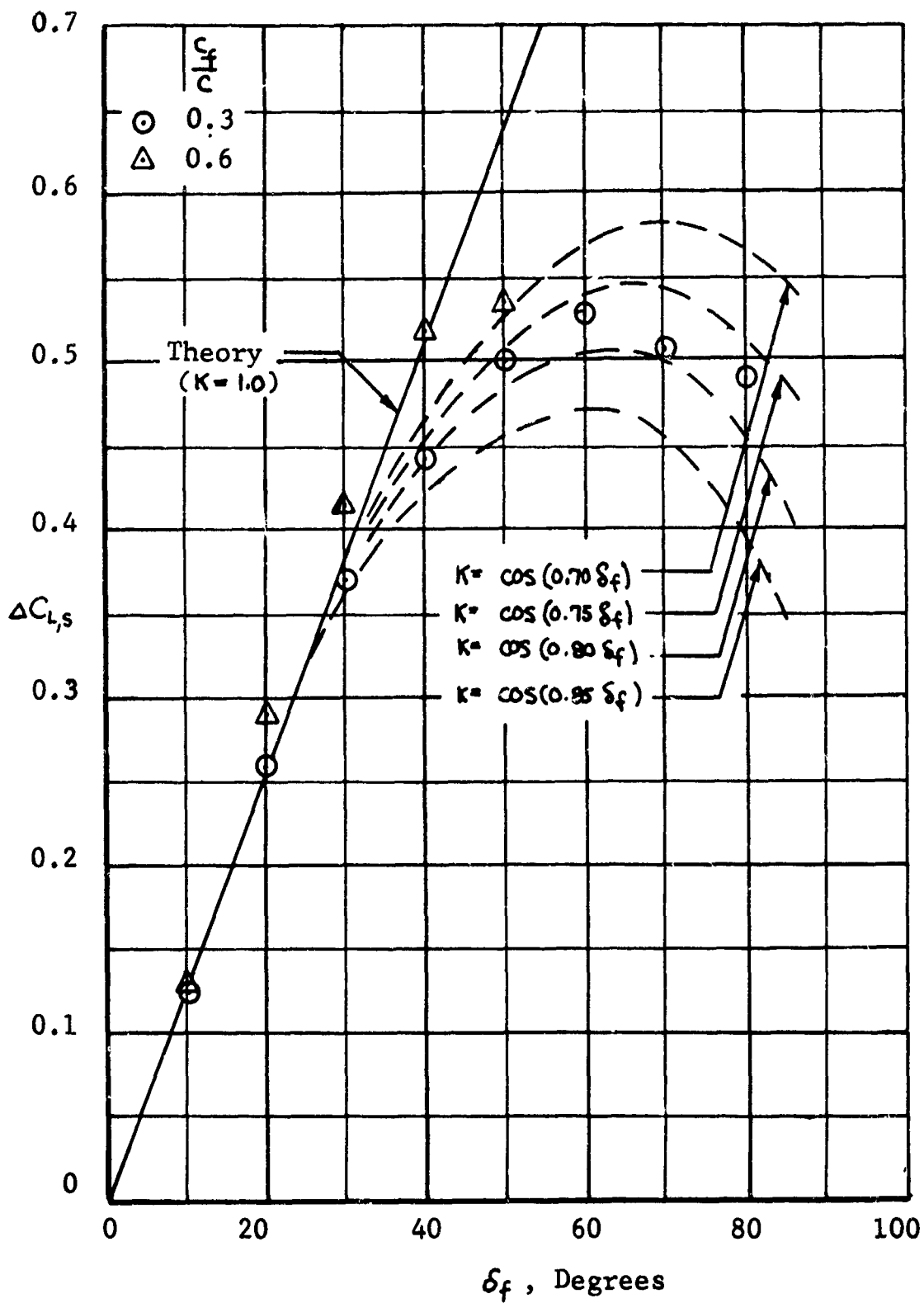
FIGURE 47. Variation of Lift Coefficient Increment with Flap Deflection Angle (Test Data from Reference 2, Figure 5a; Plain Flap, $C_{T,s} = 1.0$).

113
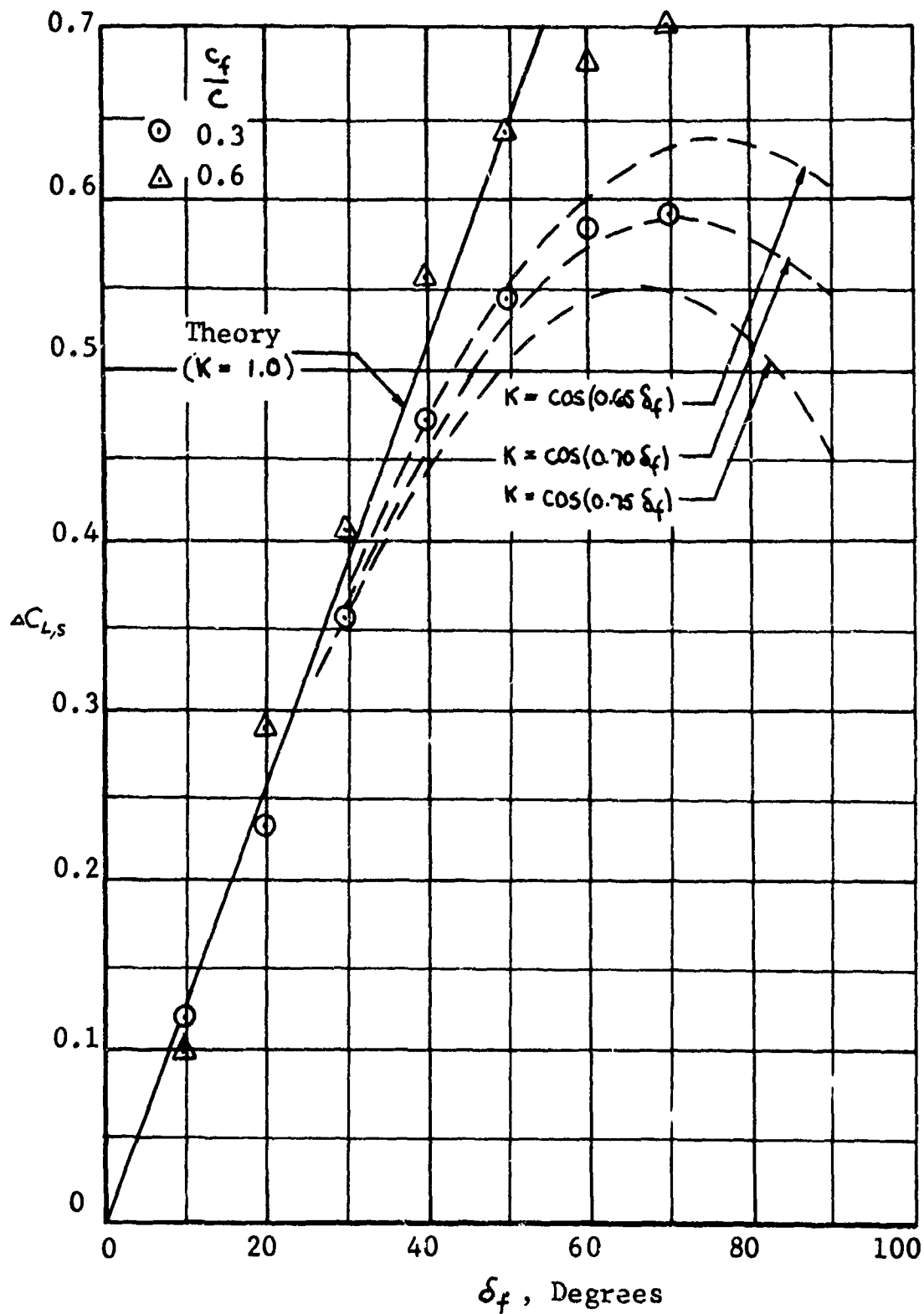
FIGURE 48. Variation of Lift Coefficient Increment with Flap Deflection Angle (Test Data from Reference 13, Figure 7a; Single-Slotted Flap, $C_{T,s} = 1.0$).

114
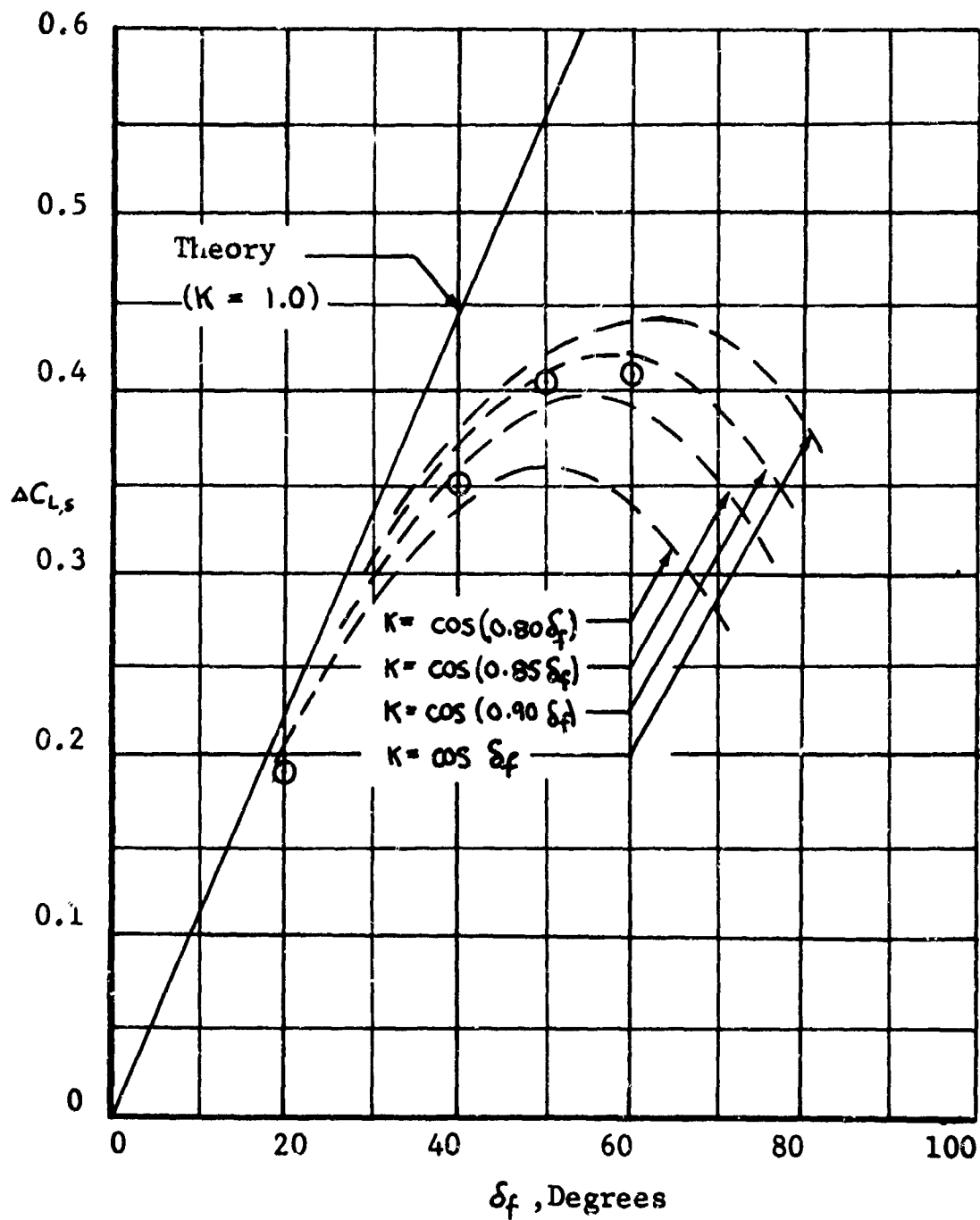
FIGURE 49. Variation of Lift Coefficient Increment with Flap
Deflection Angle (Test Data from Reference 4, Fowler Type
Flap, $c_f/c = 0.4$, $C_{\mu,s} = 1.0$).

115

the theory used here indicates that linear twist does not
change the wing lift. Because of a lack of appropriate test
data, this conclusion could not be verified.

PROPELLER-WING ORIENTATION AND POSITION

Orientation

The theory presented in Reference 3 can be used to
evaluate the effect of propeller-wing orientation angle,
i_T . This angle appears in the expression for the effective
angle of attack in the slipstream as follows:

$$\alpha_s = i_T + \phi - \alpha_{lo} + K\delta_f \tag{136}$$

where

$$\phi = \tan^{-1}\left[\frac{\sin(\alpha_p - i_T)}{\sqrt{\cos^2(\alpha_p - i_T) + \frac{C_{T_s}}{1 - C_{T_s}}}}\right] \tag{137}$$

The theory is compared in Figure 50 with the test
data of a double-slotted flap of Reference 13. The correction
factor K_1 = 0.75 was utilized in the calculations. It
is noted from Figure 50 that except for the low values of
flap deflection, the correlation between theory and test
data is very good.

Position

No theoretical analysis of the effect of the posi-
tion of the slipstreams on the lift coefficient of a wing
partially immersed in one or more propeller slipstreams has
been found in the literature. The following represents a
summary of findings from test results contained in a number
of experimental reports:
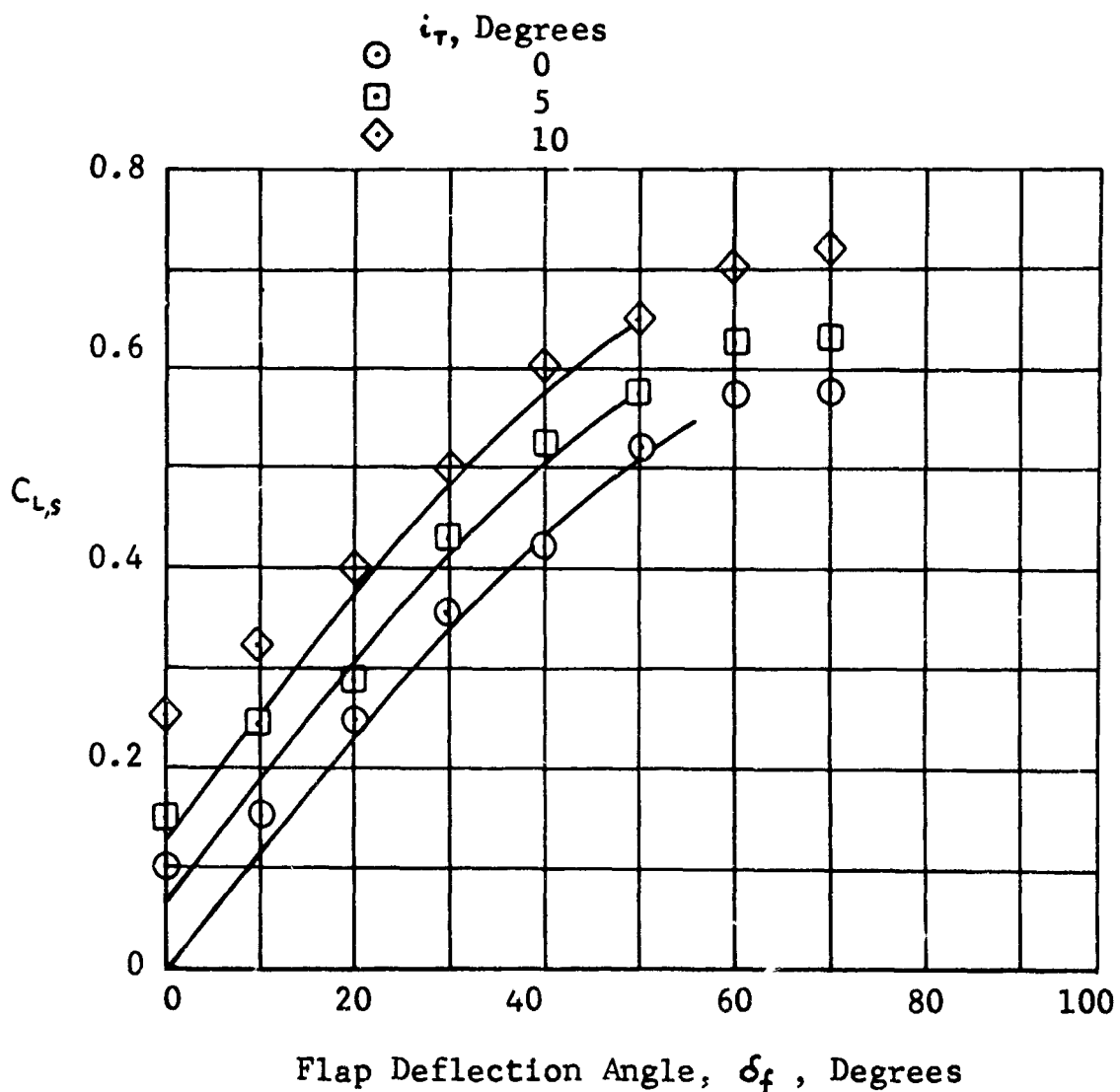
FIGURE 50. Effect of Wing Incidence on Lift Coefficient (Test Data from Reference 13, Figure 9a; Double-Slotted Flap, $C_{T,S} = 1.0$).

Longitudinal

References 2, 9, and 11 show some data on the effect of the longitudinal position. These data, which are not entirely consistent, indicate that the optimum wing-propeller relative position is such that the wing leading edge is about 0.3 to 0.5 propeller diameter behind the propeller disc plane.

Vertical

The test data presented in References 2, 9, and 11 indicate that maximum lift is obtained when the vertical position of the wing is close to the propeller center.

BIBLIOGRAPHY

1.   Anderson, R. F., Determination of the Characteristics of Tapered Wings, NACA TR 572, 1936.

2.   Draper, J.W., and Kuhn, R.E., Some Effects of Propeller Operation and Location on Ability of a Wing with Plain Flaps to Deflect Propeller Slipstream Downward for Vertical Take-Off, NACA TN 3360, 1955.

3.   Dynasciences Corporation, Effects of Propeller Slipstream on V/STOL Aircraft Performance and Stability, TRECOM Technical Report 64-47, U.S. Army Aviation Materiel Laboratories,* Fort Eustis, Virginia, August 1964.

4.   Fink, M.P., Mitchell, R.G., and White, L.C., Aerodynamic Data on a Large Semispan Tilting Wing with 0.6-Diameter Chord, Fowler Flap, and Single Propeller Rotating Up at Tip, NASA TN D-2180, 1964.

5.   Fink, M.P., Mitchell, R.G., and White, L.C., Aerodynamic Data on Large Semispan Tilting Wing with 0.6-Diameter Chord, Single-Slotted Flap, and Single Propeller Rotating Down at Tip, NASA TN D-2412, 1964.

6.   Gessow, A., and Myers, G.C., Aerodynamics of the Helicopter, The MacMillan Co., New York, New York, 1952.

7.   Hamilton Standard Division, United Aircraft Corporation, Generalized Performance of Conventional Propellers for VTOL-STOL Aircraft, Report No. HS-1829, Hamilton Standard Division, United Aircraft Corporation, Windsor Locks, Connecticut, March 1958.

8.   Harper, C.W., and Maki, R.L., A Review of the Stall Characteristics of Swept Wings, NASA TN D-2373, July 1964.

---

*Formerly U.S. Army Transportation Research Command

9.   Hayes, W.C., Kuhn, R.E., and Sherman, I.R., _Effects of Propeller Position and Develop on the Slipstream Deflection Characteristics of a Wing-Propeller Configuration Equipped with a Sliding and Fowler Flap_, NACA TN 4404, 1958.

10.   Jacobs, E.N., and Sherman A., _Airfoil Section Characteristics as Affected by Variations in Reynolds Number_, NACA TR 586, 1939.

11.   Kuhn, R.E., _Investigation of the Effects of Ground Proximity and Propeller Position on the Effectiveness of a Wing with Large-Chord Slotted Flaps in Redirecting Propeller Slipstreams Downward for Vertical Take-Off_, NACA TN 3629, 1956.

12.   Kuhn, R.E., and Draper, J.W., _An Investigation of a Wing Propeller Configuration Employing Large Chord Plain Flaps and Large-Diameter Propellers for Low-Speed Flight and Vertical Take-Off_, NACA TN 3307, 1954.

13.   Kuhn, R.E., and Draper, J.W., _Investigation of Effectiveness of Large-Chord Slotted Flaps in Deflecting Propeller Slipstreams Downward for Vertical Take-Off and Low Speed Flight_, NACA TN 3364, 1955.

14.   Kuhn, R.E., and Draper, J.W., _Investigation of the Aerodynamic Characteristics of a Model Wing-Propeller Combination and of the Wing and Propeller Separately at Angles of Attack up to 90°_, NACA TR 1263, 1956.

15.   Kuhn, R.E., and Hayes, W.C., Jr., _Wind-Tunnel Investigation of Longitudinal Aerodynamic Characteristics of Three Propeller-Driven VTOL Configurations in the Transition Speed Range, Including Effects of Ground Proximity_, NASA TN D-55, 1960.

16. Mort, K.W., and Yaggy, P.F., <u>Aerodynamic Charac-</u><u>teristics of a Full-Scale Propeller Tested with</u><u>Both Rigid and Flapping Blades and with Cyclic</u><u>Pitch Control</u>, NASA TN D-1774, May 1963.

17. Newson, W., and Kirby, H., <u>Flight Investigation of</u><u>Stability and Control Characteristics of a 1/9 Scale</u><u>Model of a Four-Propeller Tilt-Wing V/STOL Trans-</u><u>port</u>, NASA TN D-2443, September 1964.

18. Newson, W.A., Jr., and Tosti, L.P., <u>Slipstream Flow</u><u>Around Several Tilt-Wing VTOL Aircraft Models Opera-</u><u>ting Near the Ground</u>, NASA TN D-1382, September 1962.

19. Olcott, J.W., <u>Tests of a Hamilton Standard Fourway</u>,<u>21-Inch-Diameter Model Propeller Employing The U.S.</u><u>Navy Airborne Model Test Facility</u>, Report No. 675,
Princeton University, Princeton, New Jersey, April
1964.

20. Payne, H.E., III, and Cromwell, C.H., III, <u>A Sta-</u><u>bility Analysis of Tilt-Wing Aircraft (Experimental)</u>
Report No. 478, Princeton University, Princeton,
New Jersey, May 1960.

21. Pegg, R.J., <u>Summary of Flight-Test Results of the</u><u>VZ-2 Tilt-Wing Aircraft</u>, NASA TN D-989, February
1962.

22. Reeder, J.P., <u>Handling Qualities Experience with</u><u>Several VTOL Research Aircraft</u>, NASA TN D-735, 1961.

23. Ribner, H.S., <u>Formulas for Propeller in Yaw and</u><u>Charts of the Side Force Derivative</u>, NACA TR 819,
1945.

24. Schrenk, O., <u>A Simple Approximation Method for</u><u>Obtaining Spanwise Lift Distribution</u>, NACA TM 948,
1940.

25.   Sleeman, W.C., and Linsley, E.L., <u>Low Speed Wind-Tunnel Investigation of the Effects of Propeller Operation at High Thrust on the Longitudinal Stability and Trim of a Twin-Engine Airplane Configuration</u>, NACA RM L52D04, 1952.

26.   Stueper, J., <u>Effect of Propeller Slipstream on Wing and Tail</u>, NACA TM 874, 1938.

27.   Taylor, R.T., <u>Wind-Tunnel Investigation of Effect of Ratio of Wing Chord to Propeller Diameter with Addition of Slats on the Aerodynamic Characteristics of Tilting-Wing VTOL Configurations in the Transition Speed Range</u>, NASA TN D-17, 1959.

28.   Ward, J.F., <u>Structural Loads Surveys on Two Tilt-Wing VTOL Configuration</u>, NASA TN D-729, 1961.

29.   Yaggy, P.F., and Mort, K.W., <u>Wind-Tunnel Tests of Two VTOL Propellers in Descent</u>, NASA TN D-1766, March 1963.

30.   Yaggy, P.F., and Rogallo, V.L., <u>A Wind-Tunnel Investigation of Three Propellers Through an Angle-of-Attack Range from 0° to 85°</u>, NASA TN D-318, May 1960.

31.   Josephs, L.C., <u>VTOL, Vought, Hiller, Ryan, VHR-447 Tri-Service Transport, Vol. 4, Stability and Control Report, Part 1, Stability and Control</u>, Report No. AER-ElR-13342, Chance Vought Corporation, April 1961.

32.   Cromwell, C.H., III, and Payne, H.E., <u>A Stability-Analysis of Tilt-Wing Aircraft</u>, Report No. 477, Princeton University, Princeton, New Jersey, May 1960.

DOCUMENT CONTROL DATA - R&D

(Security classification of title body of abstract and indexing annotation must be entered when the overall report is classified)

1 ORIGINATING ACTIVITY (Corporate author)	2a REPORT SECURITY CLASSIFICATION
Dynasciences Corporation	Unclassified
Township Line Road	2b GROUP
Blue Bell, Pennsylvania	

3 REPORT TITLE

An Investigation of Propeller Slipstream Effects on V/STOL Aircraft Performance and Stability

4 DESCRIPTIVE NOTES *(Type of report and inclusive dates,*

Final Report

5 AUTHOR(S) *(Last name, first name, initial)*

Huang, Kuo P.
Butler, Lawrence
Goland, Leonard

6 REPORT DATE	7a TOTAL NO OF PAGES	7b NO OF REFS
February 1966	123	32

8a CONTRACT OR GRANT NO	9a ORIGINATOR'S REPORT NUMBER(S)
DA 44-177-AMC-48(T)	
b PROJECT NO	USAAVLABS Technical Report 65-81
Task 1D121401A14203	
c	9b OTHER REPORT NO(S) (Any other numbers that may be assigned this report)
d	

10 AVAILABILITY/LIMITATION NOTICES

Distribution of this document is unlimited.

11 SUPPLEMENTARY NOTES	12 SPONSORING MILITARY ACTIVITY
	US Army Aviation Materiel Laboratories Fort Eustis, Virginia

13 ABSTRACT

This report constitutes an investigation of the effects of propeller slipstream on several aspects of V/STOL aircraft performance and stability. Specific areas investigated included wing stall during transition, minimum wing size for stall-free transition, and the effects of propeller slipstream on aircraft pitching moments. In addition, a stability analysis was performed and analog computer techniques were applied to determine the feasibility of using the slipstream for stability augmentation. Finally, an analysis was performed of the effect on performance of slipstream velocity nonuniformity, and wing modification.

DD FORM 1473
1 JAN 64

14. KEY WORDS	LINK A		LINK B		LINK C	
	ROLE	WT	ROLE	WT	ROLE	WT
Slipstream: effects of propeller on V/STOL aircraft stability and performance						
V/STOL Aircraft: effect of propeller slipstream on stability and performance						

INSTRUCTIONS

1. ORIGINATING ACTIVITY: Enter the name and address of the contractor, subcontractor, grantee, Department of Defense activity or other organization (corporate author) issuing the report.

2a. REPORT SECURITY CLASSIFICATION: Enter the overall security classification of the report. Indicate whether "Restricted Data" is included. Marking is to be in accordance with appropriate security regulations.

2b. GROUP: Automatic downgrading is specified in DoD Directive 5200.10 and Armed Forces Industrial Manual. Enter the group number. Also, when applicable, show that optional markings have been used for Group 3 and Group 4 as authorized.

3. REPORT TITLE: Enter the complete report title in all capital letters. Titles in all cases should be unclassified. If a meaningful title cannot be selected without classification, show title classification in all capitals in parenthesis immediately following the title.

4. DESCRIPTIVE NOTES: If appropriate, enter the type of report, e.g., interim, progress, summary, annual, or final. Give the inclusive dates when a specific reporting period is covered.

5. AUTHOR(S): Enter the name(s) of author(s) as shown on or in the report. Enter last name, first name, middle initial. If military, show rank and branch of service. The name of the principal author is an absolute minimum requirement.

6. REPORT DATE: Enter the date of the report as day, month, year; or month, year. If more than one date appears on the report, use date of publication.

7a. TOTAL NUMBER OF PAGES: The total page count should follow normal pagination procedures, i.e., enter the number of pages containing information.

7b. NUMBER OF REFERENCES: Enter the total number of references cited in the report.

8a. CONTRACT OR GRANT NUMBER: If appropriate, enter the applicable number of the contract or grant under which the report was written.

8b, 8c, & 8d. PROJECT NUMBER: Enter the appropriate military department identification, such as project number, subproject number, system numbers, task number, etc.

9a. ORIGINATOR'S REPORT NUMBER(S): Enter the official report number by which the document will be identified and controlled by the originating activity. This number must be unique to this report.

9b. OTHER REPORT NUMBER(S): If the report has been assigned any other report numbers (either by the originator or by the sponsor), also enter this number(s).

10. AVAILABILITY/LIMITATION NOTICES: Enter any limitations on further dissemination of the report, other than those imposed by security classification, using standard statements such as:

(1) "Qualified requesters may obtain copies of this report from DDC."

(2) "Foreign announcement and dissemination of this report by DDC is not authorized."

(3) "U. S. Government agencies may obtain copies of this report directly from DDC. Other qualified DDC users shall request through
_____."

(4) "U. S. military agencies may obtain copies of this report directly from DDC. Other qualified users shall request through
_____."

(5) "All distribution of this report is controlled. Qualified DDC users shall request through
_____."

If the report has been furnished to the Office of Technical Services, Department of Commerce, for sale to the public, indicate this fact and enter the price, if known.

11. SUPPLEMENTARY NOTES: Use for additional explanatory notes.

12. SPONSORING MILITARY ACTIVITY: Enter the name of the departmental project office or laboratory sponsoring (paying for) the research and development. Include address.

13. ABSTRACT: Enter an abstract giving a brief and factual summary of the document indicative of the report, even though it may also appear elsewhere in the body of the technical report. If additional space is required, a continuation sheet shall be attached.

It is highly desirable that the abstract of classified reports be unclassified. Each paragraph of the abstract shall end with an indication of the military security classification of the information in the paragraph, represented as (TS), (S), (C), or (U).

There is no limitation on the length of the abstract. However, the suggested length is from 150 to 225 words.

14. KEY WORDS: Key words are technically meaningful terms or short phrases that characterize a report and may be used as index entries for cataloging the report. Key words must be selected so that no security classification is required. Identifiers, such as equipment model designation, trade name, military project code name, geographic location, may be used as key words but will be followed by an indication of technical context. The assignment of links, rules, and weights is optional.